WIDEBAND AND FLAT-GAIN OPTICAL AMPLIFIER WITH HAFNIA-BISMUTH ERBIUM CO-DOPED FIBER

ALABBAS AHMED ABDULJABBAR AL-AZZAWI

FACULTY OF ENGINEERING
UNIVERSITY OF MALAYA
KUALA LUMPUR

2020

WIDEBAND AND FLAT-GAIN OPTICAL AMPLIFIER WITH HAFNIA-BISMUTH ERBIUM CO-DOPED FIBER

ALABBAS AHMED ABDULJABBAR AL-AZZAWI

THESIS SUBMITTED IN FULFILMENT OF THE REQUIREMENTS FOR THE DEGREE OF DOCTOR OF PHILOSOPHY / ELECTRICAL ENGINEERING

FACULTY OF ENGINEERING
UNIVERSITY OF MALAYA
KUALA LUMPUR

2020

UNIVERSITY OF MALAYA

ORIGINAL LITERARY WORK DECLARATION

Name of Candidate: **ALABBAS AHMED ABDULJABBAR AL-AZZAWI**

Matric No: **KVA170021**

Name of Degree: **DOCTOR OF PHILOSOPHY (Ph.D)**

Title of Project Paper/Research Report/Dissertation/Thesis ("this Work"): **WIDEBAND AND FLAT-GAIN OPTICAL AMPLIFIER WITH HAFNIA-BISMUTH ERBIUM CO-DOPED FIBER**

Field of Study: **PHOTONICS**

I do solemnly and sincerely declare that:

(1) I am the sole author/writer of this Work;
(2) This Work is original;
(3) Any use of any work in which copyright exists was done by way of fair dealing and for permitted purposes and any excerpt or extract from, or reference to or reproduction of any copyright work has been disclosed expressly and sufficiently and the title of the Work and its authorship have been acknowledged in this Work;
(4) I do not have any actual knowledge nor do I ought reasonably to know that the making of this work constitutes an infringement of any copyright work;
(5) I hereby assign all and every rights in the copyright to this Work to the University of Malaya ("UM"), who henceforth shall be owner of the copyright in this Work and that any reproduction or use in any form or by any means whatsoever is prohibited without the written consent of UM having been first had and obtained;
(6) I am fully aware that if in the course of making this Work I have infringed any copyright whether intentionally or otherwise, I may be subject to legal action or any other action as may be determined by UM.

Candidate's Signature Date:

Subscribed and solemnly declared before,

Witness's Signature Date:

Name:

Designation:

WIDEBAND AND FLAT-GAIN OPTICAL AMPLIFIER WITH HAFNIA-BISMUTH ERBIUM CO-DOPED FIBER

ABSTRACT

A compact optical amplifier with a flat-gain characteristic is demonstrated using hafnia-bismuth-erbium co-doped fiber (HB-EDF) as the gain medium. The HB-EDF was recently fabricated using a modified chemical vapor deposition (MCVD) process in conjunction with solution doping (SD) technique. The fiber has an Erbium ions concentration of 12500 wt. ppm, which was realized due to the co-doping with Hafnium and Aluminum ions. Firstly, the proposed amplifier was investigated for both single and double-pass configurations. It is found that the 0.5m long HB-EDF is the optimum length for the C-band region. For double-pass HB-EDFA, at input signal power of -10 dBm, a flat-gain of 15.9 dB was realized with a gain ripple of less than 1.4 dB, along the 45 nm wavelength region from 1525 to 1570 nm. Within the flat-gain region, the noise figure was less than 8.1 dB. Secondly, a wideband HB-EDFA was demonstrated, utilizing two short lengths of HB-EDF to fulfill amplification in both C- and L-bands. The wideband HB-EDFA was achieved using two-stage in both series and parallel structures. It is found that both parallel and backward pumping-based series HB-EDFAs obtained flat-gain characteristics over a wideband operation wavelength. For instance, in parallel HB-EDFA using 1.72 m long HB-EDF, a flat-gain of 12.1 dB was realized with a gain ripple of less than 2 dB, along the wavelength region of 80 nm from 1525 to 1605 nm. Within the flat-gain region, the noise figure values vary from 6 to 11.8 dB. Besides, in backward pumping-based series HB-EDFA using 2 m long HB-EDF, a flat-gain of 14.6 dB was realized with a gain ripple of less than 2 dB, along the wavelength region of 65 nm from 1530 to 1595 nm. Within the flat-gain region, the noise figure values vary from 6.8 to 10.2 dB. Finally, a wideband and flat-gain hybrid EDFA was investigated, by employing

HB-EDF and zirconia-erbium doped fiber (Zr-EDF) as a hybrid active fiber, to improve the amplification bandwidth, flat-gain, and noise figure. In parallel hybrid EDFA, at -10 dBm input signal, a flat-gain of 15.6 dB was realized with a gain ripple of less than 1 dB, along the wideband wavelength region of 75 nm from 1525 to 1600 nm. Within the flat-gain region, the noise figure values vary from 4.1 to 8.7 dB. Besides, for backward pumping-based series hybrid EDFA, at input signal level of -10 dBm, a flat-gain of 14.6 dB was realized with a gain ripple of less than 1.8 dB, along the 70 nm wavelength region from 1530 to 1600 nm. Within the-flat gain region, the noise figure values vary from 4.3 to 7.9 dB. The proposed amplifiers are successfully realized not only the functional requirements but also the economically viable, by mitigation the complexity and devices used. A broadband ASE light was also successfully demonstrated to cover both C- and L-bands, using the hybrid active fibers in series and parallel structures. It is found that a broader and higher ASE spectrum can be achieved at the backward pumping-based series configuration.

Keywords: Erbium doped fiber amplifier, Wideband optical amplifier, Flat-gain, hafnia-bismuth-erbium co-doped fiber, hybrid active fibers.

PENGGANDA JALUR LEBAR AND GADAAN DATAR DENGAN GENTIAN BERDOPAN HAFNIA-BISMUTH-ERBIUM

ABSTRAK

Penyelidikan terhadap pengganda gentian optik yang padat dengan prestasi gandaan datar dibentangkan dengan menggunakan gentian berdopan hafnia-bismuth-erbium (HB-EDF) sebagai medium gandaan. HB-EDF baru ini direka-bentuk dengan menggunakan proses pemendapan wap kimia (MCVD) bersamaan dengan teknik doping penyelesaian (SD). Gentian optik ini yang mempunyai kepekatan ion Erbium tinggi sebanyak 12500 wt. ppm telah direalisasikan dengan doping bersama ion Hafnium dan Aluminium. Pertama, pengganda gentian yang dicadangkan dikaji dengan konfigurasi tunggal dan ganda lalu. Adalah didapati bahawa 0.5 m panjang HB-EDF adalah panjang optimum bagi gelombang konventional (lajur-C). Bagi konfigurasi HB-EDFA ganda lalu pada kuasa isyarat input -10 dBm, gandaaan mendatar 15.9 dB direalisasikan dengan riak gandaan kurang daripada 1.4 dB, sepanjang rantau panjang gelombang 45 nm dari 1525 hingga 1570 nm. Dalam rantau mendatar ini, angka hingar adalah kurang daripada 8.1 dB. Kemudian, jalur-lebar HB-EDFA telah direalisasikan dengan menggunakan dua HB-EDF pendek dalam memenuhi amplifikasi di kedua-dua jalur-C- dan jalur-L. Jalur-lebar HB-EDFA dicapai dengan menggunakan dua peringkat dalam kedua-dua struktur siri dan selari. Didapati bahawa kedua-dua struktur selari and siri HB-EDFA berasaskan mengepam ke-belakang memperoleh prestasi gandaan mendatar sepanjang gelombang operasi. Contohnya, HB-EDFA yang selari menggunakan HB-EDF yang panjangnya 1.72 m, gandaan mendatar 12.1 dB direalisasikan dengan riak gandaan kurang daripada 2 dB, di sepanjang rentang panjang gelombang 80 nm dari 1525 hingga 1605 nm. Dalam rentang datar ini, nilai angka hingar berbeza dari 6 hingga 11.8 dB. Selain itu, HB- EDFA siri berasaskan mengepam ke-belakang menggunakan HB-EDF panjangnya 2 m, gandaan

mendatar 14.6 dB direalisasikan dengan riak gandaan kurang daripada 2 dB, sepanjang rentang panjang gelombang 65 nm dari 1530 hingga 1595 nm. Dalam rentang datar ini, nilai angka hingar berbeza-beza dari 6.8 hingga 10.2 dB. Akhirnya, EDFA hibrid yang bersifat jalur-lebar dengan gadaan mendatar telah dikaji, dengan menggunakan HB-EDF dan gentian optik zirconia-erbium (Zr-EDF) sebagai gentian hybrid aktif, untuk meningkatkan bandwidth gandaan, kerataan gandaan, dan prestasi kebisingan. Dalam EDFA hibrid selari, pada isyarat input -10 dBm, gandaan mendatar 15.6 dB direalisasikan dengan riak gandaan kurang daripada 1 dB, di sepanjang rantau panjang gelombang lebar 75 nm dari 1525 hingga 1600 nm. Dalam rantau datar ini, nilai angka hingar berbeza dari 4.1 hingga 8.7 dB. Selain itu, bagi EDFA hibrid siri berasaskan mengepam ke-belakang, pada tahap isyarat input -10 dBm, gandaan mendatar 14.6 dB direalisasikan dengan riak gandaan kurang daripada 1.8 dB, sepanjang rantau panjang gelombang 70 nm dari 1530 hingga 1600 nm. Dalam rantau gandaan datar ini, nilai angka hingar berbeza-beza dari 4.3 hingga 7.9 dB. Pengganda gentian yang berjaya direalisasikan ini bukan sahaja untuk keperluan fungsional tetapi juga bersifat ekonomi, dengan mengurangkan kerumitan dan peranti yang digunakan. Cahaya jalur-lebar ASE juga telah berjaya diperkenalkan untuk menampung kedua-dua jalur-C dan jalur-L, dengan menggunakan gentian hybrid aktif dalam struktur siri dan selari. Adalah didapati bahawa spektrum ASE yang lebih luas dan lebih tinggi boleh dicapai dengan konfigurasi siri berasaskan mengepam ke-belakang.

Kata kunci: Pengganda gentian optik berdopan Erbium, Pengganda optic jalur-lebar, gadaan datar, gentian optik berdopan hafnia-bismuth-erbium, gentian optik hibrid aktif.

ACKNOWLEDGEMENTS

First and foremost, I would like to thank Allah almighty for giving me the strength, knowledge, ability and opportunity to undertake this research study and to persevere and complete it satisfactorily.

I would like to express my heartiest gratitude to my supervisor Prof. Dr. Sulaiman Wadi Harun for his continuous support, encouragement, guidance, and advice that helped me in completing this thesis. I also would like to express my deepest appreciation to my co-supervisor Prof. Dr. Harith Ahmad for his support and permission to doing the experiments at Photonics Research Center.

I would like to express my gratefulness and my full-hearted thank to my beloved parents; Mr. Ahmed Al-Azzawi and Mrs. Asmaa Alsandooq, for their endless love, support and prayers. They have always sought to see my success and sacrificed their life to raise me to be a better person. Without their support, this achievement would not have been possible. I also would like to convey my appreciation to my lovely sister; Zahraa Al-Azzawi for her encouragement.

I would like to convey a special thanks to my colleague Dr. Aya A. Almukhtar, for being a part of this journey and for her frequent help and support. My sincere thanks and appreciations also go to Dr. Jassim K. Hmood, Dr. Belal A. Hamida, and Dr. Xiau S. Cheng for their comments, suggestion, and constructive criticism.

I also would like to thank my colleagues at the laboratory; Aminah Ahmad, Muhammad Farid, and Ahmad Haziq for their kindness and cooperation.

Finally, I dedicate this thesis to my family, and to my beloved country; Iraq.

TABLE OF CONTENTS

LIST OF FIGURES

LIST OF TABLES

LIST OF SYMBOLS AND ABBREVIATIONS

SMF	:	Single mode fiber
LAN	:	Local area network
DWDM	:	Dense wavelength division multiplexing
SOA	:	Semiconductor optical amplifier
EDFA	:	Erbium doped fiber amplifier
ROA	:	Raman optical amplifier
PCE	:	Power conversion efficiency
C-band	:	Conventional band
L-band	:	Long band
HB-EDF	:	Hafnia-bismuth erbium co-doped fiber
NIR	:	Near-infrared
RI	:	Refractive index
Er	:	Erbium
Bi	:	Bismuth
Al	:	Aluminum
Hf	:	Hafnium
Yb	:	Ytterbium
FWHM	:	Full-width-half-maximum
Bi-EDF	:	Bismuth-based erbium doped fiber
ASE	:	Amplified spontaneous emission
EDF	:	Erbium doped fiber
HB-EDFA	:	Hafnia-bismuth erbium co-doped fiber amplifier
Si-EDFA	:	Silica-based erbium co-doped fiber amplifier
Zr-EDFA	:	Zirconia-based erbium co-doped fiber amplifier

CWDM	:	Coarse wavelength division multiplexing
WSC	:	Wavelength selective coupler
LD	:	Laser diode
h	:	Plank's constant
K	:	Blotzmann's constant
v	:	Operating frequency
σ_a	:	Absorption cross section
σ_e	:	Emission cross section
T	:	Absolute temperature
$^4I_{15/2}$	:	Ground energy level of Er^{3+}
$^4I_{13/2}$	:	Metastable energy level of Er^{3+}
$^4I_{11/2}$	:	Excited energy level of Er^{3+}
WDM	:	Wavelength division multiplexer
G	:	Gain
dB	:	Decibels
P_{out}	:	Output signal power
P_{in}	:	Input signal power
P_{ASE}	:	ASE noise power
P_p	:	Pump power
λ_p	:	Pump wavelength
λ_{in}	:	Input signal wavelength
NF	:	Noise figure
OSNR	:	Optical signal-to-noise ratio
Δv	:	Frequency bandwidth
OADM	:	Optical add/drop multiplexing
MZF	:	Mach-Zehnder filter

GFF	:	Gain filtering filters
$n_{sp}^{\pm}$	:	Spontaneous emission factor
FBG	:	Fiber Bragg grating
OCT	:	Optical coherence tomography
Si-EDF	:	Silica-based erbium doped fiber
Zr-EDF	:	Zirconia-based erbium co-doped fiber
UFBG	:	Uniform fiber Bragg grating
Bi-EDFA	:	Bismuth-based erbium doped fiber amplifier
EDPF	:	Erbium doped phosphate glass fiber
ZYAB-EDF	:	Zirconia-yttria-alumina-baria silica fiber
PIQ	:	Pair-induced quenching
MCVD	:	Modified chemical vapor deposition
SD	:	Solution doping
EPMA	:	Electron probe micro analysis
NA	:	Numerical aperture
TLS	:	Tunable laser source
POA	:	Programmable optical attenuator
OSA	:	Optical spectrum analyzer
ESA	:	Excited state absorption
S-band	:	Short band

CHAPTER 1: INTRODUCTION

1.1 Fiber optic communication system

The transmission of light by using optical fibers as a transmission medium, was first seriously investigated and demonstrated at the middle of the 20th century (Kao & Hockham, 1966). In general, a fiber optic communication system consists of three process which are, transmitter, electrical-optical-electrical conversion, and receiver. A transmitter provides an electrical signal which is obtained by the information signal. An optical source is used to converts the electrical signal to optical signal by modulating it with optical carrier. On the other hand, an optical detector is used to demodulate the signal and thus extract the electrical signal to the receiver. An optical fiber cable is used as a transmission medium for the optical signal (Senior & Jamro, 2009). Figure 1.1 illustrates the block diagram of the general fiber optic communication system. Compared to the conventional communication system, the fiber optic communication system provides attractive features such as; enormous bandwidth, low transmission loss, signal security, and electrical isolation (Agrawal, 2012).

The most two signal degradation factors which affect the performance of optical fibers are attenuation (or transmission loss) and dispersion (Kaushal & Kaddoum, 2016). As it is well known, the attenuation is the loss in optical power when the signal passes through an optical fiber from the source to destination. Another important factor is the dispersion which determines the available bandwidth, by limiting the pulse spreading in the fiber. Besides, there are other signal degradation factors that are less obvious such as; polarization, modal noise, and nonlinearities phenomena (Bhusari Shraddha et al., 2016; Caillaud et al., 2012). An optical fiber attenuation has proven to be one of the most significant key factors that should be minimized to the acceptance level in

telecommunications networks. In optical fibers, attenuation may be produced from material absorption, material scattering, and bending losses (Cardenas et al., 2009). A major advance in fiber optic communication system took place in 1970 when researchers produced a first fiber with transmission loss of less than 20 dB/km (Kapron et al., 1970). After that, massive improvements have been made, resulting in silica-based glass fibers with transmission loss below 0.2 dB/km (Yin et al., 2010).

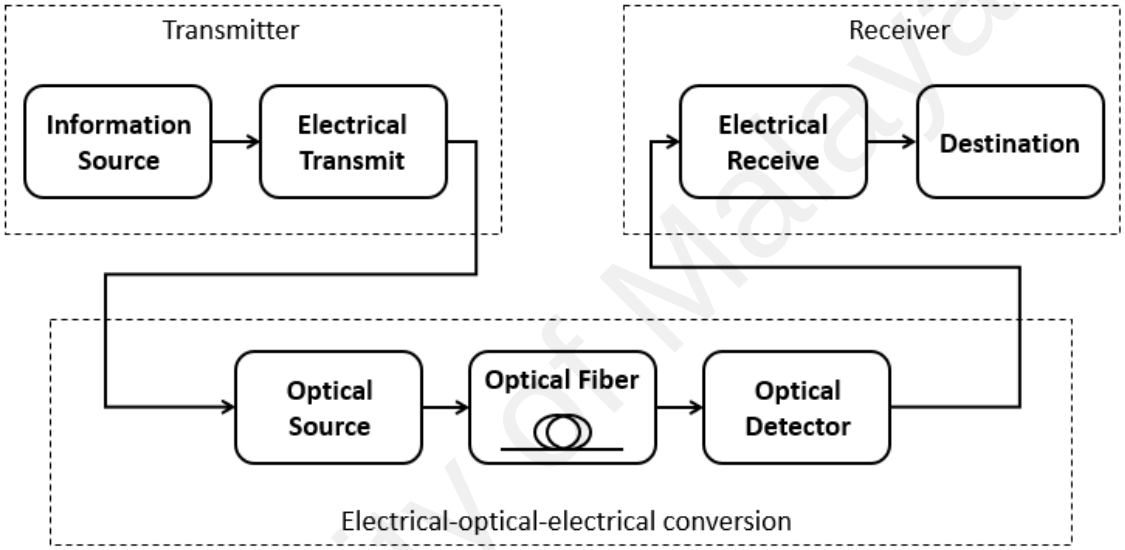

Figure 1.1: The fiber optic communication system.

Up to date, various optical fibers have been developed to operate at different optimized wavelengths. The telecommunication transmission windows of a standard silica-based single mode fiber (SMF) is illustrated in Figure 1.2. The dotted and solid curves refer to early 1980s fiber and modern fiber, respectively. As apparent, the optical loss has been significantly minimized in the modern fiber. Three operating transmission windows have been used for optical communications which are; 850 nm (1^{st} window), 1310 nm (2^{nd} window), and 1550 nm (3^{rd} and 4^{th} windows). The fiber optic systems begun at a 1^{st} window operating region, which was interesting at first. However, this region got

less interest as technology advance, due to its comparatively high attenuation limit of 3 dB/km. The 2nd window operating region has a lower attenuation of around 0.5 dB/km. Nowadays, the 1st window is still being employed for inter-premises transmission and local area network (LAN) (Jurado-Navas et al., 2015). On the other hand, some short-haul optical network still works at the 2nd window. The 3rd and 4th operating windows attain the most interest for long transmission distance owing to the minimum attenuation provided, which is around 0.2 dB/km (Allwood et al., 2011).

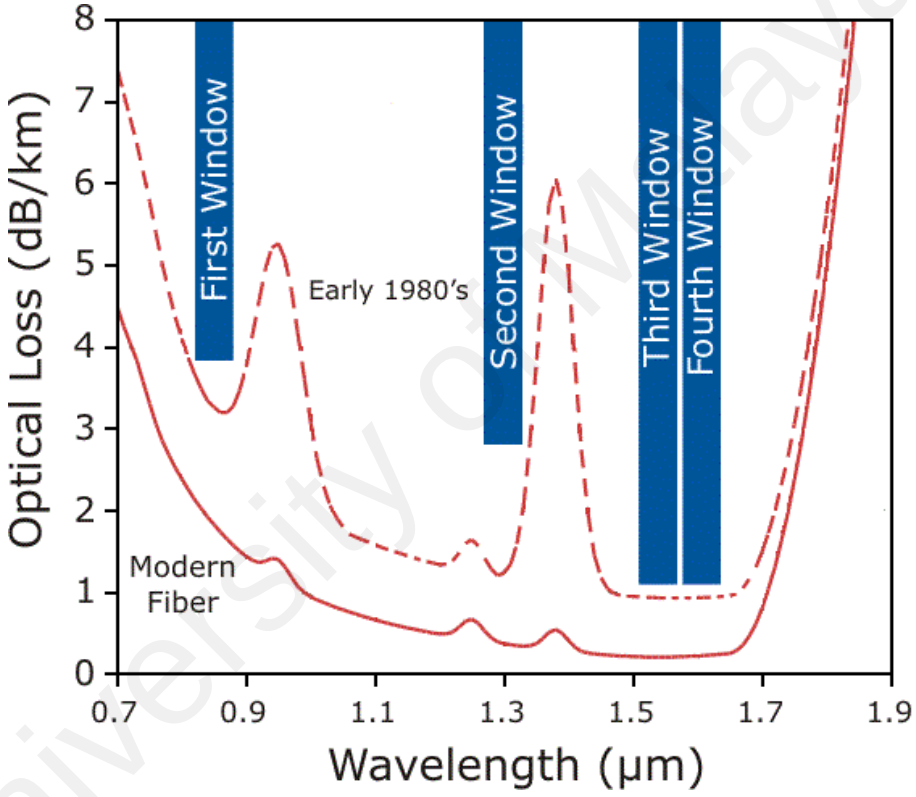

Figure 1.2: The attenuation spectra of early 1980s and modern SMFs.

1.2 Optical amplifier

The use of modern optical fiber which was optimized for the 3rd operating window, have reduced transmission loss to the lowest limit. However, the attenuation of signal power over a long distance is inevitable. It is important to overcome the problem of

attenuation in order to increase the transmission distance. During the transmission, the transmitted signal power declines, and thus it should be restored by using amplifier to keep it above the detection threshold at the receiver (Ahlawat et al., 2019). At first, an electrical repeater was used to compensate of the power loss during the long transmission distance. An optical signal undergoes four processes in the electrical repeater which are; optical-electrical conversion, amplifying the electrical signal, retiming and shaping, and lastly electrical-optical conversion. These various processing levels stimulate to the manufacturing of the optical amplifiers. This is due to the complexity, time consuming, and high cost which reduce the reliability of the electrical repeater (Rajini & Selvi, 2015).

Optical amplifiers were used and developed to amplify the optical signals directly in the optical domain, without having the optical-electrical-optical conversion process. Furthermore, optical amplifiers are suitable for dense wavelength division multiplexing (DWDM) techniques, as different optical signals wavelengths can be simultaneously amplified (Singh, 2018). At present, optical amplifiers can be classified into three main types which are; Semiconductor optical amplifiers (SOAs) (Volet et al., 2017), Erbium doped fiber amplifiers (EDFAs) (Ono et al., 2019), and Raman optical amplifiers (ROAs) (Mahran & Aly, 2016). Overall, the optical amplifier selection depends on various factors such as reliability, size and cost, gain and noise figure characteristics, power conversion efficiency (PCE), etc. SOAs display a good feature owing to their small size and low power requirement. However, several drawbacks still require more investigating in these amplifiers. SOA provides gain variations which result in nonlinear crosstalk and polarization among the wavelengths, due to the very quick gain response (picoseconds). ROA achieves a lower gain although that it requires a higher pumping power as compared to SOA and EDFA (Singh & Kaler, 2015). Currently, EDFAs are one kind of the most important optical amplifiers, that are widely used in different kinds of fiber optic communication systems. This is attributed to their interesting merits such as; flexibility

in pumping wavelength, polarization independent gain, immune to crosstalk, low coupling loss, high gain, and low noise figure. Besides, their large bandwidth which allows upgrading the DWDM system whereas various channels can be simultaneously amplified (Duarte et al., 2019).

In fiber optic communication system, the DWDM technique was used to enable a wideband transmission bandwidth, by the transferring of several optical signals in single optical fiber simultaneously (Pradhan & Mandloi, 2016). Hence, the EDFAs can be considered as the essential devices in DWDM systems. However, the number of transmitted signals in the DWDM system are limited by the bandwidth of the amplifier. The EDFAs only cover the conventional band (C-band) region which are ranging from 1530 to 1565 nm. Therefore, many researches turned to achieve amplification in long band (L-band) region which are ranging from 1565 to 1600 nm. The DWDM system could be doubled upgraded with exploit both of C- and L- telecommunication bands (Rademacher et al., 2018; Yang et al., 2016). Figure 1.3 illustrates the diagram of a DWDM system using EDFAs over the transmission path. The EDFAs are connected at intervals along the optical transmission link to obtain a linear amplification for the transmitted signal.

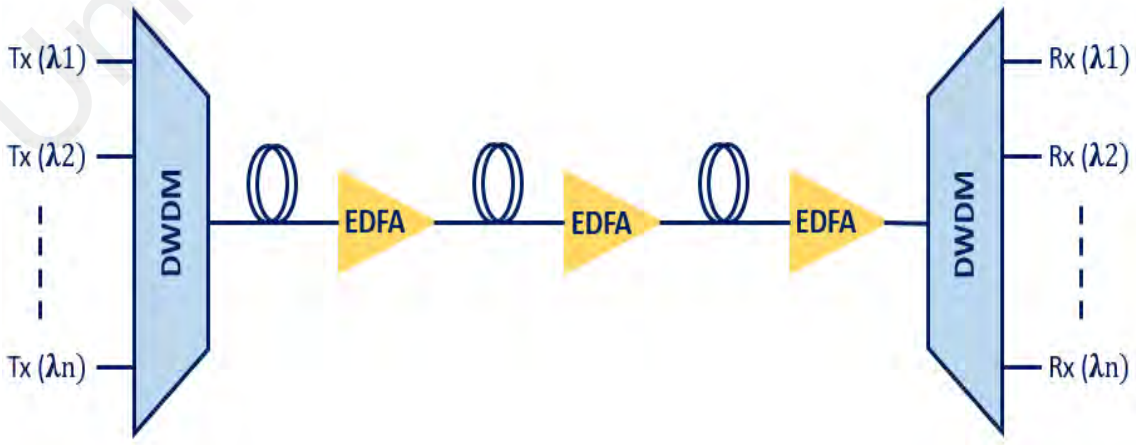

Figure 1.3: The diagram of a DWDM system using EDFAs over the transmission path.

The actual accomplishment of a commercially viable EDFA demands the combination of several unique fiber optic components in its construction, to fulfill the maximum amplifier performance efficiency. Nowadays, the cost of the EDFA is a dominant part of the system cost. This make it has necessary to be decreased by approximately an order of magnitude to make the system economically viable. The erbium doped fiber using in the EDFA has proven most practical for decreasing the complexity and cost in fiber optic communication environments, due to its ability to makes direct amplification of optical signals feasible without converting them into electrical pulses. However, there is still a challenge in reducing the instruments and the several separated stages used inside the EDFAs. Besides the functional requirements, economic feasible should be carefully optimized to fulfill the requirements imposed by fiber optic communication environments (Ganbold et al., 2018).

The EDFAs use silica fibers that doped with rare-earth materials like erbium ions. Different hosts and co-doped materials such as Tellurite (Dong et al., 2011), Phosphate (Goel et al., 2014), Bismuth (Firstov et al., 2016), and Zirconia (Duarte et al., 2019) have been proposed to enhance the erbium ion concentration. The literature review indicates that the proposed materials or elements provide different characteristics which can significantly affect the comprehensive performance of an EDFA. Some of these elements achieve higher erbium ion concentrations which prevent the concentration quenching and clustering effects, and thus reduce the active fiber lengths to get a more compact amplifier. Others achieve a broader emission wavelength which is compatible for DWDM technology (Harun et al., 2011).

Recently, there are interests in hafnia-bismuth erbium co-doped fibers (HB-EDFs) that can be useful for near-infrared (NIR) applications. This is attributed to its large effective phonon energy which reduces fundamental loss in the NIR (Kir'yanov et al., 2018). The choice of SiO_2-HfO_2 network of core-glass stems from the known fact that

HfO_2 is a material with a high refractive index (RI), transparent over a wide wavelength range, 0.4 - 6 μm (Rahman et al., 2019). Doping of Hafnia (HfO_2) having more than four coordination numbers in silica glass creates non-bridging oxygens in silica network, which allow the host glass to accommodate other optically-active in NIR co-dopants such as rare-earths Er, Yb etc along with Bi (Kir'yanov et al., 2017). By incorporating Bismuth (Bi_2O_3) and Alumina (Al_2O_3) as the main glass network, the local glass basicity near the Erbium (Er^{3+}) ions sites can be expanded. As a result, Bismuth incorporation could be broadened the 1530 nm fluorescence full-width-half-maximum (FWHM) spectrum (Yang et al., 2003). Doping HfO_2 along with Al_2O_3 maximizes the limit of erbium doping concentration while preventing the detrimental effects such as pair-induced quenching (PIQ) and cluster formation. The addition of germanium (GeO_2) in the fiber preform allows increasing the refractive index of the silica glass. This property is often used in the field of the fiber optic technology for the elaboration of the waveguiding structure in fibers with pure SiO_2 cladding (Leon et al., 2016). A minor amount of yttria (Y_2O_3) is used in the preform to prevent cracking problem. In addition, the HfO_2 can be capable to slightly modify the overall core-glass structure, and thus facilitating dispersion of active co-dopants for development of wideband optical amplifier at NIR region. Therefore, the use of HB-EDF sounds attractive to be investigated in optical amplifier devices.

1.3 Problem statement

An EDFA is a key device in DWDM technology and fiber optic communication system. However, there are several drawbacks that still require to be solved in EDFAs such as; high gain ripple. One of the drawbacks of current standard EDFAs is their relatively limited capacity for producing large gain per unit length, where they are employing long fiber lengths (10 – 50 m) and requiring fiber wraps with bend radii of

more than 30 mm. Bismuth-based erbium doped fibers (Bi-EDFs) were proposed as good alternative fibers for EDFA. Unfortunately, Bi-EDFs have a problem in splicing with standard SMFs by utilizing a standard splicing machine, due to the variance in melting temperatures. On the other hand, using several separated stages and the complexity in the design of EDFAs are unbeneficial both economically and technically.

1.4 Objectives of the study

This study introduces an original research on EDFA and the amplified spontaneous emission (ASE) source, by using the newly fabricated HB-EDF. The main reason for this study is to propose, investigate, and develop of EDFA that realizes not only the functional requirements but also the economically viable. Our study concentrates on the following objectives:

a) To demonstrate an EDFA using a shorter length of the erbium doped fiber (EDF) as an active fiber.

b) To develop a compact EDFA with flat gain characteristics over a wideband operation that covers both C- and L-telecommunication bands.

c) To propose and investigate a new EDFA based on series configuration scheme to provide flat gain and wide bandwidth amplification.

d) To demonstrate an EDFA realizing not only the functional requirements but also the economically viable, by mitigation the complexity and devices used.

e) To demonstrate a wideband ASE light source covers both C- and L-telecommunication bands.

1.5 Original contributions

The major original contributions of this study in fiber optic communication system are illustrated as following:

a) Demonstration of a compact single-pass EDFA with a flat gain characteristic at C-band region, using only 0.5 m long of new HB-EDF as the gain medium.

b) Demonstration of a compact double-pass HB-EDF amplifier (HB-EDFA) with a flat gain characteristic at C-band region, using 0.5 m long HB-EDF. Besides, the shorter length of 0.2 m long HB-EDF also achieved an efficient performance with flat gain characteristics. The comparison showed that the proposed HB-EDFA obtains a more efficient gain and lower noise figure as compared to that of the previous EDFAs such as; Silica-based erbium doped fiber amplifier (Si-EDFA) and Zirconia-based erbium co-doped fiber amplifier (Zr-EDFA).

c) Demonstration of a wideband and flat gain HB-EDFA utilizing two stages with two short pieces of HB-EDFs. The proposed amplifier was investigated in both series and parallel configurations, using 22 cm and 150 cm long HB-EDFs to realize amplification in C- and L-band wavelength region, respectively. A novel configuration using the coarse wavelength division multiplexing (CWDM) filter was employed to obtain amplification for the series HB-EDFA. Both the series and parallel amplifiers obtained a wideband operation at wavelength region from 1520 to 1610 nm.

d) Development an efficient wideband and flat gain series hybrid EDFA, comprises a 0.5 m long HB-EDF and 4 m long Zr-EDF as a hybrid active fiber to improve the amplification performance in C- and L-telecommunication bands, respectively. The performance of the hybrid EDFA was examined in

both forward and backward pumping schemes. Comparison showed that both forward and backward pumping amplifiers achieve a wideband amplification throughout a wavelength span from 1520 nm to 1610 nm. However, the backward pumping amplifier obtains a higher gain and lower noise figure than that of the forward pumping amplifier. A novel technique was proposed using the backward pumping distribution technique, to demonstrates not only an efficient performance, but also a cost reduction since only one laser diode is utilized to pump two stages.

e) Demonstration of wideband and flat gain parallel hybrid EDFA comprises a 0.5 m long HB-EDF and 4 m long Zr-EDF as a hybrid active fiber. The parallel hybrid amplifier has a better performance than the series hybrid amplifier. The proposed amplifier is successfully realized not only the functional requirements but also the economically viable, by mitigation the complexity and devices used.

f) Demonstration of broadband ASE light source covers both C- and L-band wavelength regions, using the proposed parallel and series configurations. The broader and higher ASE light spectrum was achieved at the backward pumping-based series configuration, using the hybrid active fiber.

1.6 Thesis structure

This thesis is arranged into six chapters, which the main aim is to demonstrate and develop a wideband and flat gain optical amplifier using HB-EDF as an active fiber. The brief introduction of fiber optic communication system and optical amplifier, the problem statement, objectives, and the major contributions are highlighted in this chapter.

Chapter 2 illustrates a detail literature review of EDFA, covering the working principle, the absorption and emission processes, and the population inversion phenomenon. The possible EDFA configurations and the pumping techniques used are also highlighted. Finally, the EDFA characteristics and the previous related works of EDFA are described and discussed based on weaknesses and strengths.

Chapter 3 presents a compact optical fiber amplifier with a flat-gain characteristic at the C-band region, using a short length of the new HB-EDF as the gain medium. The HB-EDF fabrication and specification are presented at the beginning of this chapter. The performance of the HB-EDFA is investigated for both single and double pass configurations, using various lengths of the HB-EDFs against various wavelengths and pump powers to determine the best of the design. The amplification performance of the HB-EDFA is compared with the previous EDFAs, such as the commercial Si-EDFA and the Zr-EDFA. Finally, the performances of single and double pass HB-EDFA are investigated using home-made multi-input wavelengths source to examine the flat gain characteristics.

Chapter 4 presents a new wideband and flat gain HB-EDFA, by utilizing two short lengths of HB-EDF sections to fulfill amplification in C- and L-band telecommunication regions. The proposed two-stage amplifier is investigated for both series and parallel structures in conjunction with double-pass scheme. The performance of the amplifier is explored for two different lengths of the HB-EDFs, as well as various pump powers to determine the optimum design. The proposed series amplifier is examined in both backward and forward pumping schemes. On the other hand, a broadband ASE light emission is also investigated and achieved using two pieces of HB-EDF in series and parallel structures. The proposed ASE source covers both C- and L-band wavelength regions.

Chapter 5 presents another wideband and flat gain hybrid EDFA with higher gain and lower noise figure, by employing a HB-EDF and Zr-EDF as the gain medium. The proposed amplifier comprises of a 0.5 m long HB-EDF and 4 m long Zr-EDF as a hybrid active fiber to fulfill amplification in C- and L-telecommunication bands, respectively. The proposed amplifier is investigated for both series and parallel structures in conjunction with double-pass scheme. In addition, the series amplifier is examined in both backward and forward pumping schemes. A new pumping distribution technique is also proposed to demonstrate not only an efficient amplification performance, but also a cost reduction since only one laser diode is utilized to pump two stages. At the end of this chapter, a broadband ASE light source is also proposed and demonstrated by using the hybrid active fibers in series and parallel structures. The proposed ASE source covers both C- and L-band wavelength regions.

Finally, all the research findings are concluded in Chapter 6. This chapter also proposes the future works.

CHAPTER 2: LITERATURE REVIEW

2.1 Introduction

From the last decades, the research interests in fiber optic communication systems is always high due to their reliability in realizing a long transmission distance with an agreeable bit error rate, and thus achieve the present and future customer requirements (Akhter et al., 2012). In the fiber optic communication systems, a large amount of information could be carried and rapidly transmitted throughout long distance, by using a semiconductor laser as a light source and an optical fiber glass as a transmission medium. Dense wavelength division multiplexing (DWDM) technology was used to maximize the information transmitting capacity of a low loss optical fiber (Pedro & Costa, 2017). DWDM transmission technology is the core of the fiber optic communications, where many information with different wavelengths could be transmitted simultaneously utilizing single-mode optical fiber. Two methods have been used to increase the transmitted signal counts which are; reducing the spacing between the channels, and full exploit of the usable low loss bandwidth (Liang et al., 2000; Singh, 2018).

Erbium doped fiber amplifiers (EDFAs) are considered to be one of the key components in the DWDM system. In this respect, DWDM transmission technology requires an EDFA with high gain to increase the transmission distance, as well as, flat gain characteristics over wide bandwidth to confirm that each transmitted signal reach the receiver with same power (Durak & Altuncu, 2018; Kumar & Kumar, 2019;). This thesis aims to demonstrate a flat-gain and wide-bandwidth optical amplifier using a newly developed hafnia-bismuth erbium co-doped optical fiber as the gain medium. In this chapter, the working principle of EDFA including the theory, the absorption and emission processes, and the population inversion phenomenon are detailly explained. The possible

EDFA configurations and the pumping techniques used are also highlighted. Finally, the EDFA characteristics and the previous related works of EDFA are described and discussed based on their weaknesses and strengths.

2.2 Erbium doped fiber amplifier (EDFA)

EDFAs were first commercially used in 1991 and they have obtained a wide recognition in the last decades for the rapid development of fiber optic communication system (Giles & Desurvire, 1991). The conventional EDFA mainly consists of erbium doped fibers (EDFs) which are silica fibers doping with parts per million by respect to weight (ppm. wt) of erbium ions (Er^{3+}). Figure 2.1 shows the basic configuration of an EDFA which also include, a laser diode (LD) pump at certain wavelength, as well as a wavelength selective coupler (WSC) to multiplex the input and LD pump signals.

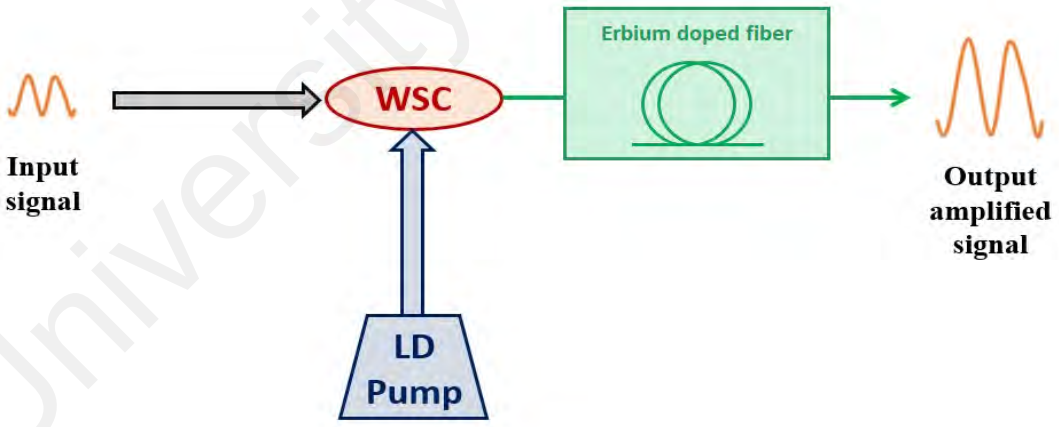

Figure 2.1: The basic configuration of the EDFA.

The optical amplification in EDF depends on spontaneous and stimulated emissions of Er^{3+} ions. The LD pumps energy to excite the Er^{3+} ions in lower energy level of EDF to higher energy levels in order to create a population inversion. Thereby, these excited

ions spontaneously emit photons as the ions release their energy to return to ground level. When an input signal photon enters the EDF at certain wavelength, this also would trigger the excited ions to drop down from higher to lower energy levels through a stimulated emission process. This process provides an amplification for the input signal inside the EDF (Pradhan & Mishra, 2015). The absorption and emission cross sections are two major parameters of EDF, which are material characteristics that quantifies the absorption or stimulated emission transition. The absorption and emission cross sections are based on a certain glass host in which the Er^{3+} is doped. Many techniques have been developed to measure the absorption and emission cross sections such as; commercial spectrophotometers (Miniscalco, 2001), Ladenburg–Fuchtbauer relation (Pollnau & Eichhorn, 2017), and McCumber relation (Ladaci et al., 2018). However, the representation of McCumber is normally utilized to link the absorption and emission cross-sections. This is attributed to its reliability and simplicity as illustrated in equation 2.1:

$$\sigma_e(\lambda) = \sigma_a(\lambda) \cdot e^{\frac{\varepsilon - h\nu}{KT}} \tag{2.1}$$

where ε, h, ν, K, and T are the energy required to excite one erbium ion, Plank's constant, operating frequency, Blotzmann's constant, and the absolute temperature, respectively. However, the absorption and emission cross sections are represented by σ_a and σ_e, respectively (Bebawi et al., 2018).

2.2.1 Population inversion

In a normal atomic system, the atom density (N_1) for lower energy level is much larger than the atom density (N_2) for upper energy level. In other word, a stimulated absorption is much higher than a stimulated emission. This condition is known as thermal

equilibrium where the atoms comply the Boltzmann distribution as illustrated in equation 2.2:

$$\frac{N_2}{N_1} = e^{-\left[\frac{(E_2 - E_1)}{KT}\right]} \tag{2.2}$$

where E_1 and E_2 represents the lower and upper energy levels, respectively. However, K and T are the Boltzmann constant and the absolute temperature, respectively.

To produce an optical amplification, the number of excited atoms at E_2 should be greater than that at E_1. In other word, N_2 is greater than N_1. Therefore, a stimulated absorption will be much lower than a stimulated emission. This is a critical condition in optical amplifier systems, which is known as population inversion (Naji et al., 2011). In EDFA, the population inversion could be obtained by pumping power to the EDF, and thus excite the erbium ions to upper energy level. The large population inversion results in getting a maximum gain. Figure 2.2 illustrates the atom density curve for both thermal equilibrium and population inversion cases.

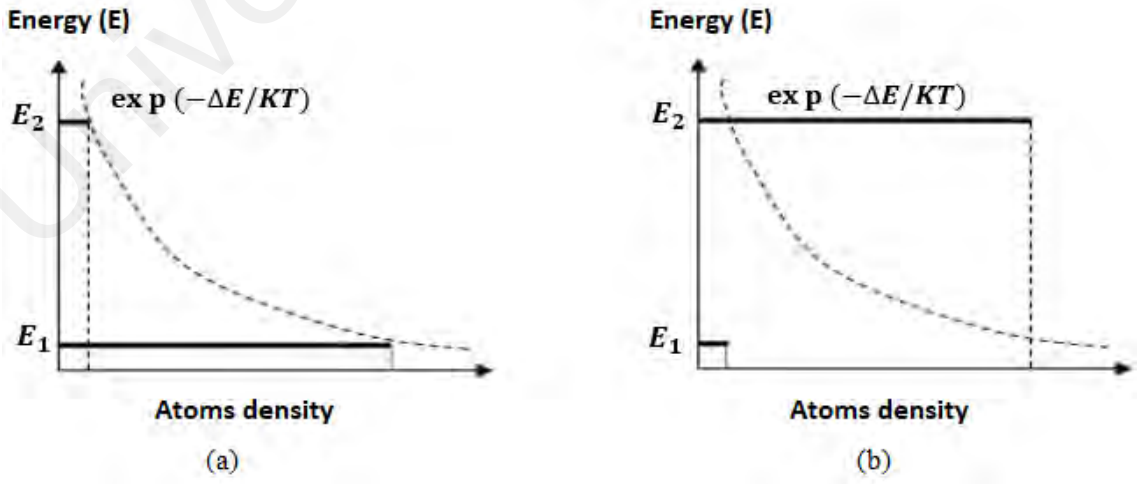

Figure 2.2: The atom density curve of two energy levels system at (a) thermal equilibrium, and (b) population inversion (Naji et al., 2011).

2.2.2 Energy levels of Er^{3+} ions

The materials ions that create two energy levels are not appropriate for optical amplifier applications. This is owing to the probabilities of absorption and spontaneous emission which are completely the same, and thus the population inversion could not be realized. At this regard, the Er^{3+} ions which provide more than two energy levels is used in EDFA. Figure 2.3 illustrates the energy levels of Er^{3+} ions that pumping with possible wavelengths. According to quantum physics laws, the energy levels are spaced by energy gaps. The ground, metastable, and excited levels which are the first three levels are represented by $^4I_{15/2}$, $^4I_{13/2}$, and $^4I_{11/2}$. respectively. The atom stabilizes at ground level and it absorbs an external energy which is provided by LD pump, to move to an upper energy level. After that, the atom at the upper energy level goes down to the ground level through spontaneous or stimulated emission processes. During these emissions, the atom releases photon with an energy equal to the difference between energy levels, as illustrated in equation 2.3:

$$hf = E_2 - E_1 \tag{2.3}$$

where *h* and *f* are the Planck's constant and photon frequency, respectively.

A spontaneous emission process happens when atom goes down to ground level spontaneously in a random phase, and thus no amplification could be occurred. Otherwise, a stimulated emission process happens due to an external energy provided by an input signal photon. Therefore, the photons produced, emit in same phase of ones that causes it. The external energy of the photons produced, add to the input signal photons, which is leading to achieve amplification (Norouzi et al., 2013). In EDFA, two pumping wavelengths are commonly used to excite Er^{3+} ions in $^4I_{15/2}$ in order to move to $^4I_{11/2}$ and $^4I_{13/2}$ levels, which are 980 nm and 1480 nm.

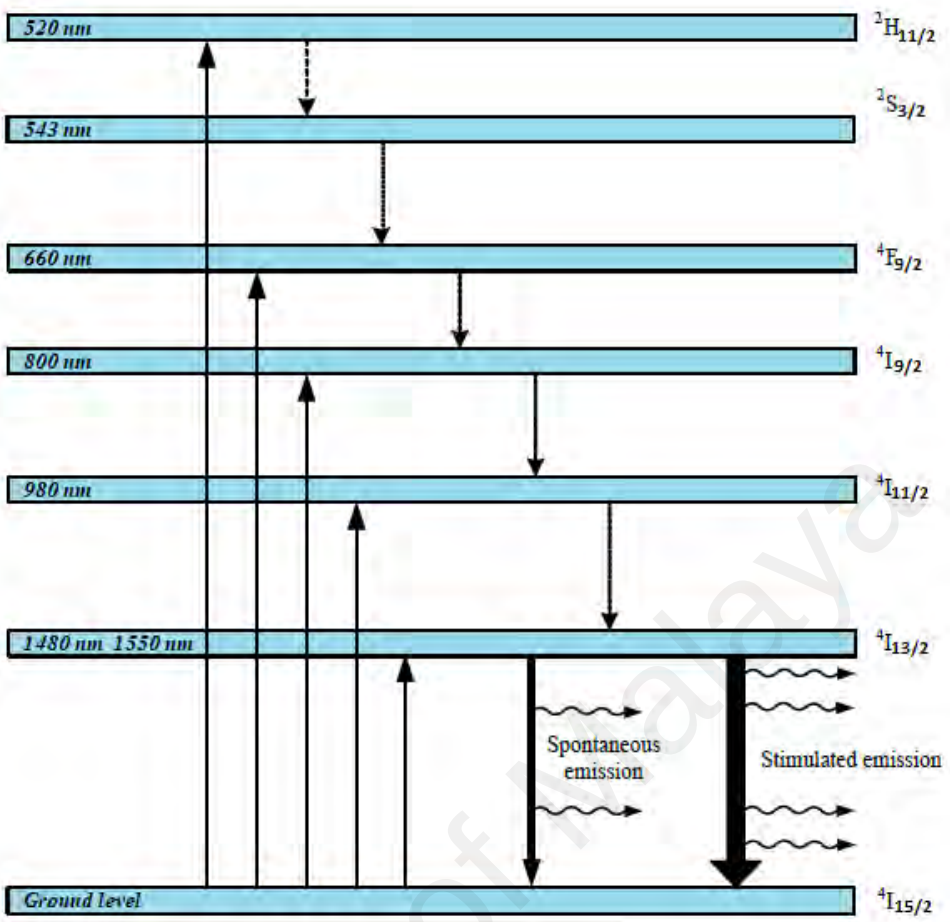

Figure 2.3: The energy levels of Er3+ ions that pumping with possible wavelengths (Norouzi et al., 2013).

2.2.2.1 Pumping at 980 nm wavelength

Pumping Er^{3+} ions at 980 nm wavelength produces three energy levels as schematically illustrated in Figure 2.4. The Er^{3+} ions in $^4I_{15/2}$ level absorb the 980 nm pump power, and thus start to move to higher level $^4I_{11/2}$. However, these excited ions quickly go down to $^4I_{13/2}$ level through a nonradiative decay transition, where the lifetime of Er^{3+} ions at $^4I_{11/2}$ level is roughly 1 µs which is very short. As compared to $^4I_{11/2}$ level, the $^4I_{13/2}$ level is more stable, and it has a longer lifetime of Er^{3+} ions which is roughly 1 ms. As a result, a population inversion could be occurred between $^4I_{13/2}$ and $^4I_{15/2}$ levels,

where the number of excited Er^{3+} ions at $^4I_{13/2}$ level is greater than $^4I_{15/2}$ level. The photons of the input signal that need to be amplified, trigger the excited Er^{3+} ions at $^4I_{13/2}$ level to decay to the $^4I_{15/2}$ level through a stimulated emission process. Hence, a new photon emits with same phase, wavelength, and polarization, resulting in amplifying the input signal (Nakandakari et al., 2017). The $^4I_{13/2}$ and $^4I_{15/2}$ levels are manifold consisting of seven and eight energy sublevels, respectively. Due to these sublevels, high levels of stimulated emissions happen at the 1525 to 1565 nm wavelengths range (Digonnet et al., 2002).

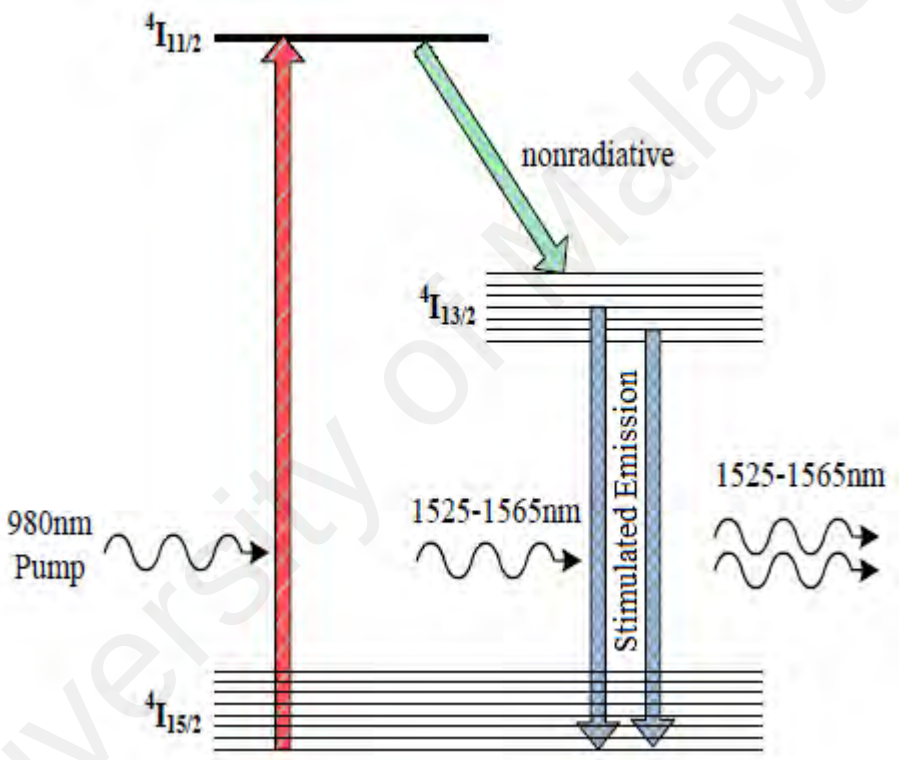

Figure 2.4: Three energy levels produced by pumping Er^{3+} ions at 980 nm wavelength.

2.2.2.2 Pumping at 1480 nm wavelength

In EDFA applications, a pumping at 1480 nm wavelength is another suitable pumping for the Er^{3+} ions. In difference with 980 nm wavelength pumping, the 1480 nm pumping provides only two energy levels as schematically illustrated in Figure 2.5. The

Er^{3+} ions in $^4I_{15/2}$ level absorb the 1480 nm pump power, and thus start to move directly to the top of $^4I_{13/2}$ level. At $^4I_{13/2}$ level, the Er^{3+} ions tend to relax down in the bottom energy sublevels, and then triggered by input signal photon to decay to $^4I_{15/2}$ level through a stimulated emission process (Harun et al., 2010).

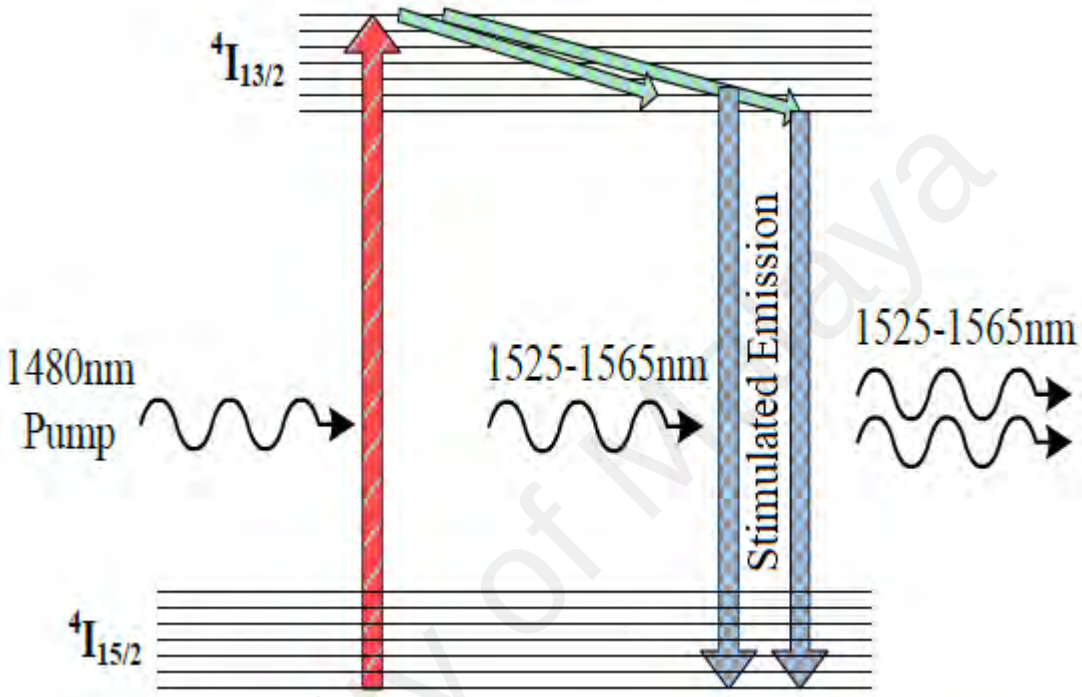

Figure 2.5: Two energy levels produced by pumping Er^{3+} ions at 1480 nm wavelength.

For operation in long wavelength band (L-band) region, an EDFA requires a longer erbium doped fiber (EDF). In this case, the energy of the pump could not be enough to produce a complete population inversion at long wavelengths. Therefore, the short wavelength photons that emitted will act as a pump power. The short wavelength photons are absorbed again by Er^{3+} ions. Hence, these excited Er^{3+} ions tend to move to $^4I_{13/2}$ level, and then emit at longer wavelength through a stimulated emission process (Nakazawa, 2014; Rivera-López et al., 2012). This process results in an EDFA that operates according to quasi-two-level system as illustrated in Figure 2.6.

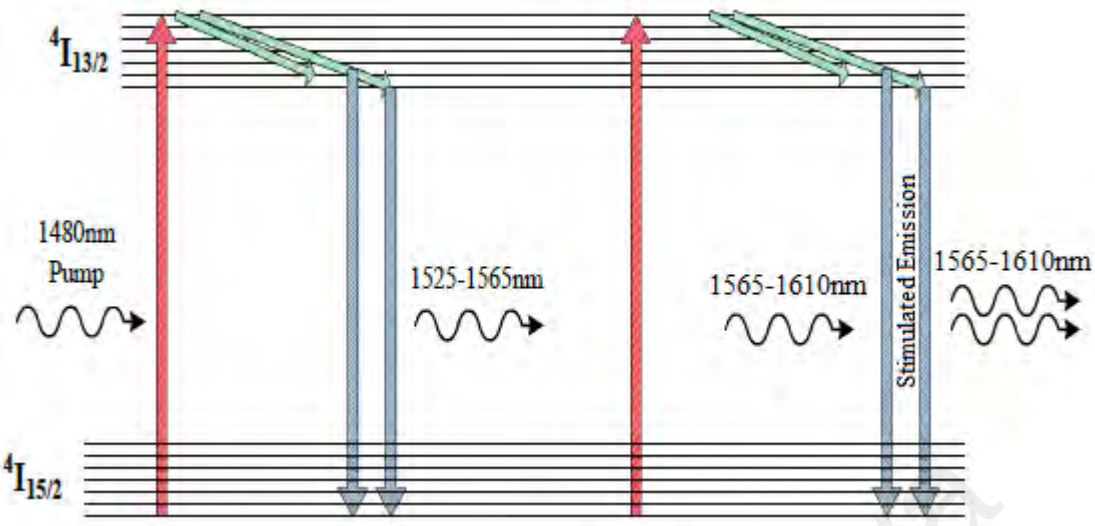

Figure 2.6: Quasi-two-level produced by pumping Er^{3+} ions at 1480 nm wavelength.

2.3 Pumping techniques

To achieve an optical amplification in the EDFA, the EDF is core pumped by using LD source at certain power and wavelength. There are three techniques to pump EDF, which are classified based on the direction. These techniques are: co-directional pumping, counter-directional pumping, and bi-directional pumping (Shukla & Kaur, 2013). In co-directional pumping (forward pumping), the pump signal is injected in same direction of the input signal, as illustrated in Figure 2.7 (a). The input and pump signals are integrated together by using wavelength division multiplexer (WDM). Then, the input signal is amplified inside the EDF, to get the output signal.

In counter-directional pumping (backward pumping), the pump signal is injected in opposite direction of the input signal, as illustrated in Figure 2.7 (b). Thus, input and pump signals are integrated and amplified in the EDF, to get the output signal. This technique achieves a higher noise figure as compared to that of co-directional pumping (Mishra et al., 2017). The bi-directional pumping (dual pumping) is a combination of co-

directional and counter-directional pumping. The input signal is amplified inside the EDF by using two pump signals. Opposed to input signal, one pump signal goes in same direction while another one goes in opposite direction, as illustrated in Figure 2.7 (c). This technique could achieve a higher gain as compared to that of co-directional and counter-directional pumping (Mishra et al., 2017). However, the residual pump power may enter the opposite LD, which could cause damage to the pump LD. Therefore, this scheme is not favorable in this study.

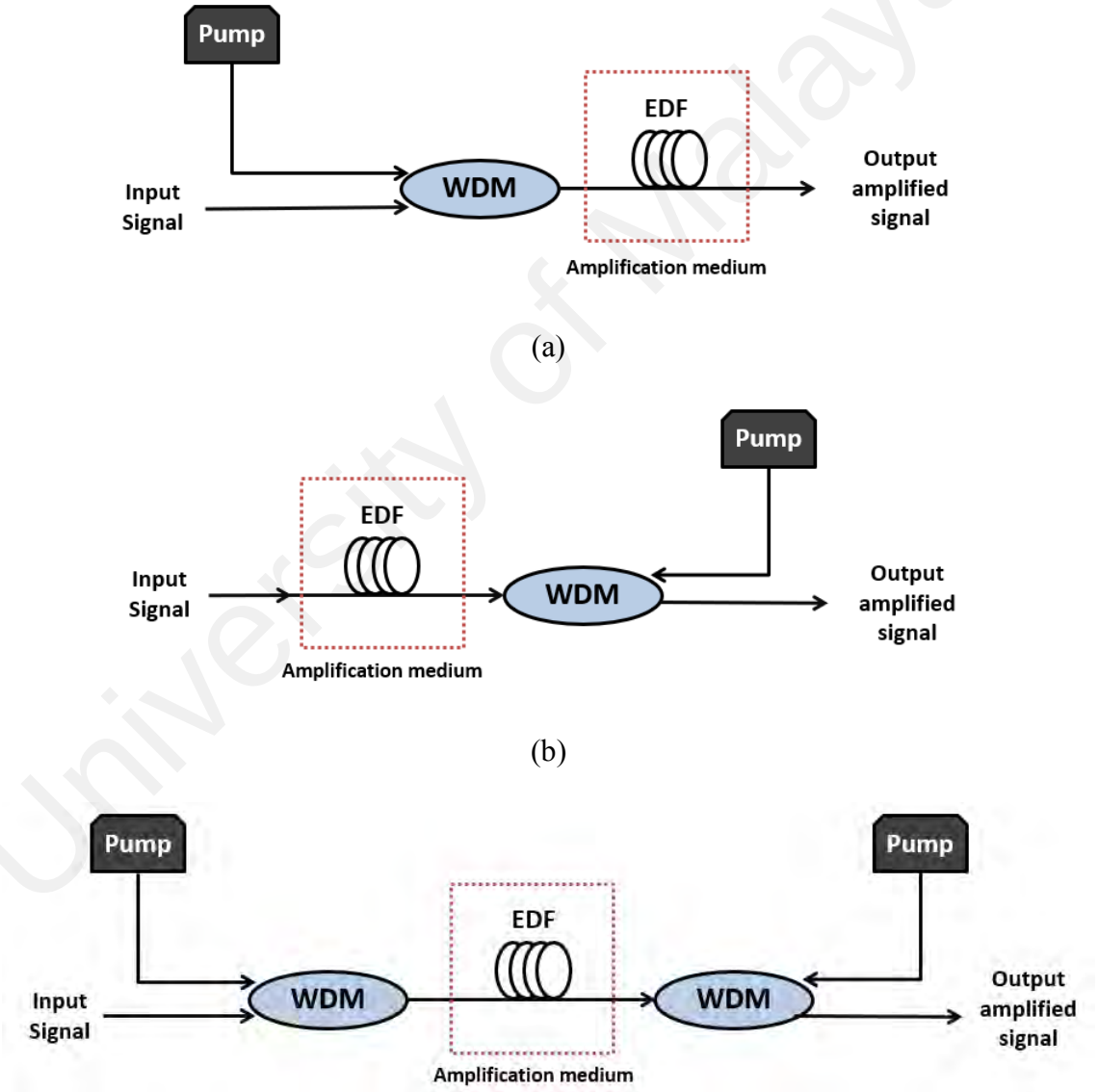

Figure 2.7: Conventional EDFA using (a) Co-directional pumping, (b) Counter-directional pumping, and (c) Bi-directional pumping.

2.4 Gain and noise figure characteristics

The performance of EDFA is described based on two main parameters; gain and noise figure. As it is well known, the gain (G) is the opposite of loss, and it is used to measure the amplification strength in an amplifier. In other word, the gain is the ratio between output and input signals powers, and it is expressed in units of decibels (dB) as illustrated in equations 2.4 and 2.5:

$$G(dB) = 10\log_{10}\left(\frac{P_{out}(mW)}{P_{in}(mW)}\right) \tag{2.4}$$

$$G(dB) = P_{out}(dBm) - P_{in}(dBm) \tag{2.5}$$

where P_{out} and P_{in} are output and input signals powers, respectively.

Practically, the output signal power consists of output signal power as well as a small amount of the amplified spontaneous emission (ASE) noise power (Suzuki et al., 2016). Hence, the real expression for the gain is illustrated in equation 2.6:

$$G(dB) = 10\log_{10}\left(\frac{P_{out}(mW) - P_{ASE}(mW)}{P_{in}(mW)}\right) \tag{2.6}$$

where P_{ASE} is the ASE noise power.

In EDFA, the signal gain is affected by various physical limitations. An energy conservation principle is one of the most major limitations, where the maximum output signal energy could not exceed the summation of input and pump signals energies (Abu-

Aisheh & Moslehpour, 2010). This principle is illustrated in equation 2.7, while it is derived and expressed in terms of gain as shown in equation 2.8:

$$P_{out} \leq P_{in} + \frac{\lambda_p}{\lambda_{in}} P_p \tag{2.7}$$

$$G \leq 1 + \frac{\lambda_p}{\lambda_{in}} \frac{P_p}{P_{in}} \tag{2.8}$$

where P_p , λ_p and λ_{in} are the pump power, pump wavelength, and input signal wavelength, respectively.

Based on equation 2.8, the gain is directly proportional with the pump power. Thus, increasing the transformation number of pump photons to signal photons could achieve a higher gain. However, the Er^{3+} ions concentration and EDF length determine the pump photons absorption (Emmanuel & Zervas, 1994). The gain is also determined by another important parameter which is the saturation effect. The amplifier's gain increases with the increasing of pumping power. However, after a certain level of pumping power, the increasing of gain becomes very small and then the saturation gain occurs (Kaler & Kaler, 2011). This is owing to that all Er^{3+} ions are excited at this pumping power level, and thus the population inversion will not increase any more. On the other hand, the gain saturation occurs easily at higher input signal power for same pump power. This causes decreasing the gain for high input signal power, due to the stimulated emission rate which tend to be similar or a bit higher than the pumping rate (Cokrak & Altuncu, 2004). The power conversion efficiency (PCE) is another important parameter is affected on the gain, which is indicating the saturation characteristics of the EDFAs. The high PCE can be obtained when a conventional EDFA is operated under highly saturated regime. Operating in such

a regime, the EDFA is normally used as a power amplifier in order to yield a maximized output signal power (Teyo et al., 2013). The PCE is defined as shown in equations 2.9 and 2.10:

$$PCE\ (\%) = \frac{(P_{out} - P_{in})}{P_p} * 100\% \tag{2.9}$$

Or

$$PCE\ (\%) = \frac{\lambda_p}{\lambda_{in}} * 100\% \tag{2.10}$$

where P_{out} , P_{in} and P_p are the amplified output, input signal, and pump powers, respectively. λ_p is the pump wavelength, while λ_{in} is the input signal wavelength.

Noise figure (NF) is the second main parameter of EDFA, which measures the quality of amplification. Noise figure is a description of an optical signal-to-noise ratio (OSNR) degradation that a signal suffered after entering the optical amplifier. In EDFA, the ASE noise that produced from spontaneous emission process is the dominant noise resulting in noise figure. The lowest noise figure could be obtained with an EDFA that provides a highest population inversion. Figure 2.8 illustrates the input and output signals of the EDFA with the amplification parameters. Similar to the signal gain, noise figure is also expressed in units of dB as illustrated in equation 2.11:

$$NF(dB) = 10 \log_{10} \left(\frac{OSNR_{in}(mW)}{OSNR_{out}(mW)} \right) \tag{2.11}$$

where $OSNR_{in}$ and $OSNR_{out}$ are the optical signal-to-noise ratio at input and output of the amplifier, respectively.

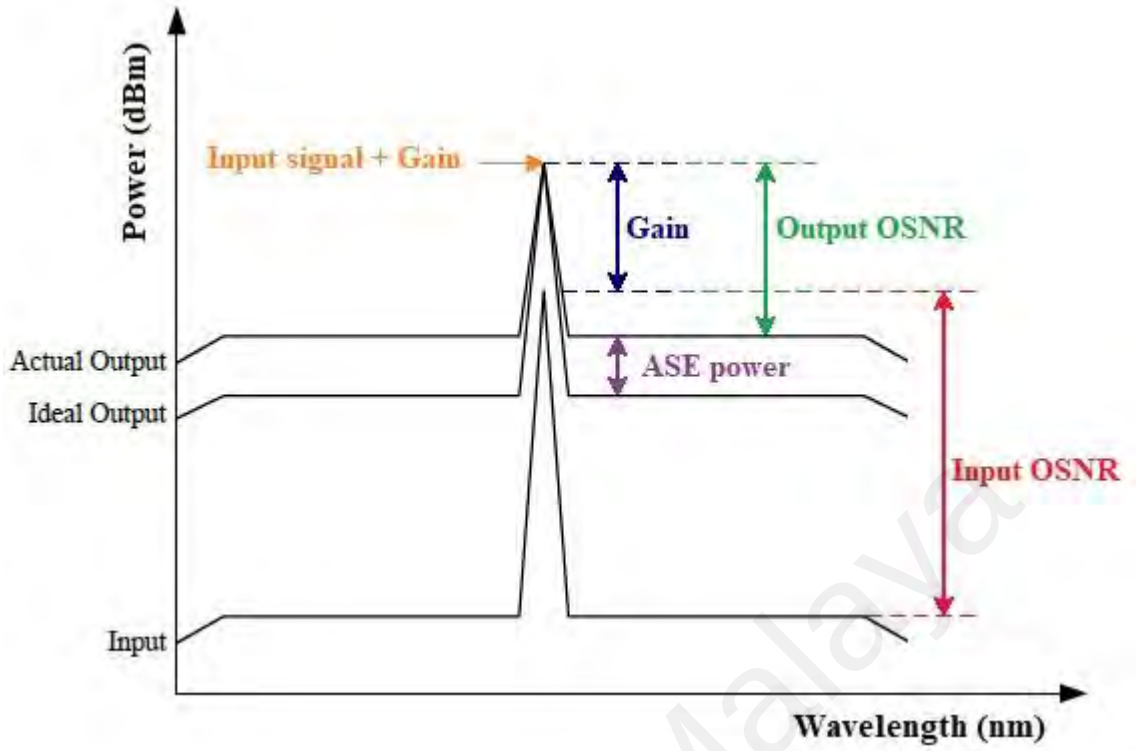

Figure 2.8: The input and output signals of the EDFA with the amplification parameters.

The $OSNR_{in}$ is always higher than $OSNR_{out}$. This is due to the noise that provided by the EDFA which is absolutely higher than the noise at the input signal. The OSNR is the signal peak power over noise peak power within the system bandwidth, as defined in the equation 2.12. Therefore, the noise figure is conclusively larger value than 1 dB. From further derivation, it was found that the lowest theoretical value of the noise figure is 3 dB (Bass et al., 2009).

$$OSNR(dB) = 10\log_{10}\left(\frac{P_{Signal}(mW)}{P_{noise}(mW)}\right) \tag{2.12}$$

Practically, the noise figure can be expressed based on the ASE power as illustrated in equation 2.13:

$$NF(dB) = 10\log_{10}\left(\frac{1}{G} + \frac{P_{ASE}}{hf\,\Delta v\,G}\right) \quad (2.13)$$

where h, f and Δv are the Planck's constant, signal frequency and frequency bandwidth, respectively.

2.5 Flat-gain characteristic

In DWDM system, it is highly advisable to design an EDFA with flat gain characteristic (i.e. uniform signal gain for all transmission wavelengths). The flat gain EDFA provides many features for DWDM system such as; optical add/drop multiplexing (OADM), link loss change, gain equalizer with low fabrication complexity, and network reconfigurations (Yusoff et al., 2010; Mahdi & Sheih, 2004). On the other hand, a high gain variation resulting in an additional noise as well as reduce the OSNR at receiver. Hence, the quest for flatting the gain spectrum of EDFA has become inevitable. Several techniques were investigated to obtain a flat gain EDFA such as; using of acousto-optic tunable filters (Varshney et al., 2007), a Mach-Zehnder filter (MZF) (Kumar & Ramachandran, 2013), and gain filtering filters (GFFs) (Shah & Mankodi, 2017). However, these methods are unpractical and uneconomical owing to the filter sensitivity with temperature varies. Furthermore, the use of external device (filter) produces extra losses and costs. Intrinsic methods were also used to obtain a flat gain amplifier, such as fabricating new active fibers by utilizing a different glass host and co-doped materials which have a high erbium ion concentration (Duarte et al., 2019). Recently, hybrid amplifiers that use several stages with different active fibers, are proven to efficiently ensure the gain flatness (Kumar & Goyal, 2019; Obaid & Shahid, 2018).

2.6 Amplified spontaneous emission (ASE)

As described previously, the stimulated emission photons that amplified in the EDF are the main cause of amplification. On the other hand, the spontaneous emission photons are also amplified in the EDF. However, these spontaneously emitted photons are not coherent with the input signal, and thus produce an optical noise typically known as the amplified spontaneous emission (ASE). In EDFA, the ASE noise reduces the stimulated emission and thus limits the maximum attainable gain. In addition, it adversely affects on the noise figure performance (Hui & O'Sullivan, 2009). ASE is produced in both forward and reverse directions, and thus the total ASE power can be expressed in equation 2.14:

$$P_{ASE}^{\pm} = n_{sp}^{\pm} hf \Delta v \, (G - 1) \tag{2.14}$$

where $P_{ASE}^{\pm}$ is the total ASE power of both directions as illustrated in equation 2.15, while $n_{sp}^{\pm}$ is the spontaneous emission factor which is defined by equation 2.16:

$$P_{ASE}^{\pm} = P_{ASE}^{+} + P_{ASE}^{-} \tag{2.15}$$

$$n_{sp} = \frac{\sigma_e \, N_2}{\sigma_e \, N_2 - \sigma_a \, N_1} \tag{2.16}$$

Pumping the EDF with sufficiently power in an open cavity (without input signal) produce ASE source spectrum. ASE light sources based on EDF are widely used due to their high output power and broad bandwidth. Practically, ASE light sources have been used in various applications, such as fiber Bragg grating (FBG) sensing, fiber optic gyroscopes, optical coherence tomography (OCT), and etc (Muniz-Cánovas et al., 2019). In addition, ASE spectrum is a measure of the available amplification band in the EDF, and thus is a helpful experimental way to optimize EDFA characteristics (Saifi, 2001).

2.7 Configurations of EDFA

EDFA could be classified according to its configuration, which affects on the gain and noise figure characteristics. There are several EDFA configurations that could be divided according to the number of stages and passes.

2.7.1 One-stage or single stage EDFA

In one-stage EDFA, the configuration includes only one active fiber (EDF) as an amplification medium. Besides, the configuration consists of one LD pump and one WDM in the case of co-directional or counter-directional pumping. However, it consists of two LDs and two WDM in the case of bi-directional pumping. The one-stage EDFA is possible to conjunct with a single-pass or double-pass schemes as shown in Figure 2.9 (a) and (b), respectively. In single pass EDFA, the input signal is passed and amplified one time within the EDF. However, in double-pass EDFA, the input signal is passed and amplified two times within the EDF (Hamzah et al., 2017). The double-pass EDFA can be obtained by using optical mirror, optical circulator, or fiber Bragg grating (FBG) to retro-pass the signal back into the gain medium.

Abass et al. (2014) compared and investigated the performance of one-stage single and double-pass EDFAs, under different input and pump signals powers. The simulation results show that the gain was improved in double-pass EDFA, using a broadband optical mirror. The gain improvement of 37.13% was obtained at input signal power of -40 dBm. On the other hand, double-pass EDFA produced a higher noise figure as compared to that of single-pass EDFA. However, the noise figure was less than 6 dB which is still in acceptable level. Yucel and Aslan (2013) improves the noise figure of the double-pass C-band EDFA, by utilizing a short length of unpumped EDF within a circulator-based loop

mirror. The unpumped EDF reduces the ASE that is routed back for a double propagation. This technique decreased the noise figure about 1.1dB to 3.34 dB. Unfortunately, this method is not useful for the EDF with high erbium ions concentration. This is due to the unpumped EDF would cause to decline the gain of the high concentration fiber.

Mishra et al. (2017) proposed a one-stage single-pass EDFA with flat gain characteristics over C-band region. The amplifier was investigated to correct the non-uniform gain for every channel of the WDM. The influence of various pumping techniques on the gain and noise figure characteristics of single-pass EDFA, was also studied. The bi-directional pumping achieved the optimum gain and acceptable noise figure, while co-directional pumping obtained the optimum noise figure.

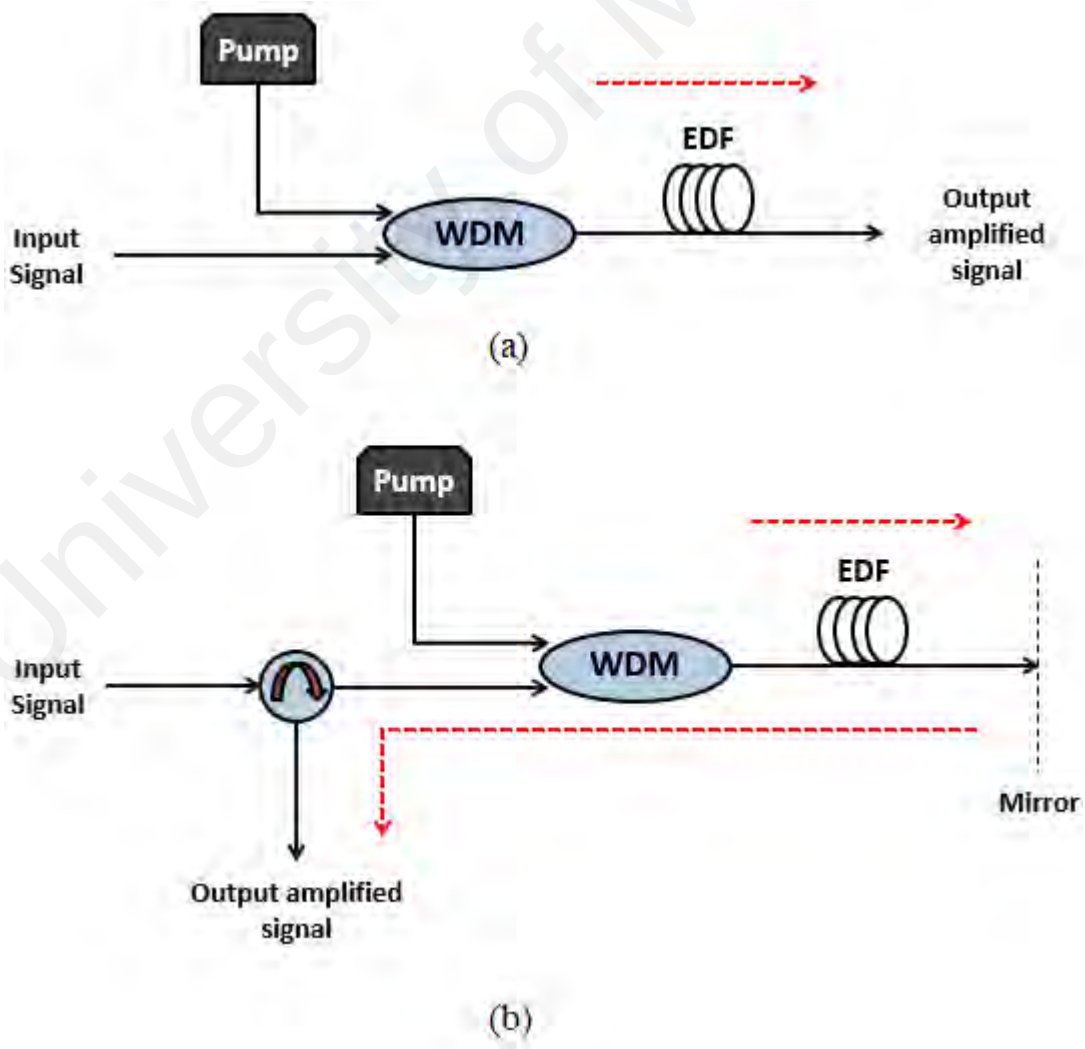

Figure 2.9: One-stage EDFA using (a) single-pass, and (b) double-pass schemes.

2.7.2 Two-stage EDFA

The two-stage EDFA is usually constructed by combining two amplifiers in series or parallel configurations, as illustrated in Figure 2.10 (a) and (b). Besides, each amplifier is possible to conjunct with a single-pass or double-pass schemes. The two-stage EDFA uses two pieces of the EDFs, where the input signals could be amplified in both EDFs, or in one of them depending on the configuration. The two-stage EDFA provides the ability to design a hybrid system that combines different active fibers. The hybrid amplifier fulfills many advantages such as; increase the gain, decrease the noise figure, broaden the bandwidth, as well as achieving a flat gain amplification characteristic. Up to date, the advance in optical fiber fabrication technology has resulted in the productions of silica-based erbium doped fiber (Si-EDF), bismuth-based erbium doped fiber (Bi-EDF), zirconia-based erbium co-doped fiber (Zr-EDF), which are effective active fibers for the two-stage hybrid applications (Hamida et al., 2015).

Gangwar et al. (2010) proposed a flat gain L-band EDFA by using two stages in series configuration. The first stage used 30 m long EDF and it was forward pumped by 980 nm LD, While, the second stage used 200 m long EDF and it was backward pumped by 1480 nm LD. At input signal power of -40 dBm, the two-stage amplifier achieved an efficient flat gain within 45 nm wavelength region. The conclusion illustrated that the two stages complement each other in such a way which the flat gain is achieved.

Cheng et al. (2012) proposed a wideband two-stage Bi-EDFA by using two sections of Bi-EDFs in parallel and series configurations. A broadband FBG was used in both the first and second stages to allow a double-pass operation. For parallel Bi-EDFA, a C/L-band splitter was used to separate the C- and L-band signals into the stages. The parallel Bi-EDFA provided a higher gain as compared to that of series Bi-EDFA. At -30 dBm input signal power, the parallel Bi-EDFA achieved average gain of 20 dB, which is

around 3 dB higher than the gain achieved by the series Bi-EDFA. The noise figures obtained were less than 10 dB within the amplification wavelength region.

Yucel and Yenilmez (2015) investigated the performance of three different configurations of two-stage EDFA, to realize a better flat gain characteristics. These configurations were two stages EDFA with uniform fiber Bragg grating (UFBG), two stages EDFA with gain filtering filter (GFF) and FBG, and two stages EDFA with optical feedback loop. A 11.5 m long was used for both EDFs in all proposed configurations. The two stages EDFA that uses GFF and FBG obtained the best flat gain results. At input signal power of -20 dBm, a flat gain of 26 dB was realized with a gain ripple of less than 1.6 dB, along the 35 nm wavelength region from 1530 to 1565 nm. As a conclusion, there are several configurations in the design of EDFA, and thus the simple design and cost are important factors that must be considered.

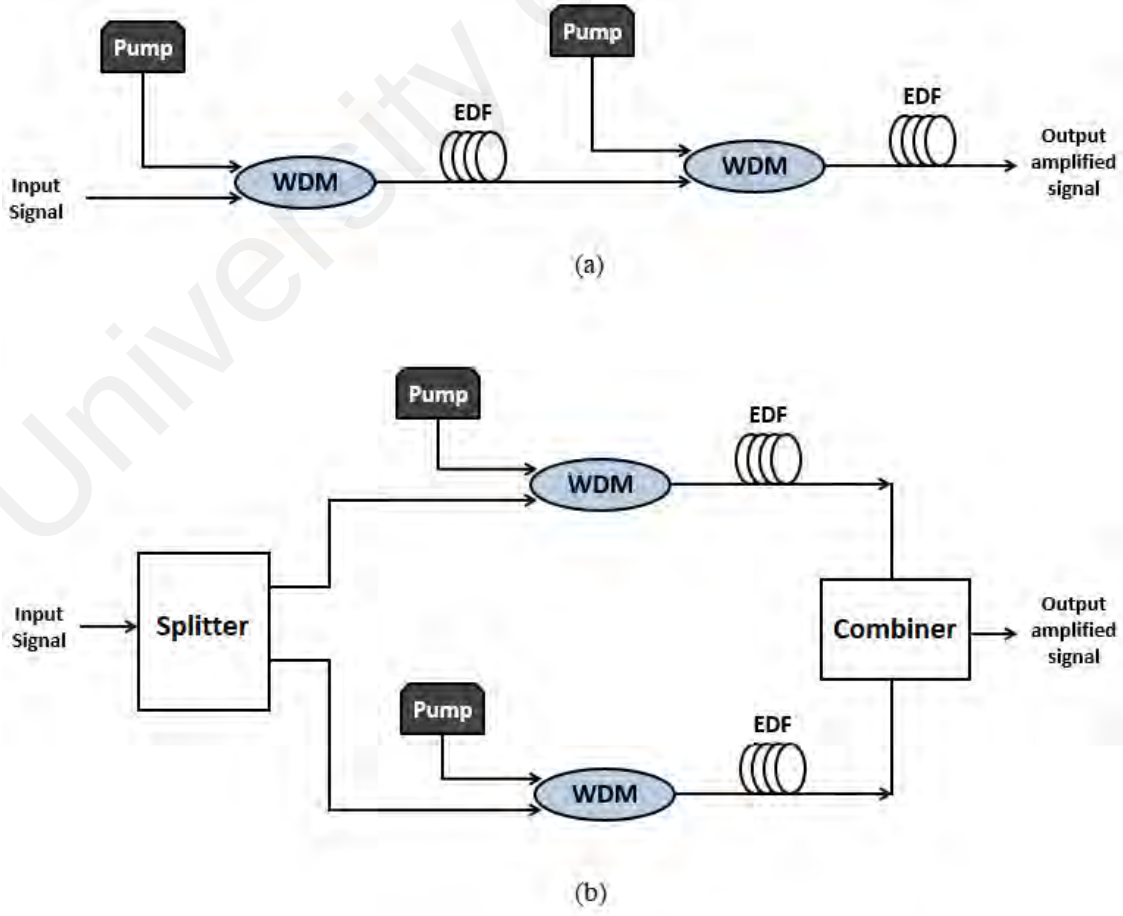

Figure 2.10: Two-stage EDFA in (a) series, and (b) parallel configurations.

2.8 Previous related works

In this section, an overview of the previous related works is presented and discussed, as illustrated in Table 2.1. The discussion is focused on the weaknesses and strengths of the previous proposed amplifiers depending on their important parameters. These parameters are; the gain, the noise figure, the amplification bandwidth, the flat gain characteristic, and the length of the active fiber.

Table 2.1: An overview of the previous related works.

Paper title	Author	Research findings	Research limitations
Wide-Band Bismuth-Based Erbium Doped Fiber Amplifier With a Flat-Gain Characteristic	Cheng et al. (2009)	A wideband bismuth-erbium doped fiber amplifier (Bi-EDFA) utilizing two stages in series structure was introduced. The wide-band operation region was obtained by using a broadband FBG as well as two sections of bismuth erbium doped fibers (Bi-EDFs). A flat gain of about 11.5 dB was achieved by using backward pumping technique.	A high noise figures were observed as com-pared to the achieved gain. The average gain was about 11.5 dB while the noise figure fluctuated from 9.5 dB to 14 dB. In addition, Bi-EDFs have a problem in splicing with standard SMFs by utilizing a standard splicing machine due to the variance in melting temperatures.
Experimental and theoretical studies on a double-pass C-band bismuth-	Harun et al. (2010)	A one stage double-pass Bi-EDFA was proposed by using 1480 nm forward pumping. At the optimum length	Within the flat gain region, the noise figure is less than 12 dB. This indicates that the noise figure was still high as

Table 2.1, continued.

Paper title	Author	Research findings	Research limitations
based erbium-doped fiber amplifier		of 49 cm long Bi-EDF, a flat gain of 14.5 dB was realized with a gain ripple of less than 1.2 dB, along wavelength region from 1530 to 1565 nm.	compared to achieved gain, which was 14 .5 dB. In addition, this amplifier covered only the C-band wavelength region.
Hybrid Flat Gain C-band Optical Amplifier with Zr-based Erbium-doped Fiber and Semiconductor Optical Amplifier	Huri et al. (2011)	A flat gain two stages optical amplifier was proposed, utilizing a hybrid stages of semiconductor optical amplifier (SOA) and Zr-EDF. At low input signal power, a flat gain of 28 dB was realized with a gain ripple of less than 4 dB, along the wavelength region from 1530 to 1560 nm.	A high gain ripple of 4 dB was observed in the flat gain region. In addition, this amplifier works only in the C-band region although its complex design. Besides, the amplifier used long length of Zr-EDF, which is 3 m.
Dual-stage L-band erbium-doped fiber amplifier with distributed pumping from single pump laser	Yusoff et al. (2012)	A two stages L-band EDFA was investigated with flat gain of 17 dB, and noise figure of less than 6.7 dB. Compared to one stage EDFA at same EDF length and pump power, the two stages EDFA achieved	This amplifier has two drawbacks which are; the high pump power required and the long EDF. The pump power and the total EDF length were 600 mW and 27 m, respectively. Besides, this amplifier

Table 2.1, continued.

Paper title	Author	Research findings	Research limitations
		a higher gain and lower noise figure. 1497 nm Raman pump power was used in this amplifier.	works only in the L-band region.
Comparative Study on Single- and Double-Pass Configurations for Serial Dual-Stage High Concentration EDFA	Latiff et al. (2013)	A wideband optical amplifier using two pieces of silica erbium doped fibers (Si-EDFs) was proposed. Two series stages were used in conjunction with single and double-pass configurations. The better performance was observed with series double-pass amplifier. At input signal power of -30 dBm, a flat gain of 22 dB was realized with a gain ripple of less than 3 dB.	The total length of the Si-EDFs used were 10.5 m which are long. Besides, at low input signal power, a high noise figures were observed as compared to the achieved gain. The average gain was about 11.5 dB while the noise figure fluctuated from 8 dB to 12 dB. The series single-pass EDFA achieved a flat gain only in the L-band region.
An optical amplifier having 5 cm long silica clad erbium doped phosphate glass fiber fabricated by	Goel et al. (2014)	An optical amplifier was introduced using only 5 cm of the new fabricated erbium - doped phosphate glass fiber (EDPF). A double pass configuration was used with backward	The gain was very low. The maximum gain of 5 dB was observed at 1535 nm wavelength. Further investigations aimed at improving the gain are required.

Table 2.1, continued.

Paper title	Author	Research findings	Research limitations
‘‘core-suction’’ technique		pumping technique. A wide gain spectrum was observed in this amplifier.	
Enhanced Erbium Zirconia–Yttria Aluminum Co Doped Fiber Amplifier	Paul et al. (2015)	A flat gain double-pass EDFA was proposed by using an enhanced Zr-EDF. The Comparison among three different lengths of enhanced Zr-EDF illustrated that the 1 m long was the optimum length. A higher gain and lower noise figure were observed with enhance Zr-EDFA as compared to that of conventional Zr-EDFA.	This amplifier could not achieve a flat gain for L-band region. Besides, at high input signal power of -10 dBm, the gain ripple and noise figure were high, within the C-band wavelength region.
Flat-gain wide-band erbium doped fiber amplifier with hybrid gain medium	Hamida et al. (2016)	An incorporation of Zr-EDF with Si-EDF were used as a hybrid active fiber to achieve a wideband EDFA. At high input signal power , a flat gain of 15 dB was realized with a gain ripple of less than 1 dB. Noise figure fluctuated from 6.2 dB to 10.8 dB.	The total length of the EDFs used were 11 m which is very long. Besides, the series amplifier could not achieve a flat gain over the wideband operation region.

Table 2.1, continued.

Paper title	Author	Research findings	Research limitations
Performance comparison of enhanced Erbium-Zirconia-Yttria-Aluminum co-doped conventional erbium-doped fiber amplifiers	Markom et al. (2017)	A flat-gain single and double pass optical amplifier was proposed using a Zr-EDF as the gain medium. The performance of the proposed amplifier was compared with the conventional Si-EDFA. A better gain and noise figure characteristics were observed with the Zr-EDFA.	This amplifier used 1 m long of Zr-EDF to achieve a flat gain only at C-band region. This length is still long for C-band region as compared to that of previous active fibers, such as, Bi-EDF.
Flat-gain and Wideband EDFA by using Dual Stage Amplifier Technique	Hamzah et al. (2018)	A wideband and flat gain amplification of two stages EDFA was investigated under different EDF lengths and pump powers. Compared to one stage EDFA, the two stages EDFA obtained a better performance for all experiments. At 0 dBm of input signal power and 100 mW of pump power, a flat gain of about 15 dB was realized throughout a wideband region.	The total length of the EDFs used were 22 m which is very long. On the other hand, this study focused only on the gain characteristic where the noise figure was ignored.

Table 2.1, continued.

Paper title	Author	Research findings	Research limitations
Optical amplification performance of erbium doped zirconia-yttria-alumina-baria silica fiber	Duarte et al. (2019)	An optical amplifier was proposed using a new fabricated erbium - doped zirconia-yttria-alumina - baria silica fiber (ZYAB-EDF). At input signal power of -20 dBm, a flat gain of 25 dB was realized with a gain ripple of less than 3 dB, along the wavelength region from 1525 to 1565 nm.	This amplifier used 1 m long of ZYAB -EDF to achieve a flat gain only at C-band region. This length is still long for C-band region as compared to Bi-EDF. Further investigations and studies on this fiber is required.

2.9 Summary

In this chapter, the basic working principle of EDFA including the theory, the absorption and emission processes, and the population inversion phenomenon have been explained in detail. The conventional EDFA mainly consists of EDF, pump power, and WSC. It was found that the optical amplification in EDF depends on the spontaneous and stimulated emissions processes into the EDF. In EDFA, two pumping wavelengths are commonly used to excite Er^{3+} ions in $^4I_{15/2}$ in order to move to $^4I_{11/2}$ and $^4I_{13/2}$ levels, which are 980 nm and 1480 nm. Pumping Er^{3+} ions at 980 nm wavelength produces three energy levels. However, the 1480 nm pumping provides only two energy levels. There are three techniques to pump EDF, which are classified based on the direction. These techniques are: co-directional pumping, counter-directional pumping, and bi-directional pumping.

EDFA could be classified according to its configuration, which affects on the amplification characteristics such as; the gain, noise figure, flat gain and ASE noise. There are several EDFA configurations, which could be divided according to the number of stages and passes. Finally, the previous related works of EDFA have been successfully described and discussed based on their weaknesses and strengths.

CHAPTER 3: HAFNIA–BISMUTH ERBIUM CO–DOPED FIBER AMPLIFIER WITH FLAT-GAIN CHARACTERISTIC

3.1 Introduction

In the telecommunications field, there is an ever-increasing demand for higher levels of integration and for smaller fiber-optic equipment and components (Xiao et al., 2018). For instance, optical amplifiers and fiber laser devices are desirable to use a gain medium with a large active ions concentration to shorten the length of the active fiber and to reduce the size and cost of the device (Wang et al., 2018; Paul et al., 2015). One of the disadvantages of current standard erbium doped fiber amplifiers (EDFAs) is their relatively limited capacity for producing large gain per unit length. This leads to gain devices composed of individually fiber pigtailed components typically employing long fiber lengths (10 – 50 m) requiring fiber wraps with bend radii of more than 30 mm. This produces amplifier or fiber laser architectures that are difficult to miniaturize, and incompatible with trends towards: automated assembly of small form factor modules, multi-channel devices, and integrated hybrid optics (Dhar et al., 2012).

To shorten the length of the gain medium, the active fiber needs to be doped with so much higher erbium ion concentration. However, a high concentration of erbium ions may result in pair-induced quenching (PIQ) effects, which potentially degrades the pump power conversion efficiency (PCE) and rise the noise figure for EDFA (Lim et al., 2012). For increasing the limit of erbium doping concentration while maintaining the amplification performance, various glass hosts and co-doped materials have been proposed and investigated (Duarte et al., 2019; Goel et al., 2014). Up to date, the advance in optical fiber fabrication technology has resulted in the productions of bismuth-based

erbium doped fiber (Bi-EDF) (Firstov et al., 2017) and zirconia-based erbium co-doped fiber (Zr-EDF) (Markom et al., 2017) which have an erbium ion concentration of 6300 and 4000 wt. ppm, respectively. Both fibers act as an effective gain medium for realizing the compact optical amplifier and laser devices. However, Bi-EDF cannot be spliced with a standard single mode fiber (SMF) using the standard splicing machine. This is attributed to the difference in their melting temperatures (Harun et al., 2011). The Bi-EDF has the Bi content of more than 50% and thus higher than Si content, which gives rise to very lower melting temperature than that of SMF where Si content is more than 96%. It was reported that the glass transition temperature of the Bi_2O_3-SiO_2 system where the Bi content above 60% is below 450 °C which becomes very much lower than that of SiO_2 based glass (George et al., 1999). On the other hand, Zr-EDF amplifier (Zr-EDFA) needs longer length of the gain medium to achieve a comparable performance with Bi-EDF amplifier (Bi-EDFA) (Paul et al., 2010).

Recently, hafnia-bismuth erbium co-doped fiber (HB-EDF) that can be highly doped with 12,500 wt. ppm of erbium ions concentration, was introduced (Kir'yanov et al., 2017). By combining Hafnium and Aluminum ions in the glass host, ion clustering effect is minimized and thus a high erbium ion concentration can be introduced. In addition, the HB-EDF can be easily spliced with a standard SMF, due to the similarity in their melting temperature. In HB-EDF, the Bi content is very low around 0.035 wt% with Si content of more than 90 wt%, which almost match with the silica content of a standard SMF fiber. Therefore, the melting temperature of the doping host of HB-EDF becomes almost similar to the melting temperature of SMF. Depending to these features, the use of HB-EDF sounds attractive to be investigated in optical amplifier devices.

In this chapter, a compact optical fiber amplifier with a flat-gain characteristic at the C-band region is demonstrated, by using a short length of the new HB-EDF as the gain medium. Firstly, the HB-EDF fabrication and specification are highlighted. The

performance of the new HB-EDF amplifier (HB-EDFA) is investigated for both single and double pass configurations, using various lengths of the HB-EDFs against various wavelengths and pump powers to determine the best of the design. The performance comparison between 980 nm and 1480 nm wavelengths pumping for double pass HB-EDFA is also investigated. The amplification performance of the HB-EDFA is compared with the previous EDFAs, such as the commercial silica erbium doped fiber amplifier (Si-EDFA) and the conventional Zr-EDFA. Finally, the performances of single and double pass HB-EDFA are investigated using home-made multi-input wavelengths source to examine the flat gain characteristics.

3.2 HB-EDF fabrication and characterization

The HB-EDF was fabricated through a standard two steps process; making of optical preform followed by fiber drawing. A fiber preform of hafnium-bismuth-erbium co-doped yttria-aluminum-silica glass was fabricated through deposition of porous silica layer at around 1500 °C temperature by using the modified chemical vapor deposition (MCVD) process followed by the solution doping (SD) technique. Suitable strength of $Al(NO_3)_3 \cdot 9H_2O$, $HfCl_3$, $Bi(NO_3)_3 \cdot xH_2O$, $Y(NO_3)_3 \cdot 6H_2O$ and $ErCl_3 \cdot xH_2O$ were used for soaking of the porous layer for a period of about one hour in the SD process, to incorporate all the co-dopants such as Al_2O_3, HfO_2, Bi_2O_3, Y_2O_3 and Er_2O_3. All the halide and nitrate salts retain into porous layer after draining out the solution. The core layer was dried with flow of N_2 gas at room temperature and then dried thermally, by heating up to 800–900 °C with flow of mixture of oxygen (O_2) and helium (He) gases, for oxidizing the salts. Sintering of the porous layer containing such oxides was done by gradually increasing temperature from 1300 to 1900 °C, to form a transparent glass. The glass was converted to a solid preform by collapsing stages where it was over-cladded with a thick silica tube

to reduce the core diameter. The final fiber was drawn from the preform and coated with acrylate resin by a conventional way using a fiber drawing tower, at ~2000 °C.

The doping level within the core region of the fabricated fiber was measured by electron probe micro analysis (EPMA) using an JEOL EPMA instrument. For this, around 1-2 mm of the fiber sample was ground and polished on both sides. Finally, EPMA of the polished fiber was carried out with the maximum spatial resolution of 1 μm after applying a thin graphite coating layer. Figure 3.1 shows the elemental distribution curve of different dopants along the diameter of the fiber core. It is found that the fiber core glass contains 6.0 wt% Al_2O_3, 1.23 wt% Er_2O_3, 2.2 wt% HfO_2 and 0.035 wt% Bi_2O_3. Figure 3.2 (a) shows the fiber cross sectional view of the fabricated fiber. As shown in the figure, the core and cladding diameters of the fiber are 3.71 μm and 123.94 μm, respectively. The refractive index (RI) profile of HB-EDF that measured by a fiber analyzer is shown in Figure 3.2 (b). Based on the RI profile, the numerical aperture (NA) is calculated to be 0.21. Figure 3.2 (c) shows the optical loss curve of the HB-EDF, which was obtained by cut-back method measurement using Bentham spectral attenuation setup. The absorption losses at 980 nm and 1530 nm are found to be 100 dB/m and 270 dB/m respectively.

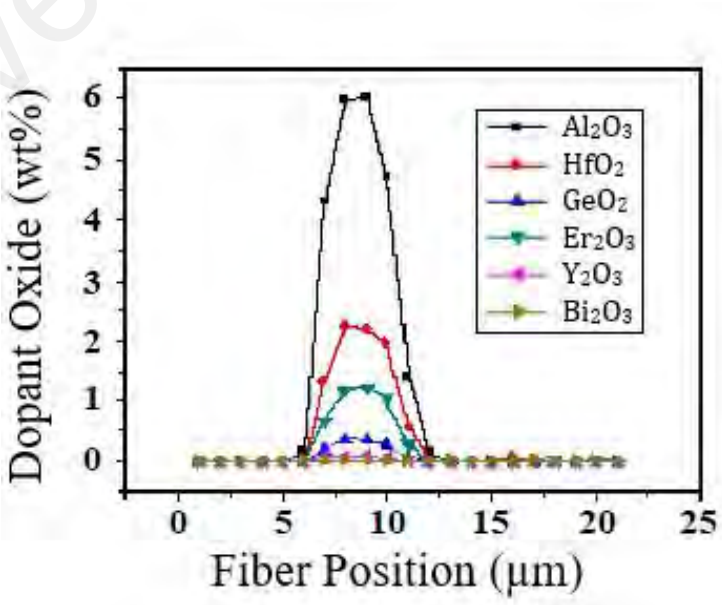

Figure 3.1: Distributions of elements constituting core-glass of the HB-EDF.

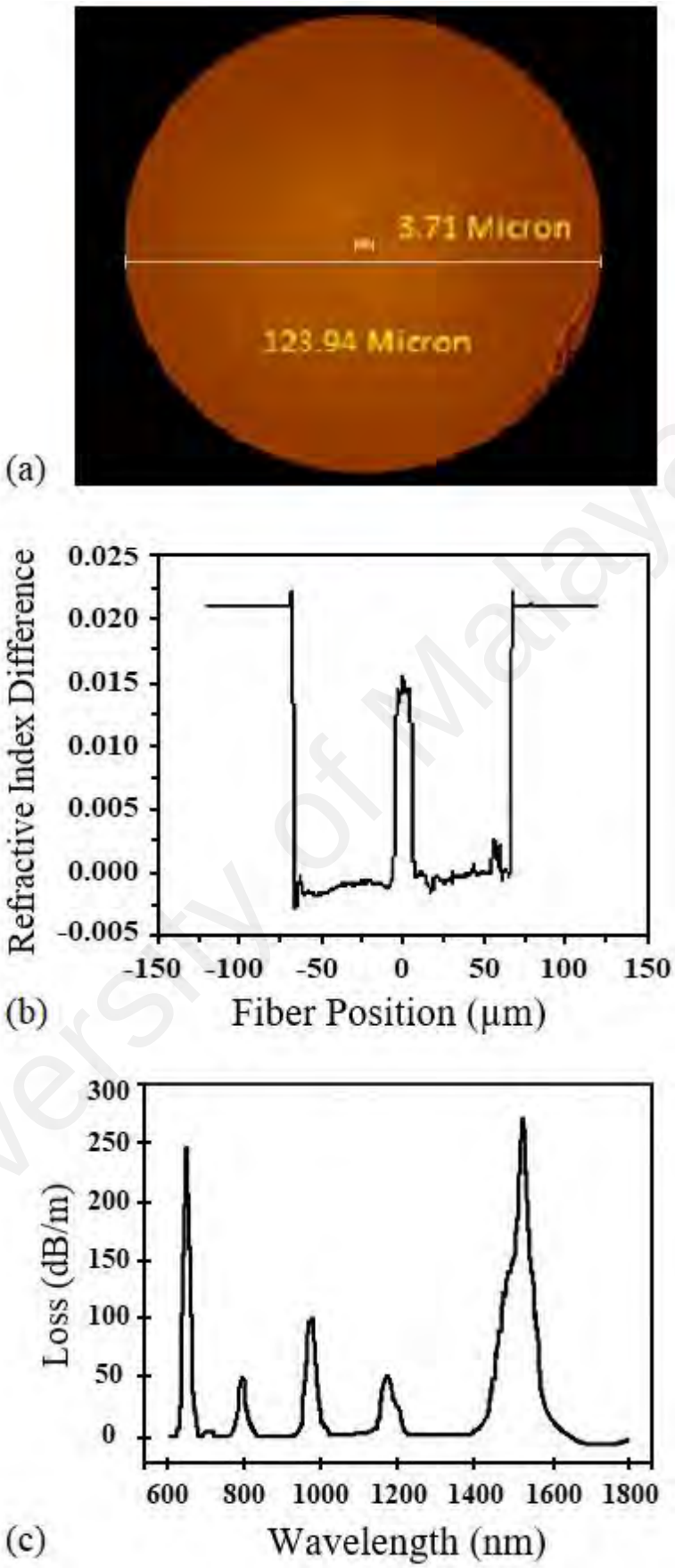

Figure 3.2: HB-EDF characteristics: (a) Microscopic view, (b) Refractive index profile, and (c) Absorption loss curve.

3.3 Amplification performance

In order to gauge the behavior of the HB-EDF, the amplification characteristics and performance of the fiber was evaluated by measuring the signal gain and noise figure. The amplification characteristics of the HB-EDF was investigated at low and high input signal powers of -30 dBm and -10 dBm, respectively. A tunable laser source (TLS) was used as a signal source while a programmable optical attenuator (POA) was used to get the exact input signal power to the amplifier. An optical spectrum analyzer (OSA) was utilized to test the gain (G) and noise figure (NF) characteristics, using the following equations;

$$G\ (dB) = \ 10\log_{10}\left(\frac{P_{out} - P_{ASE}}{P_{in}}\right) \tag{3.1}$$

$$NF(dB) = \ 10\log_{10}\left(\frac{1}{G} + \frac{P_{ASE}}{h\nu\Delta\nu G}\right) \tag{3.2}$$

where P_{in}, P_{out} and P_{ASE} are the input signal power, output signal power and the ASE noise power, respectively. hν is the photon energy while Δν is the OSA's resolution.

3.3.1 Single pass HB-EDFA

Firstly, the amplified spontaneous emission (ASE) spectrum of the new HB-EDF is investigated at three different doped fiber lengths, 0.2 m, 0.5 m and 1 m as the gain medium. Figure 3.3 shows the ASE spectrum of the HB-EDFs that are forward pumped with 980 nm wavelength at maximum power of 170 mW. It is shown that the ASE power is improved as the length is increased from 0.2 to 0.5 m. The ASE level of 0.5 m long HB-EDF is around 10 dB higher as compared to that of 0.2 m long HB-EDF. This is

attributed to the number of Erbium ions in the fiber, which increases with the length. The more ions enhance the population inversion and thus increases the spontaneous and stimulated emission in the active fiber. However, as the HB-EDF is increased above 0.5 m, the population inversion starts to be saturated. The 1550 nm photons are absorbed by the Erbium ions to emit in longer wavelength. Therefore, at 1 m long HB-EDF, the peak of ASE spectrum shifted to the longer wavelength at around 1565 nm instead of 1530 nm.

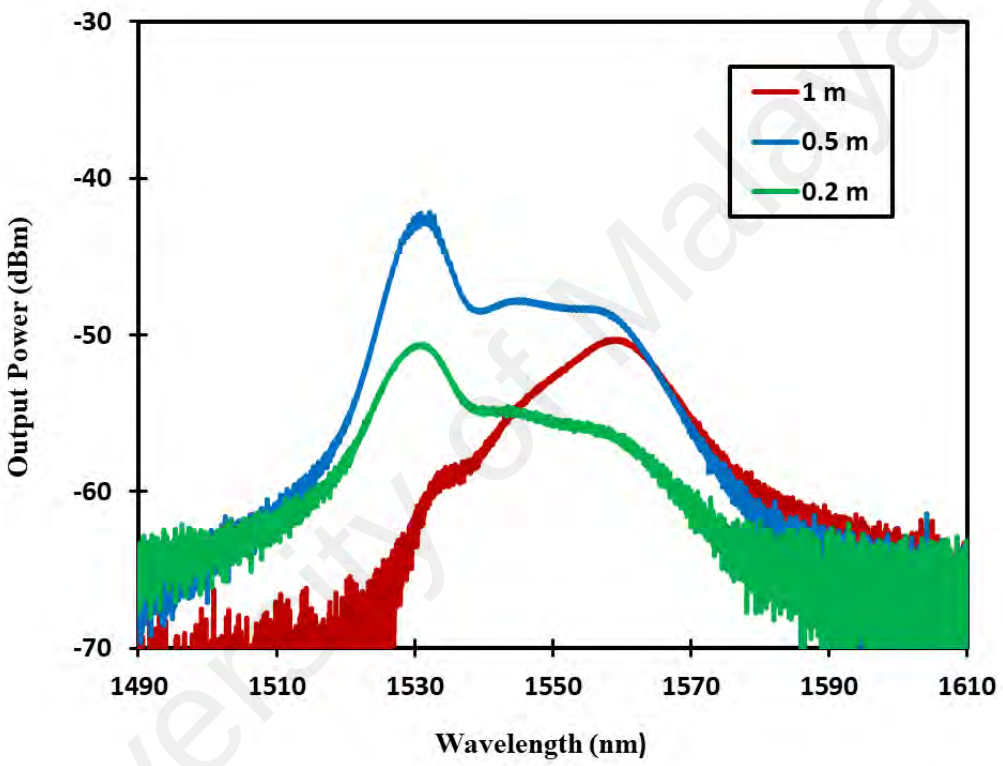

Figure 3.3: ASE spectrum from the HB-EDFs with 980 nm pumping at 170 mW.

The amplification performance of the HB-EDF is then investigated based on a single pass scheme as shown in Figure 3.4. In the experiment, the HB-EDF is forward pumped by a 980 nm laser diode with the maximum power of 170 mW. The 980 nm pump power is launched into the active HB-EDF via a 980/1550 nm wavelength division multiplexer (WDM) coupler. The HB-EDF is pumped by a 980 nm laser diode to create

a population inversion between the ground state ($^4I_{15/2}$) and metastable state ($^4I_{13/2}$) of Er^{3+}. The signal amplification is obtained as a signal passes through the core fiber doped with erbium ion (Er^{+3}) under the effect of pump, absorption, stimulated, and spontaneous emission. The stimulated emission is occurred exactly at the same wavelength of the input signal but the spontaneous is occurred at wide range of wavelengths.

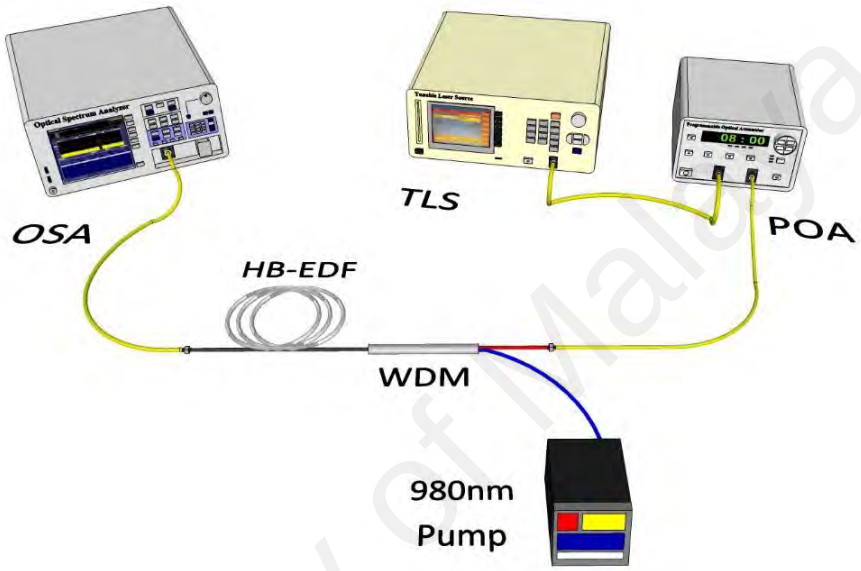

Figure 3.4: Experimental setup of the single pass HB-EDFA.

Figure 3.5 shows the gain and noise figure spectra of the single pass HB-EDFA at three different gain medium lengths, for input signal power of -30 dBm. It is found that the gain of the amplifier peaks at 1530 nm with the use of both 0.5 m and 0.2 m long active HB-EDF. However, at 1 m long HB-EDF, the gain spectrum peak shifts to a longer wavelength of 1560 nm. This indicates that the optimum length of the amplifier operation in the C-band region is around 0.5 m. As the length of the gain medium increases, the operating wavelength shifts to the L-band region due to a quasi-two-level absorption effect. At 0.5 m long of HB-EDF, the amplifier's gain varies from 17 to 22.2 dB within a wavelength range from 1525 to 1565 nm. The corresponding noise figures vary from 3.1

to 4.9 dB within the same wavelength region. On the other hand, a significant gain spectrum is also obtained at short length of 0.2 m long HB-EDF. For 0.2 m long HB-EDF, a flat gain of 11.9 dB is realized with a gain ripple of less than 1.3 dB, along the 35 nm wavelength region from 1525 to 1560 nm. Within the flat gain region, the noise figure is less than 5.3 dB.

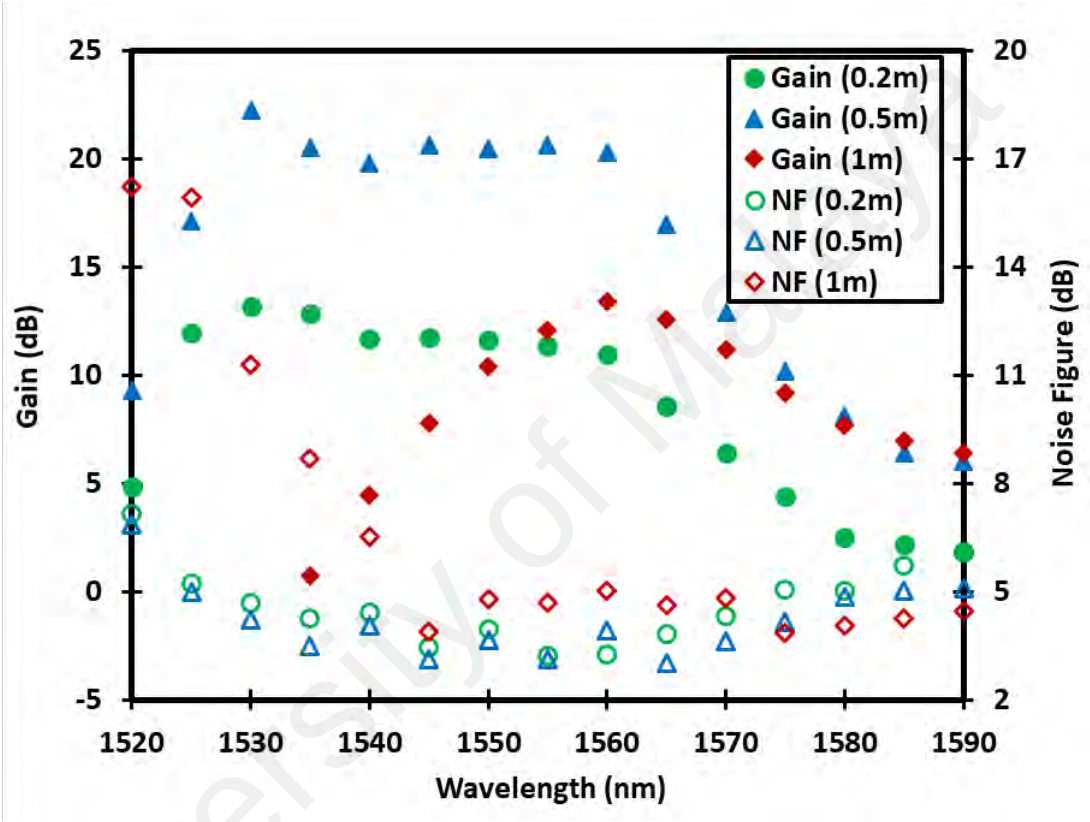

Figure 3.5: Gain and noise figure spectra of the single pass HB-EDFA at input signal power of -30 dBm.

Figure 3.6 shows the gain and noise figure spectra of the single pass HB-EDFA, for input signal power of -10 dBm. At the optimum length of 0.5 m long HB-EDF, a flat gain of 12.4 dB is realized with a gain ripple of less than 1.4 dB, along the 45 nm wavelength region from 1525 to 1570 nm. Within the flat gain region, the noise figure is less than 4.6 dB. Higher flat gain is observed in low input signal power of -30 dBm as compared to

that in high input signal power of -10 dBm. This is due to the influence of the population inversion which is larger at low input signals powers, whereas the high input signals powers suppress the population inversion and hence reduce the attainable gain.

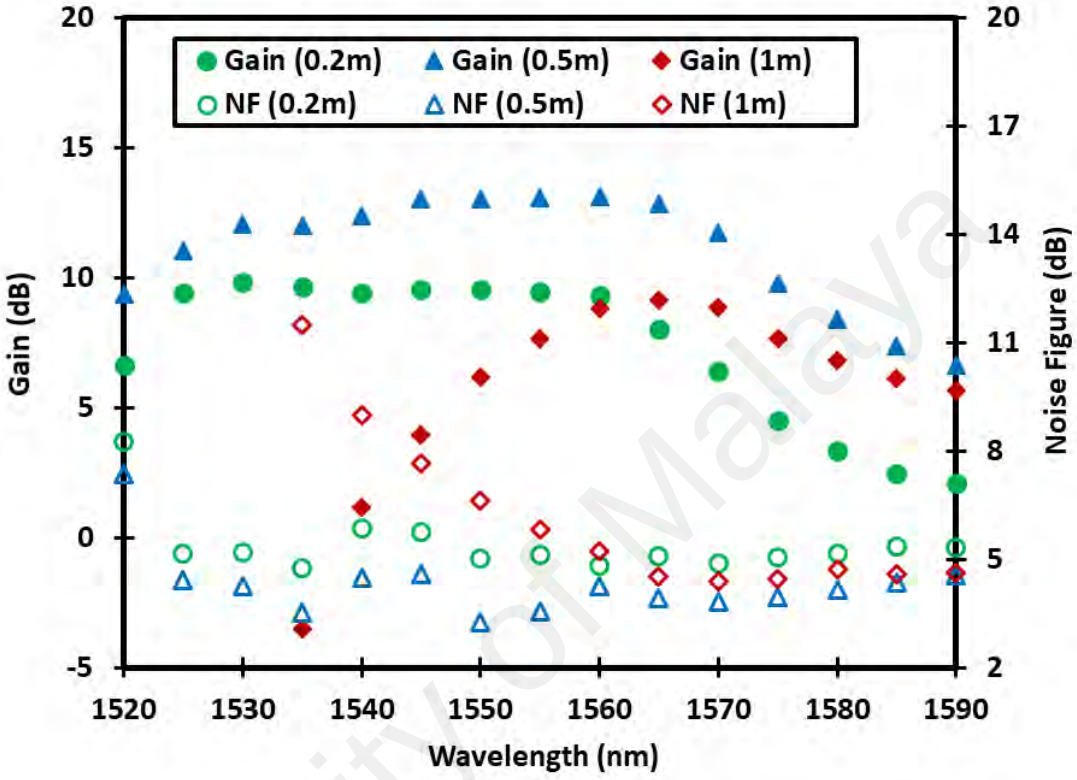

Figure 3.6: Gain and noise figure spectra of the single pass HB-EDFA at input signal power of -10 dBm.

The gain and noise figure characteristics of the single pass HB-EDFA against different pump powers are also measured for both input signal powers of -30 dBm and -10 dBm, as depicted in Figure 3.7 and Figure 3.8, respectively. In the experiment, the input signal wavelength is adjusted at 1550 nm and the 980 nm pump power is varied from 20 to 170 mW. As shown in the Figures, the gains increase as the pump power increases while the noise figure is decreased. At low input signal power of -30 dBm, the saturation gain occurs when the pump power exceeds 140 mW for 0.2 m long HB-EDF.

However, the 0.5 m long HB-EDF realizes the saturation gain when the pump power exceeds 150 mW. This is attributed to the population inversion, which requires more pump power for longer EDF.

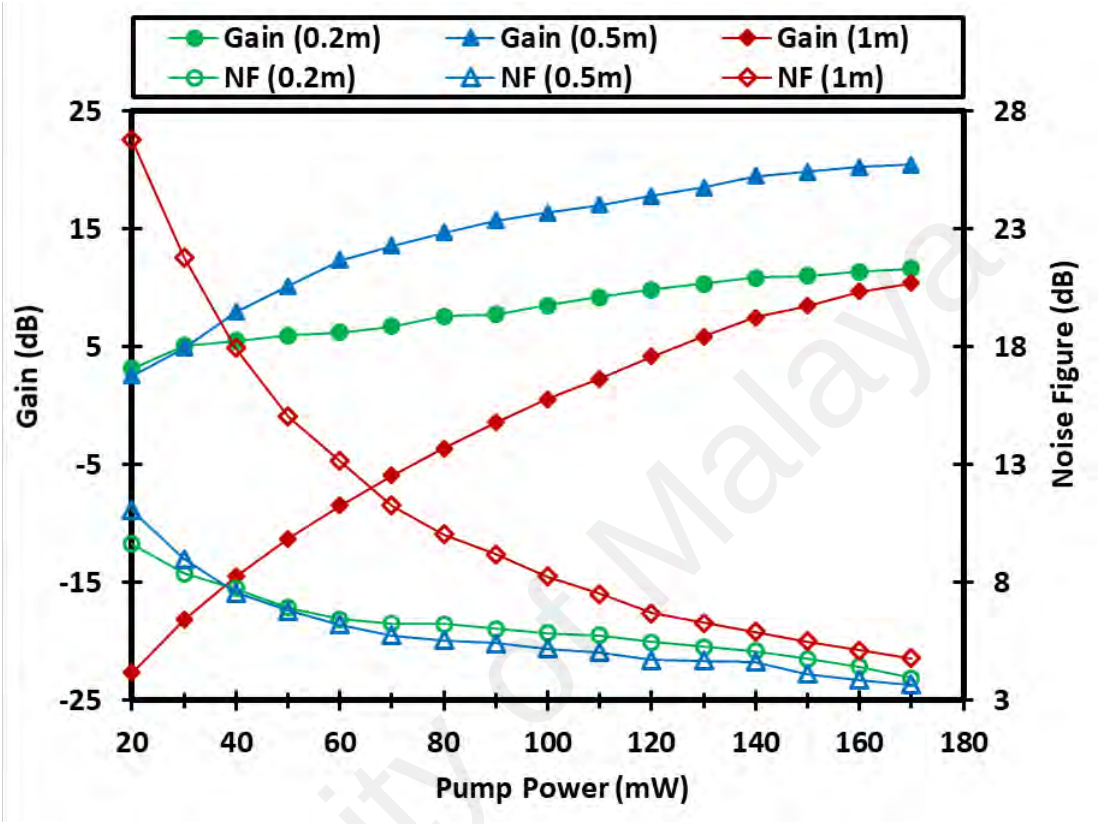

Figure 3.7: The performance of single pass HB-EDFA against various pump powers for input signal power of -30 dBm.

At high input signal power of -10 dBm, the saturation gain occurs when the pump power exceeds 120 mW and 140 mW for 0.2 m long HB-EDF and 0.5 m long HB-EDF, respectively. It can be concluded that the amplifier requires high pump power for high input signal power as compared to that for low input signal power, to realize the saturation status. This indicates that the population inversion is smaller at higher input signal powers. On the other hand, 1 m long HB-EDF requires more than 170 mW of the pump power to get the saturation effect. This is due to the length of HB-EDF which is long, and it is not convenient for shorter wavelength region.

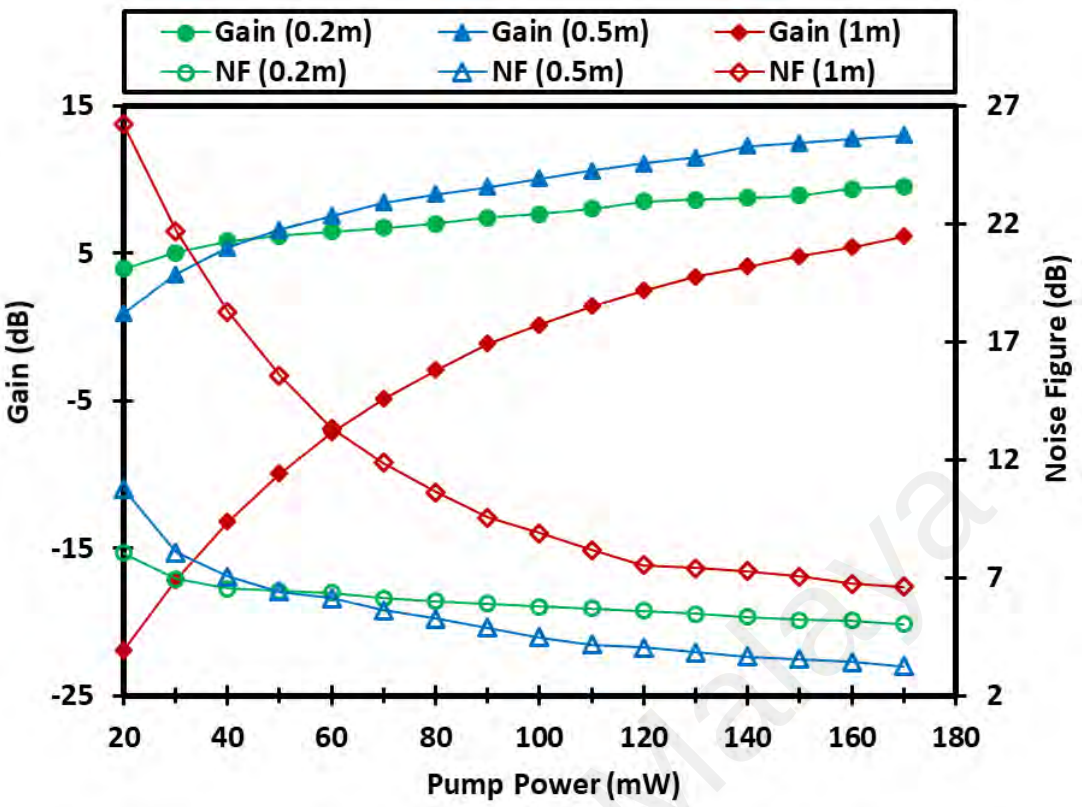

Figure 3.8: The performance of single pass HB-EDFA against various pump powers for input signal power of -10 dBm.

3.3.2 Double pass HB-EDFA

The double pass HB-EDFA setup is shown in Figure 3.9. A 980 nm laser diode is used to forward pumped the HB-EDF via a 980/1550 nm WDM coupler. Two optical circulators are utilized at the input and output ports of the amplifier to permit double propagation of the signal in the erbium fiber. At the input port, an optical circulator is utilized to deliver the input signal into the WDM, and to extract the double amplified signal to the OSA. At the output port, another optical circulator is utilized as a broadband loop mirror for reflecting the amplified signal into the erbium fiber. The broadband loop mirror is constructed by joining port 3 with port 1 so that the signal from port 2 is routed

back into the same port. The performance of double pass HB-EDFA is also investigated at three different doped fiber lengths, 0.2 m, 0.5 m and 1 m.

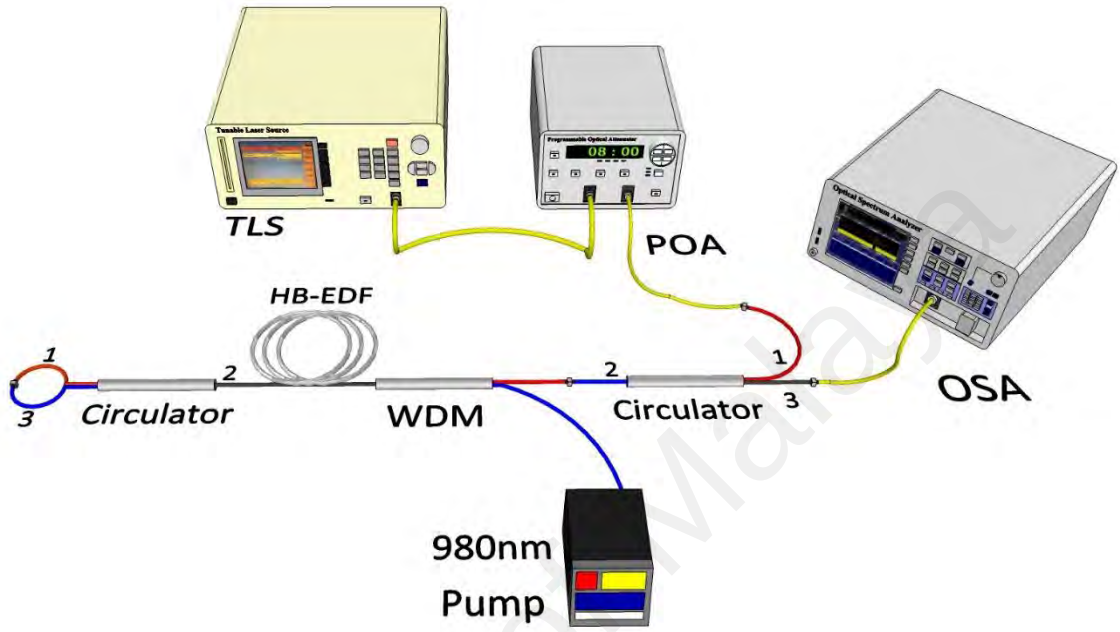

Figure 3.9: Experimental setup of the double pass HB-EDFA.

Figure 3.10 and Figure 3.11 represent the spectra of the gain and the noise figure of the double pass HB-EDFA for the input signal powers of -30 dBm and -10 dBm, respectively. These measured results are obtained under the maximum pumping power of 170 mW. At the input signal power of -30 dBm, it is found that the amplifier configured with 0.5 m long HB-EDF obtains the best amplification performance especially in the C-band region. At 0.5 m long HB-EDF, a flat gain of 30.8 dB is realized with a gain ripple of less than 1.3 dB, along the 30 nm wavelength region from 1530 to 1560 nm. Within the flat gain region, the noise figure is less than 7 dB. However, 0.2 m long HB-EDF also achieved a flat gain spectrum but with lower values as compared to that of 0.5 m long HB-EDF. At 0.2 m long HB-EDF, a flat gain of 19.7 dB is realized with a gain ripple of

less than 1.5 dB, along the 30 nm wavelength region from 1525 to 1555 nm. Within the flat gain region, the noise figure is less than 7.6 dB.

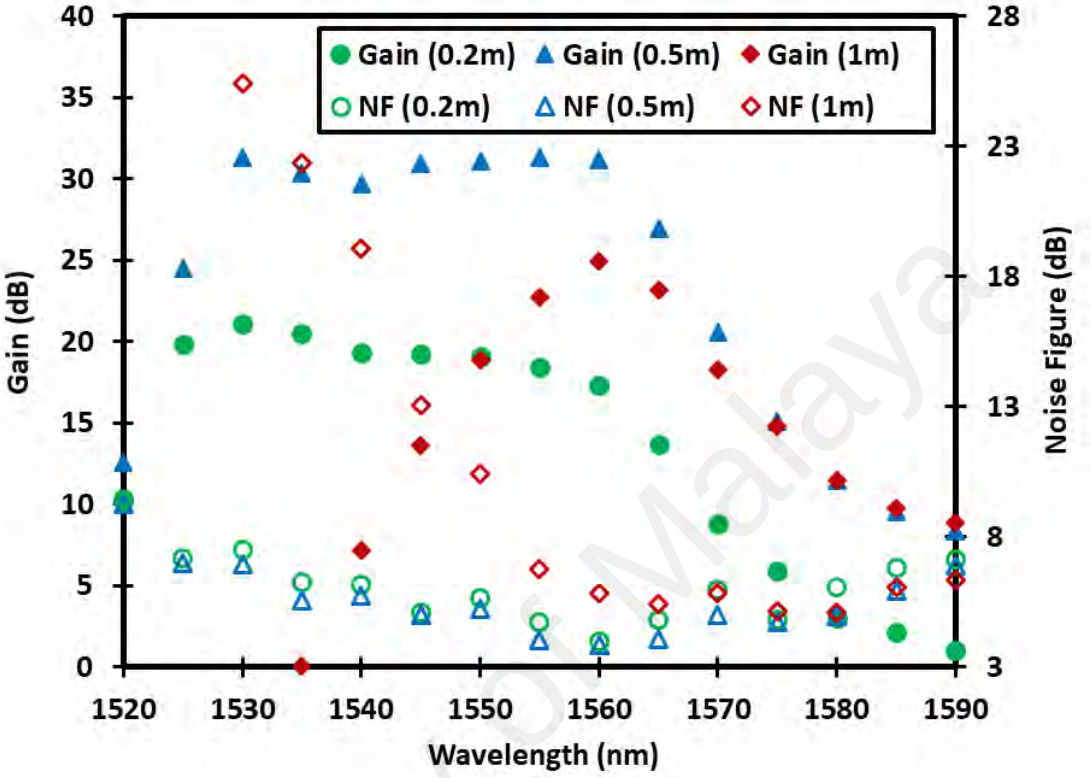

Figure 3.10: Gain and noise figure spectra of the double pass HB-EDFA at input signal power of -30 dBm.

For input signal power of -10 dBm, it is found that both 0.2 m long HB-EDF and 0.5 m HB-EDF achieved an efficient amplification performance with flat gain characteristics at C-band wavelengths region. At 0.5 m long HB-EDF, a flat gain of 15.9 dB is realized with a gain ripple of less than 1.4 dB, along the 45 nm wavelength region from 1525 to 1570 nm. Within the flat gain region, the noise figure is less than 8.1 dB. Whereas at 0.2 m long HB-EDF, a flat gain of 11.8 dB is realized with a gain ripple of less than 1.1 dB, along the 40 nm wavelength region from 1525 to 1565 nm. Within the flat gain region, the noise figure is less than 8.8 dB. On the other hand, at the 1 m long

HB-EDF, the gain spectrum shifts to the L-band region but with lower values. This is attributed to insufficient pump power to support population inversion with a longer gain medium.

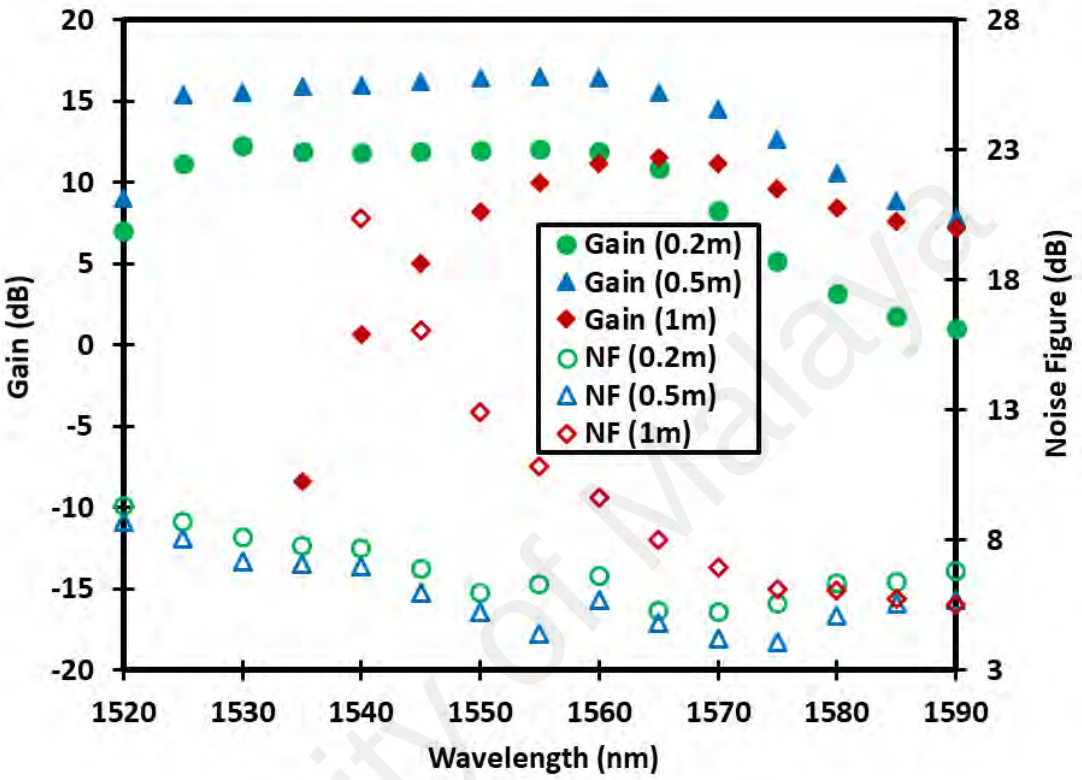

Figure 3.11: Gain and noise figure spectra of the double pass HB-EDFA at input signal power of -10 dBm.

The gain and noise figure characteristics of the double pass HB-EDFA against different pump powers are measured, at both input signal powers of -30 dBm and -10 dBm, as depicted in Figures 3.12 and 3.13, respectively. In the experiment, the input signal wavelength is adjusted at 1550 nm and the 980 nm pump power is varied from 20 to 170 mW. As shown in the Figures, the gain increases as the pump power increases while the noise figure is decreased. At low input signal power of -30 dBm, the saturation gain occurs when the pump power exceeds 150 mW for 0.2 m long HB-EDF. However,

the 0.5 m long HB-EDF realizes the saturation gain when the pump power exceeds 160 mW. This is attributed to the population inversion, which requires more pump power for longer EDF. At high input signal power of -10 dBm, the saturation gain occurs when the pump power exceeds 130 mW and 150 mW for 0.2 m long HB-EDF and 0.5 m long HB-EDF, respectively. On the other hand, 1 m long HB-EDF requires more than 170 mW of the pump power to get the saturation effect. This is due to the length of HB-EDF which is long, and it is not convenient for shorter wavelength region.

It can be inferred that double pass HB-EDFA requires more pump power to realize the saturation status as compared to that for single pass HB-EDFA. This is owing to the 1550 nm wavelength signal which is absorbed at the output portion of the HB-EDF, for the double pass amplifier when the pump power is low.

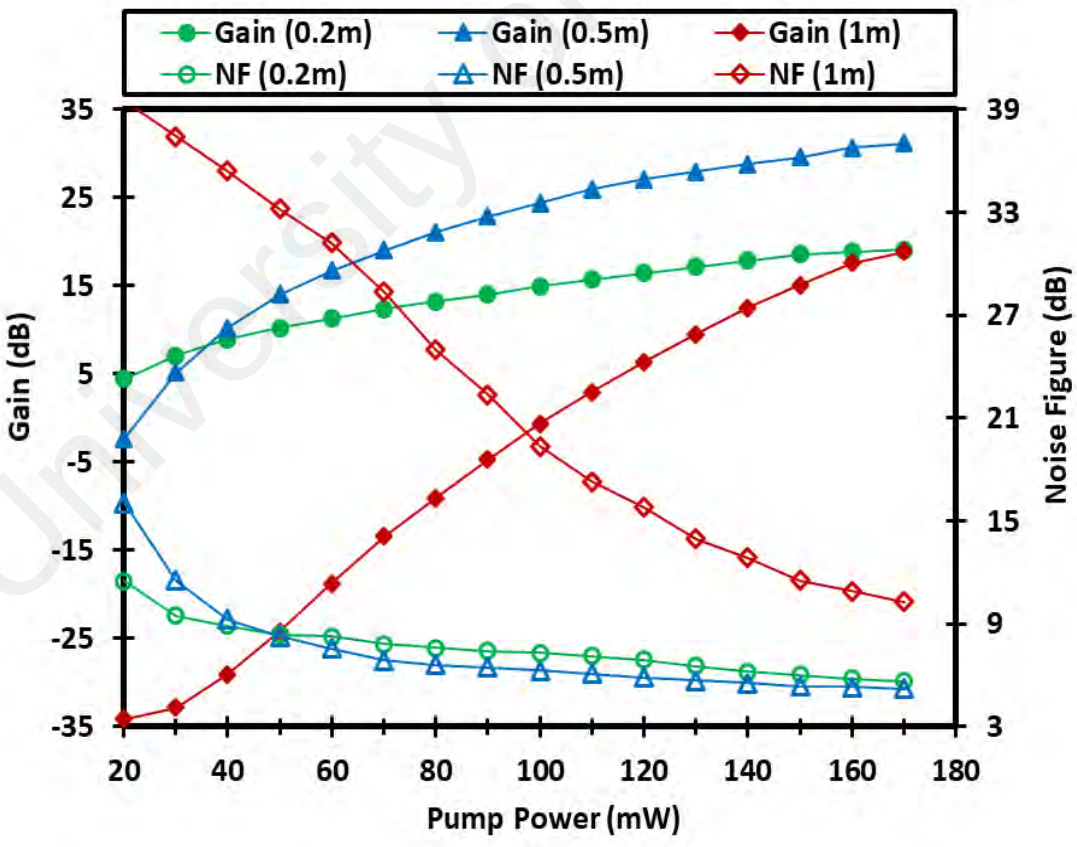

Figure 3.12: The performance of double pass HB-EDFA against various pump powers for input signal power of -30 dBm.

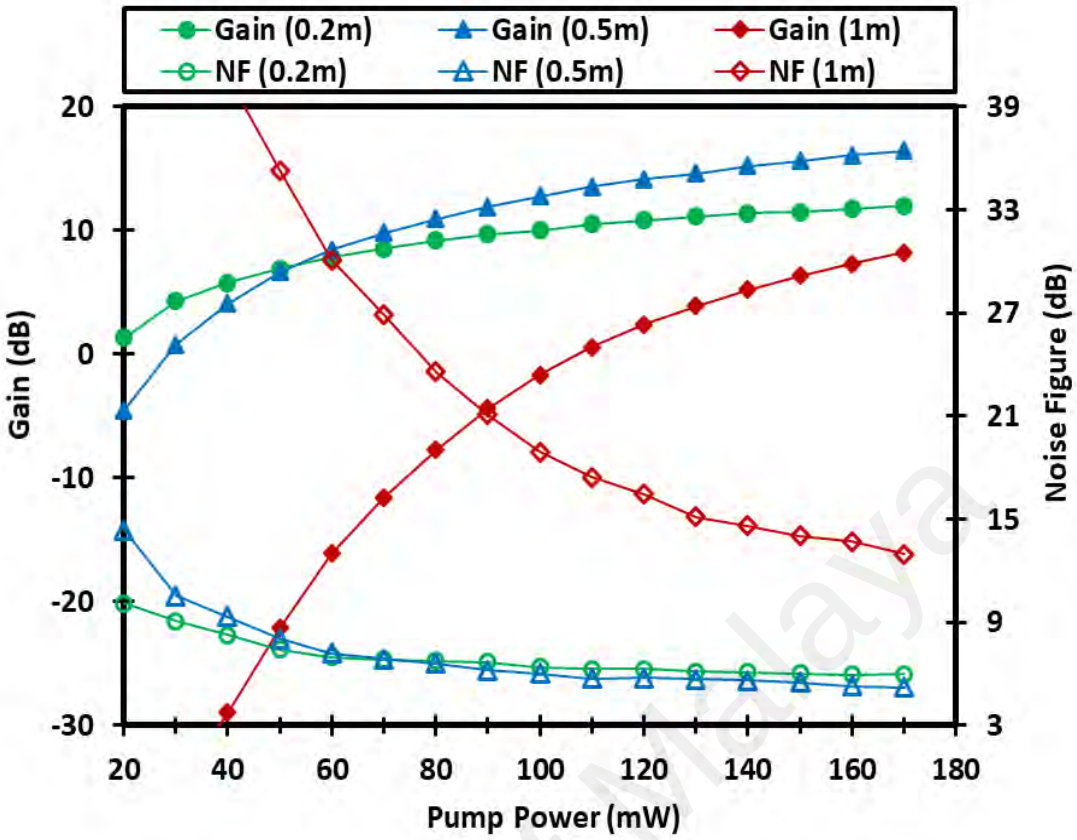

Figure 3.13: The performance of double pass HB-EDFA against various pump powers for input signal power of -10 dBm.

3.3.3 Performance comparison of single and double pass HB-EDFAs

Figure 3.14 compares the measured gain and noise figure results between the single and double pass C-band HB-EDFA, when the input signal and LD pump powers are fixed at -30 dBm and 170 mW, respectively. The single and double pass amplifiers are compared at the optimum length of 0.5 m long HB-EDF. As illustrated, the gain of the double pass HB-EDFA is significantly better than that of the single pass HB-EDFA. This is attributed to population inversion, which increases with double propagation of signal. An average gain improvement of about 9.6 dB is achieved along a wavelength region from 1525 to 1570 nm.

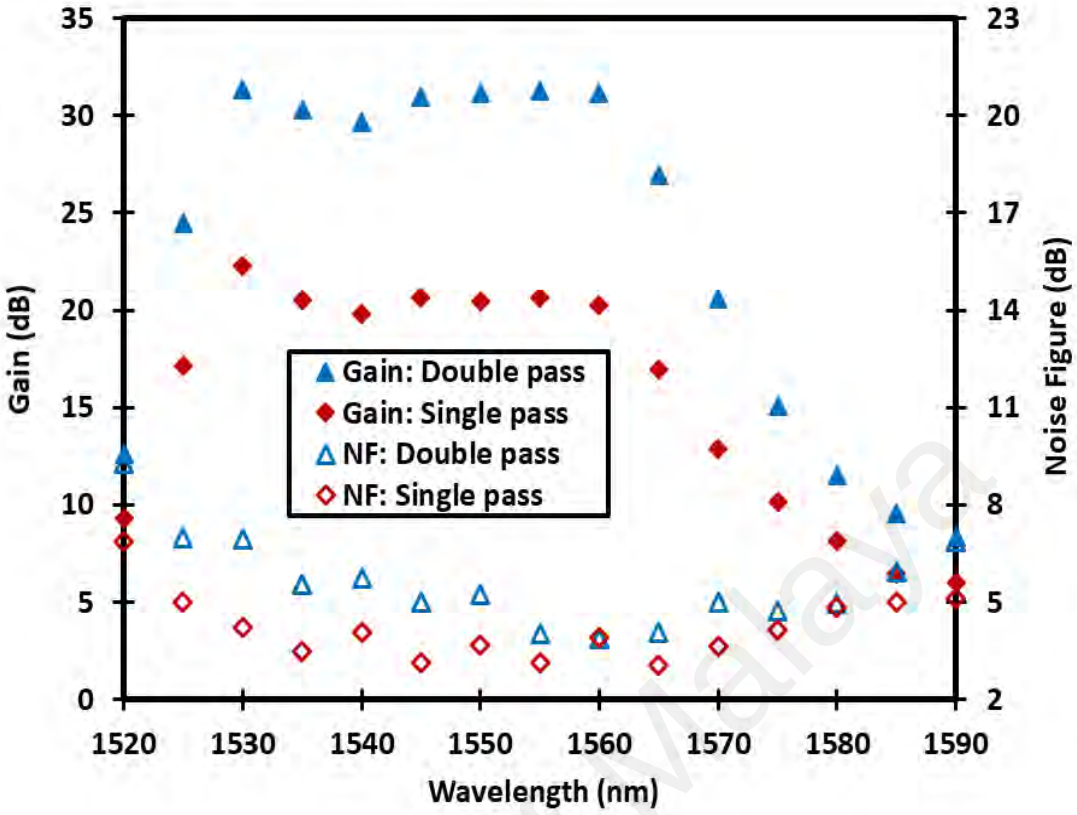

Figure 3.14: Measured gain and noise figure comparisons of single and double pass HB-EDFAs at input signal power of -30 dBm.

The gain and noise figure results are also measured and compared at high input signal power of -10 dBm, as illustrated in Figure 3.15. It is obvious that the gain enhancement with double pass HB-EDFA is not significant at high input signal power. This indicates that the population inversion is smaller at higher input signal powers, and therefore the attainable gain is reduced. The average gain improvement of about 3.4 dB is achieved over a wavelength region from 1525 to 1570 nm. As seen in Figures 3.14 and 3.15, the noise figures for double pass HB-EDFA are reasonably higher compared to those of the single pass HB-EDFA. This is due to the impact of the higher amplified spontaneous emission (ASE), which increases the noise figures.

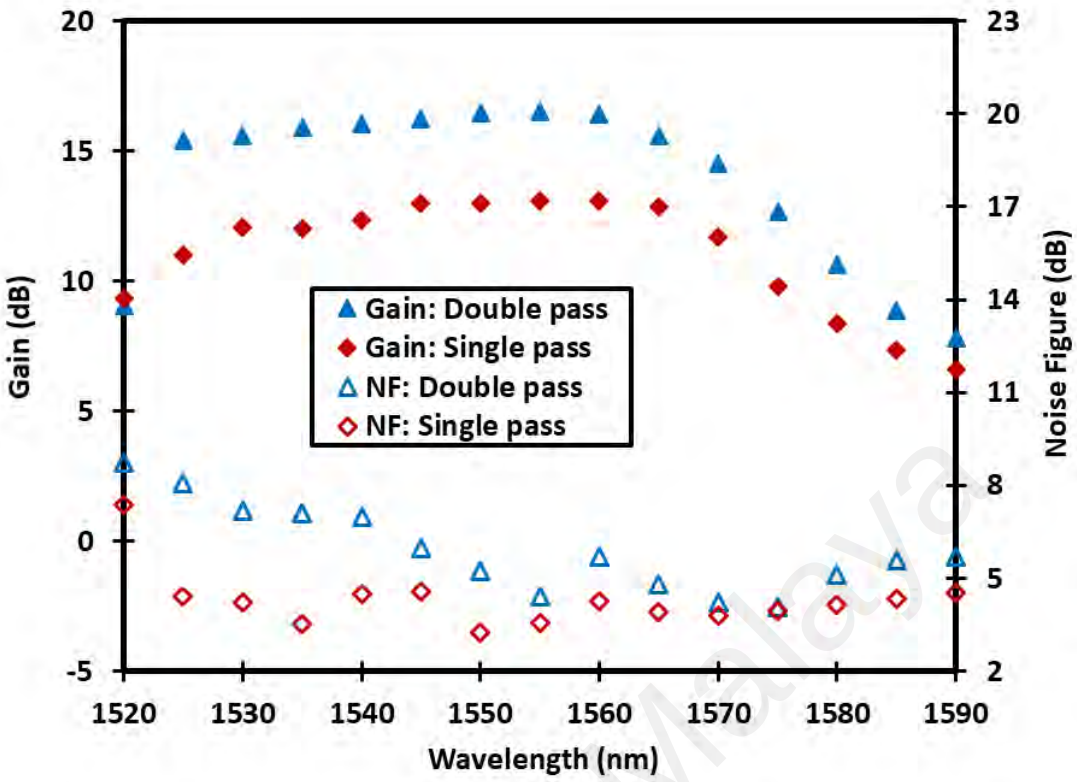

Figure 3.15: Measured gain and noise figure comparisons of single and double pass HB-EDFAs at input signal power of -10 dBm.

3.4 Effect of pumping wavelength on the performance of double pass HB-EDFA

The performance comparison between 980 nm and 1480 nm wavelengths pumping for double pass HB-EDFA is investigated, at the optimum length of 0.5 m long HB-EDF. The double pass HB-EDFA pumping with 1480 nm is obtained by replacing the 980 nm laser diode and the 980/1550 WDM with 1480 nm laser diode and 1480/1550 WDM, respectively. In the experiment, the pump power is fixed at the maximum power of 170 mW for both 980 nm and 1480 nm pumping wavelengths. Figures 3.16 and 3.17 show the amplification performance comparisons at input signal power of -30 dBm and -10 dBm, respectively. It is obvious that the double pass HB-EDFA that pumping with 980 nm wavelength achieves a better amplification performance especially at C-band region, as compared to that pumping with 1480 nm wavelength. This is most likely due

to a wider separation between the 980 nm laser wavelength and pump wavelength. This reduces the loss at WDM and thus increases the attainable gain. The absorption coefficient for the Erbium ions is also higher at 980 nm region, which provides a higher gain through population inversion.

At input signal power of -30 dBm, the average gain improvement of about 4.6 dB is achieved throughout a wavelength region from 1520 to 1560 nm, when the amplifier pumped at 980 nm wavelength. Furthermore, 980 nm wavelength pumping achieves a flatter gain spectrum for input signal power of -10 dBm. However, 1480 nm wavelength pumping gives a relatively gain improvement and lower noise figure at L-band region. This is because the 1480 nm pumping achieves a higher optical power conversion efficiency (PCE) in the L-band region, compared to that of 980 nm pumping. On the other hand, the noise figure is lower with 980 nm wavelength pumping, for both input signal powers at C-band region.

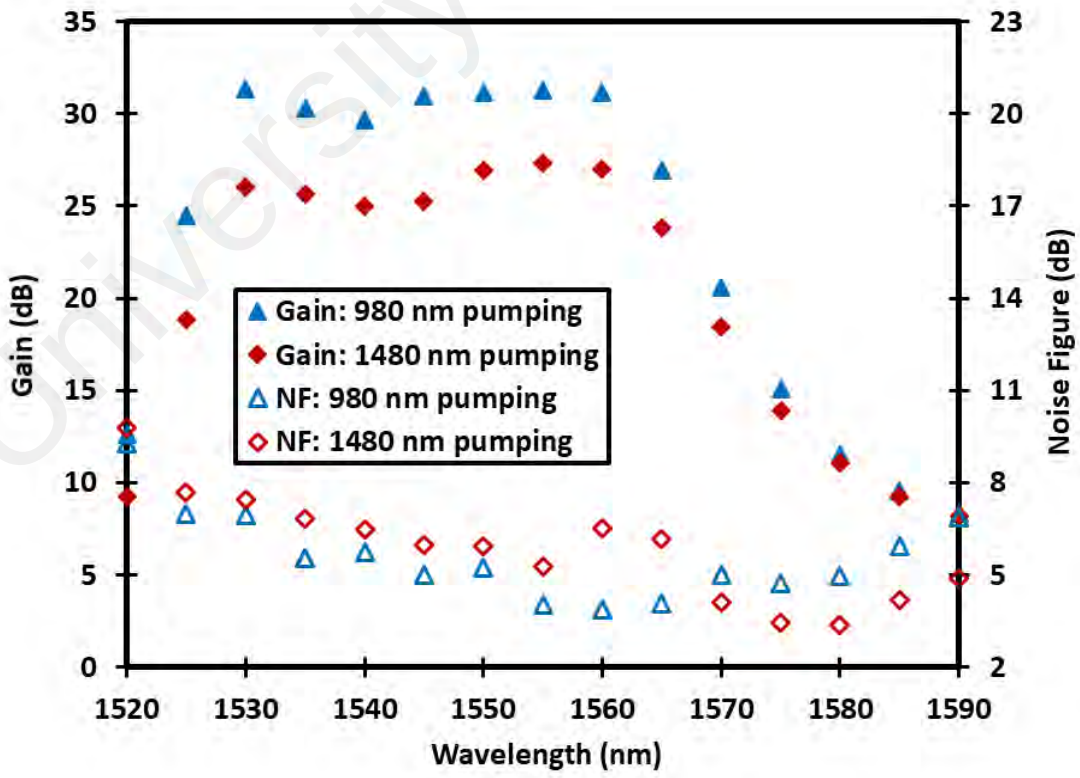

Figure 3.16: The performance comparison between 980 nm and 1480 nm pumping wavelength for double pass HB-EDFA at input signal power of -30 dBm.

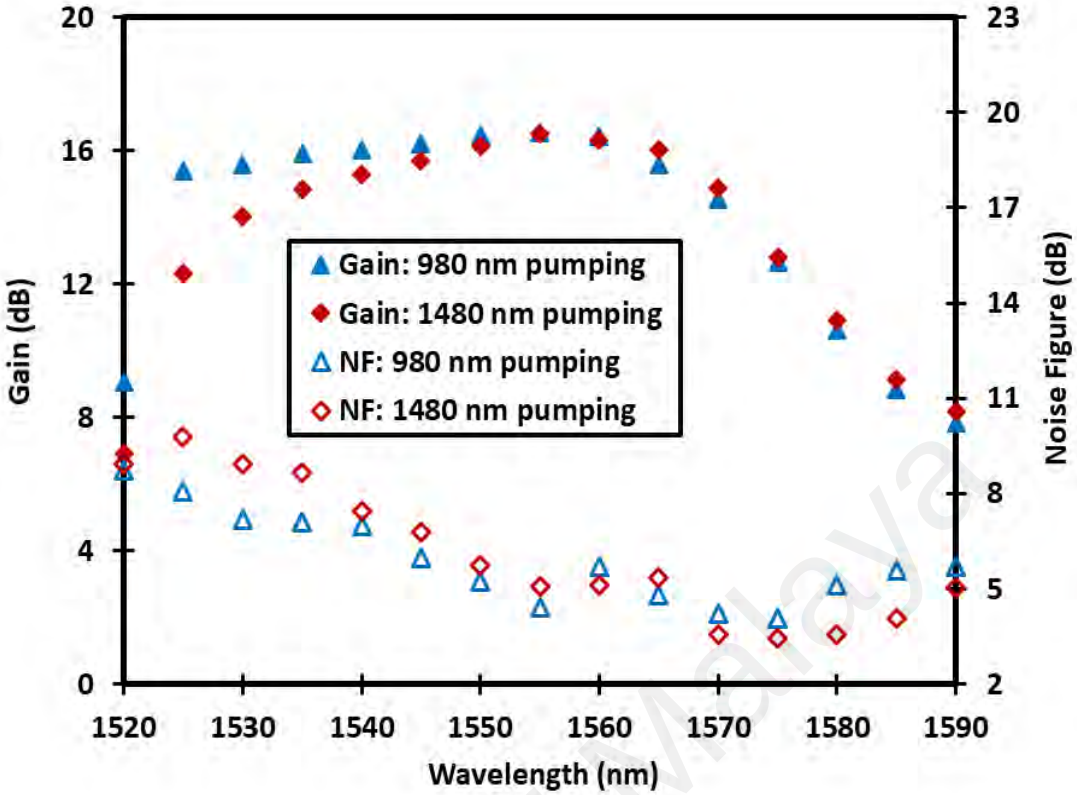

Figure 3.17: The performance comparison between 980 nm and 1480 nm pumping wavelength for double pass HB-EDFA at input signal power of -10 dBm.

3.5 Performance comparison between HB-EDFA and commercial Si-EDFA

In the choice of fiber glass host, many studies have focused on silica fiber due to its proven reliability and compatibility with conventional fiber optic components. In this section, the performance of the new HB-EDFA is compared with the commercial silica erbium doped fiber amplifier (Si-EDFA), which is known as IsoGain^{TM} I-25. The silica erbium doped fiber (Si-EDF) has an absorption loss of 23 dB/m at 980 nm, which translates to the erbium ion concentration of 2200 wt. ppm. For fair comparison, The EDFs are fixed at the optimum length of 0.5 m and 1 m for HB-EDF and Si-EDF, respectively. The literature review shows that the optimum length for Si-EDF in the C-bad region is 1 m (Markom et al., 2016). The comparison of the optical fiber specifications between HB-EDF and Si-EDF are illustrated at Table 3.1.

Table 3.1: The optical fiber specifications of HB-EDF and Si-EDF.

Merit	HB-EDF	Si-EDF
Fibers preform	Hafnium bismuth erbium co-doped yttria aluminum silica fiber	Erbium doped silica fiber
Erbium ion concentration	12500 wt. ppm	2200 wt. ppm
Absorption loss	100 dB/m at 980 nm	23 dB/m at 980 nm
Fiber Diameter	123.94 μm	125 μm
Numerical Aperture	0.21	0.17

In the experiment, the performance amplification is compared based on double pass configuration, by replacing the HB-EDF section with Si-EDF section. The comparison performances of both double pass amplifiers are depicted in Figure 3.18, as the input signal and the pump power are fixed at -30 dBm and 170 mW, respectively. As shown in the figure, the proposed HB-EDFA achieves a higher gain at all wavelengths tested compared with Si-EDFA. This is due to the population inversion, which is higher in the new HB-EDFA. For instance, the gain enhancements of 2.7 dB and 4.6 dB are obtained with HB-EDFA at 1550 nm and 1565 nm, respectively. Furthermore, the new HB-EDFA obtains a higher flat gain compared with Si-EDFA at the wavelength region from 1530 to 1560 nm. On the other hand, the noise figure is comparatively improved in the proposed HB-EDFA. This is due to the lower gain and higher loss related to the Si-EDFA as compared to that of HB-EDFA. The noise figures are maintained below 7 dB and 8.3 dB at a flat gain region for the HB-EDFA and Si-EDFA, respectively.

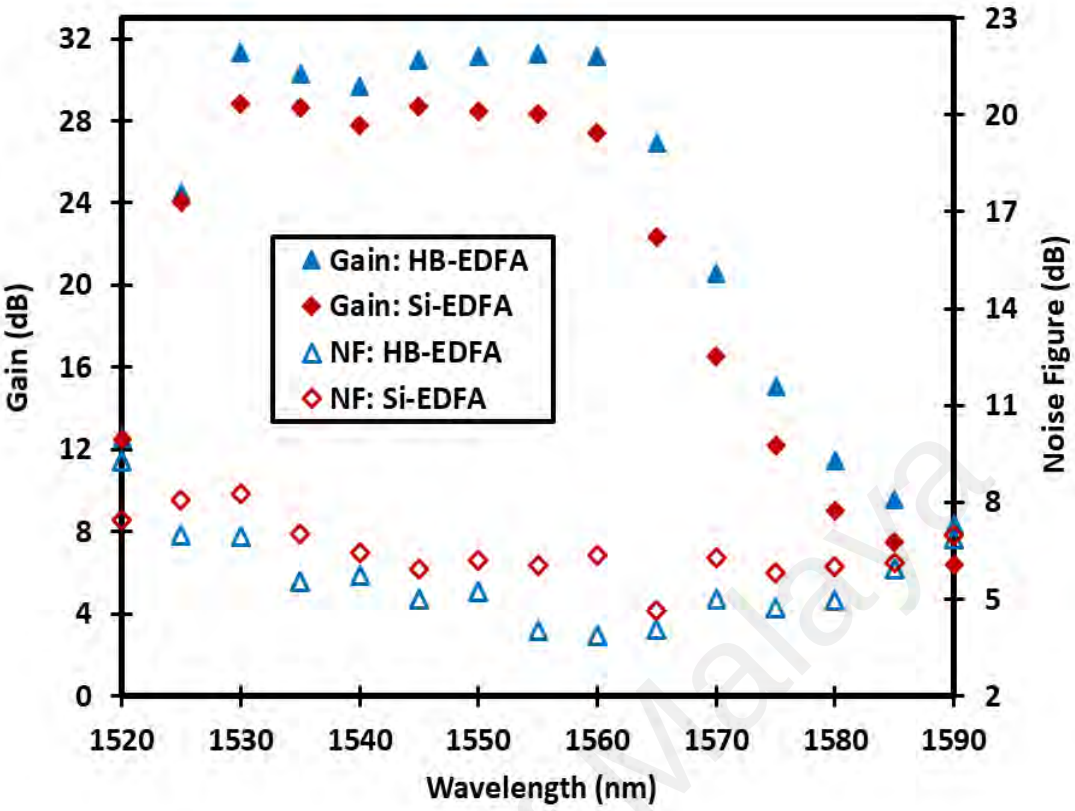

Figure 3.18: Comparison of the gain and noise figure performances between the HB-EDFA and Si-EDFA at an input signal power of -30 dBm.

Figure 3.19 shows the gain and noise figure characteristics across the wavelength region from 1520 to 1590 nm for an input signal and a pump power of -10 dBm and 170 mW, respectively. It is observed that the gains of the HB-EDFA are almost comparable with Si-EDFA, for the C-band wavelength region. In addition, the gain is higher with the HB-EDFA at the L-band region. This is due to the higher concentration ion erbium doping in the proposed HB-EDF, which improves the number of excited ions to be stimulated. Thereby, the attainable optical gain for broader wavelengths is improved. The noise figures are maintained below 8.1 dB and 8.4 dB at a flat gain region for the HB-EDFA and Si-EDFA, respectively. The comparison shows that the proposed HB-EDFA obtains a more efficient gain and lower noise figure as compared to that of Si- EDFA.

Furthermore, the proposed HB-EDFA used a shorter gain medium length than that of Si-EDFA.

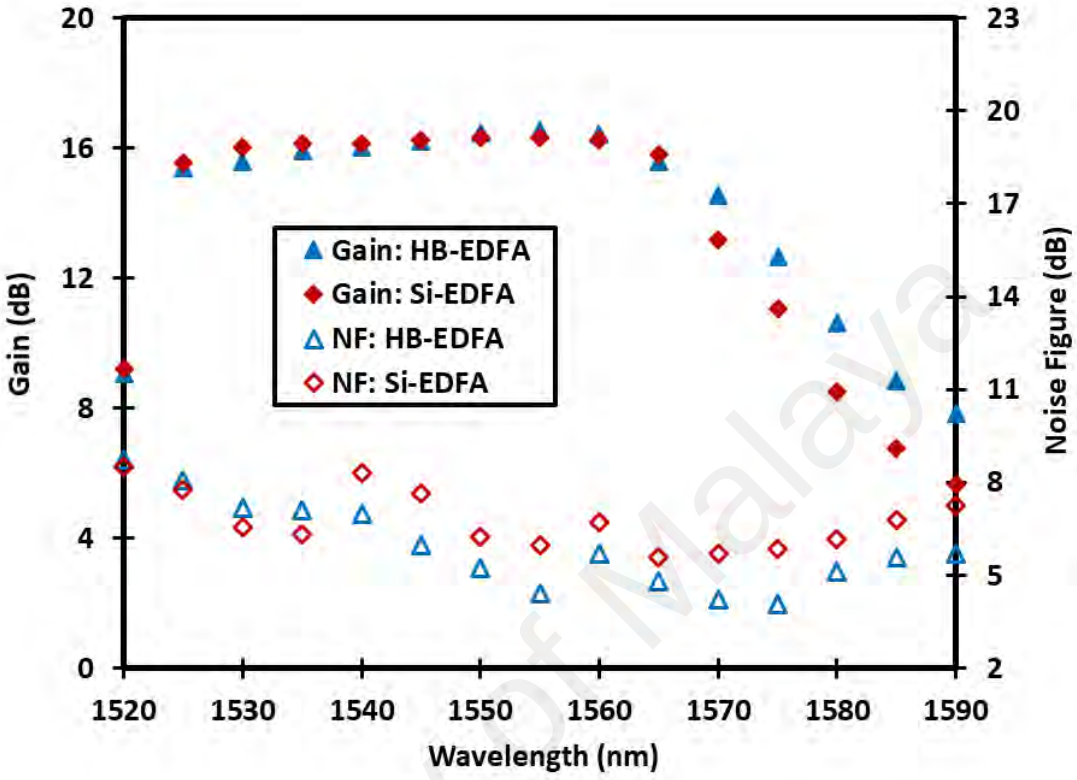

Figure 3.19: Comparison of the gain and noise figure performances between the HB-EDFA and Si-EDFA at an input signal power of -10 dBm.

3.6 Performance comparison between HB-EDFA and Zr-EDFA

The performance of the new HB-EDFA is also compared with the conventional Zr-EDFA, which is considered the latest effective EDF that fabricated based on optical fiber fabrication technology. The conventional Zr-EDF is obtained from a fiber perform, which is fabricated in a ternary class host, zirconia-yttria-aluminum co-doped silica fiber using MCVD. The Zr-EDF has an absorption loss of 80 dB/m at 980 nm, which translates to the erbium ion concentration of 4000 wt. ppm. The comparison of the optical fiber specifications between HB-EDF and Zi-EDF are illustrated at Table 3.2.

Table 3.2: The optical fiber specifications of HB-EDF and Zr-EDF.

Merit	HB-EDF	Zr-EDF
Fibers preform	Hafnium-bismuth-erbium co-doped yttria-aluminum silica fiber	Zirconia-yttria–aluminum–erbium co-doped silica fiber
Erbium ion concentration	12500 wt. ppm	4000 wt. ppm
Absorption loss	100 dB/m at 980 nm	80 dB/m at 980 nm
Fiber Diameter	123.94 μm	126.83 μm
Numerical Aperture	0.21	0.17

In the experiment, the performance of the amplifiers is compared based on double pass configuration, which was obtained by replacing the HB-EDF section with Zr-EDF section. The EDF lengths are fixed at the optimum length of 0.5 m for both HB-EDF and Zr-EDF. Figure 3.20 shows the gain and noise figure spectra for both double pass amplifiers when the input signal and the pump power are fixed at -30 dBm and 170 mW, respectively. As shown in the figure, the proposed HB-EDFA achieves a higher gain at all wavelengths tested compared with Zr-EDFA. For instance, the gain enhancements of 2.4 dB and 3 dB are obtained with HB-EDFA at 1530 nm and 1560 nm, respectively. This is due to the population inversion, which is higher in the new HB-EDFA. On the other hand, the noise figure is relatively improved in the proposed amplifier configured with HB-EDF. This is owing to lower ASE noise resulting from an efficient population inversion of HB-EDF. However, the noise figure for Zr-EDF is better than HB-EDFA at some wavelengths such as 1535 nm and 1540 nm. This is due to the improvement of the inhomogeneous distribution of erbium ion sites at these wavelengths.

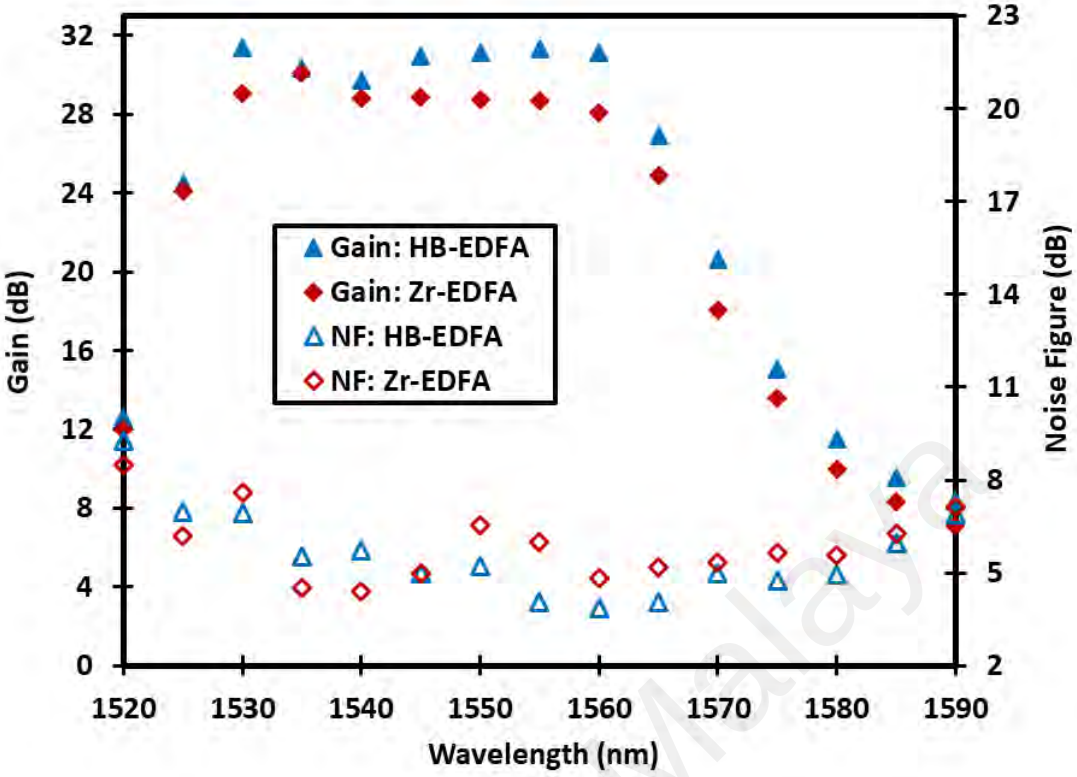

Figure 3.20: Comparison of the gain and noise figure performances between the HB-EDFA and Zr-EDFA at an input signal power of -30 dBm.

Figure 3.21 compares the gain and noise figure characteristics when the input signal power and a pump power are fixed at -10 dBm and 140mW, respectively. It is observed that the gain is slightly higher with HB-EDFA as compared to that of Zr-EDFA for the wavelength region from 1520 nm to 1590 nm. Besides the gain improvement, the gain spectrum is also broader with HB-EDFA due to the improvement of the inhomogeneous distribution of erbium ion sites and the suppression of signal excited state absorption (ESA). ESA is absorption of light by ions in an excited state, rather than in the ground state. The noise figure is relatively improved in the proposed HB-EDF. The results indicate that the proposed HB-EDFA could provide a more efficient gain and lower noise figure as compared to that of Zr-EDFA.

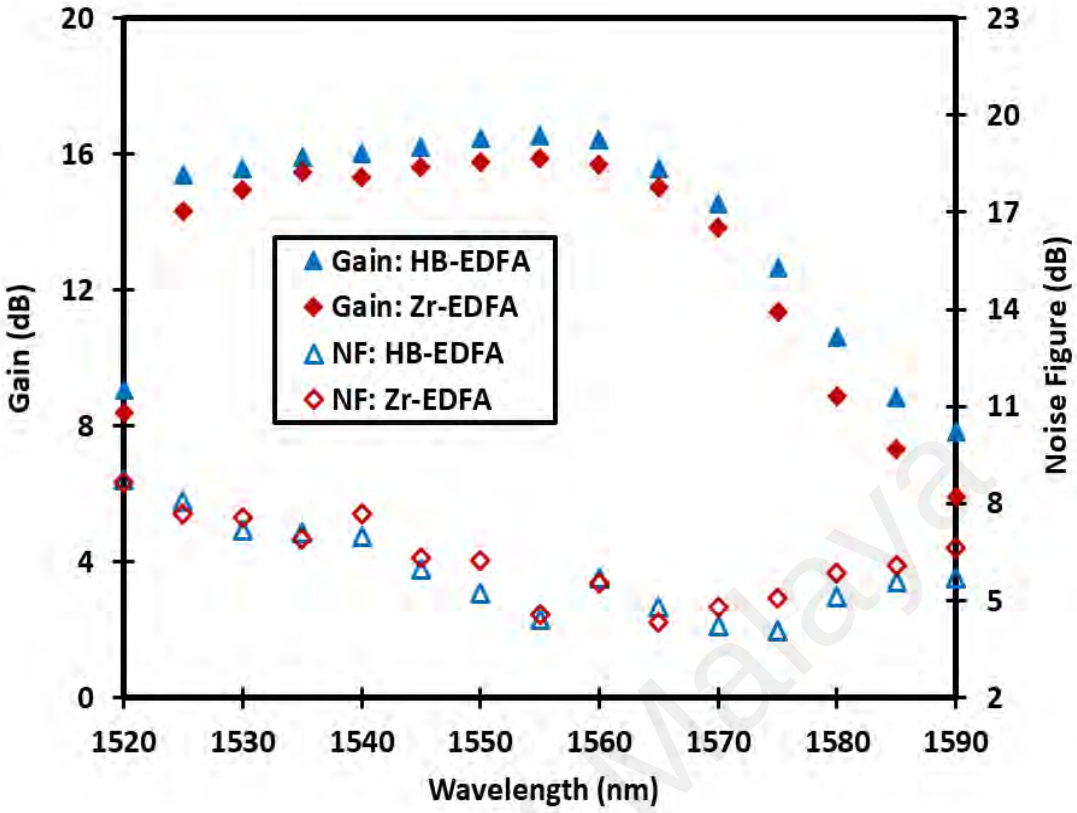

Figure 3.21: Comparison of the gain and noise figure performances between the HB-EDFA and Zr-EDFA at an input signal power of -10 dBm.

3.7 The performance of HB-EDFA with multi-input wavelengths

In this section, the performances of both single and double pass HB-EDFA are investigated using home-made multi-input wavelengths source to examine the flat gain characteristics. Figure 3.22 shows the home-made multi-input wavelengths source. As shown in the Figure, four TLS are linked with four POA in order to provide four input wavelengths with same input power of -10 dBm. A three 3-dB optical couplers are used to combine the input wavelengths, and to extract the output to the input port of the amplifier. The input signal wavelengths are fixed at 1540 nm, 1545 nm, 1550 nm and 1555 nm where the OSA span wavelength is set at 20 nm. The performances of both

single and double pass HB-EDFA are obtained for the optimum length of 0.5 m long HB-EDF when the pump power is fixed at 170 mW.

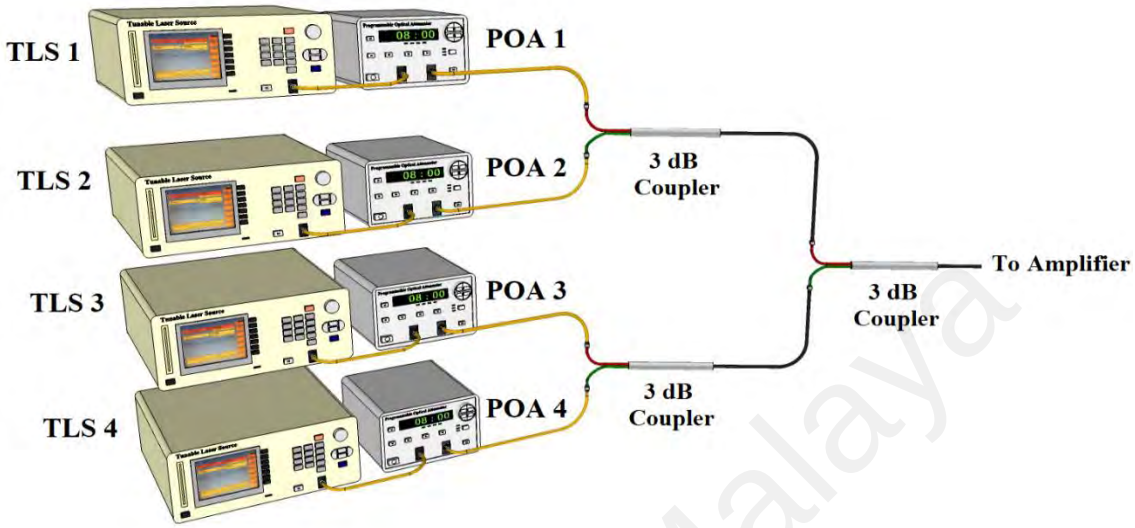

Figure 3.22: The home-made multi-input wavelengths source.

Figures 3.23 (a) and (b) show the input and output laser spectrum for the single and double pass HB-EDFA, respectively. It can be seen that input signals are amplified after propagating through both single and double pass amplifiers. The amplification is obtained from the energy stored outside the input signal wavelength, by suppressing the ASE generated within the gain region. This owing to the homogeneous expansion feature of EDFA. A flat output peaks powers of around 1.9 dBm and 5 dBm are realized for the single and double pass HB-EDFA, respectively.

The performance of the HB-EDFA using multi-input wavelengths source is compared to the one that using single input wavelength source as shown in Figures 3.24 and 3.25, for single and double pass configurations, respectively. The comparisons show a relatively lower gain is obtained with HB-EDFA that using multi-input wavelengths source. This is attributed to the sharing of the pump energy among the input signals. For

instance, the average gain decrements are 0.9 dB and 1.2 dB in the single and double pass amplifiers, respectively. Besides, a higher noise figure is observed with the amplifier that using multi-input wavelengths source. This is owing to the lower gain in addition to a resolution used which is lower with the amplifier using multi-input source. The OSA span wavelength is fixed at 20 nm to characterize the amplifier using multi-input source. However, the OSA span wavelength is fixed at 3 nm with the amplifier using single input source. For this reason, the OSA resolution is lower with the amplifier using multi-input source.

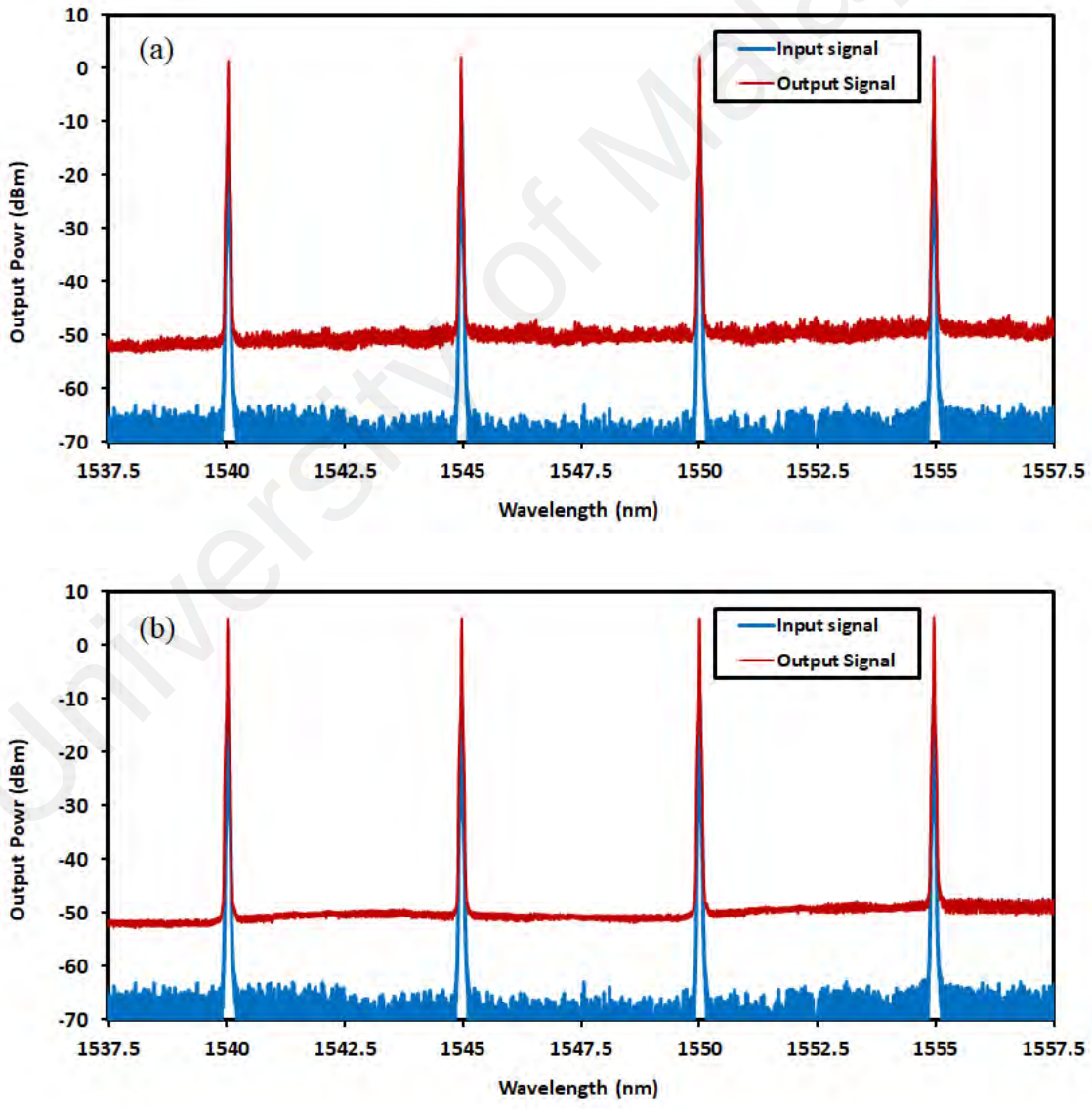

Figure 3.23: The input and output laser spectrum using multi-input wavelength source for (a) single pass HB-EDFA and (b) double pass HB-EDFA.

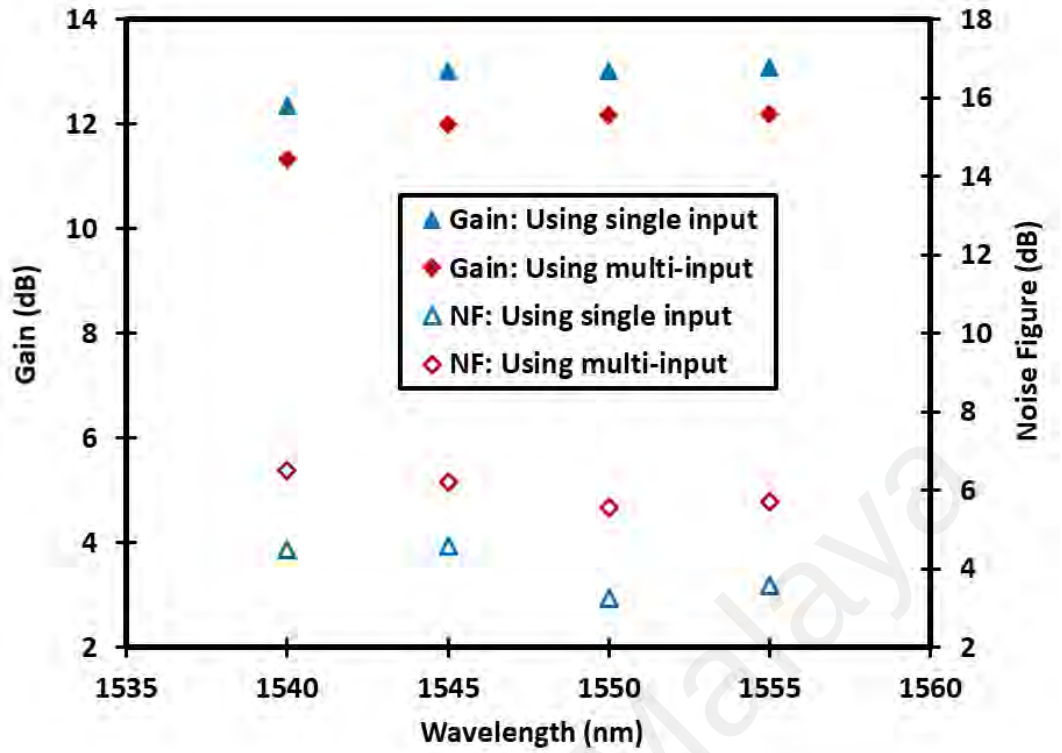

Figure 3.24: The comparison performance between HB-EDFA using multi-input source and that using single input source for single pass configuration.

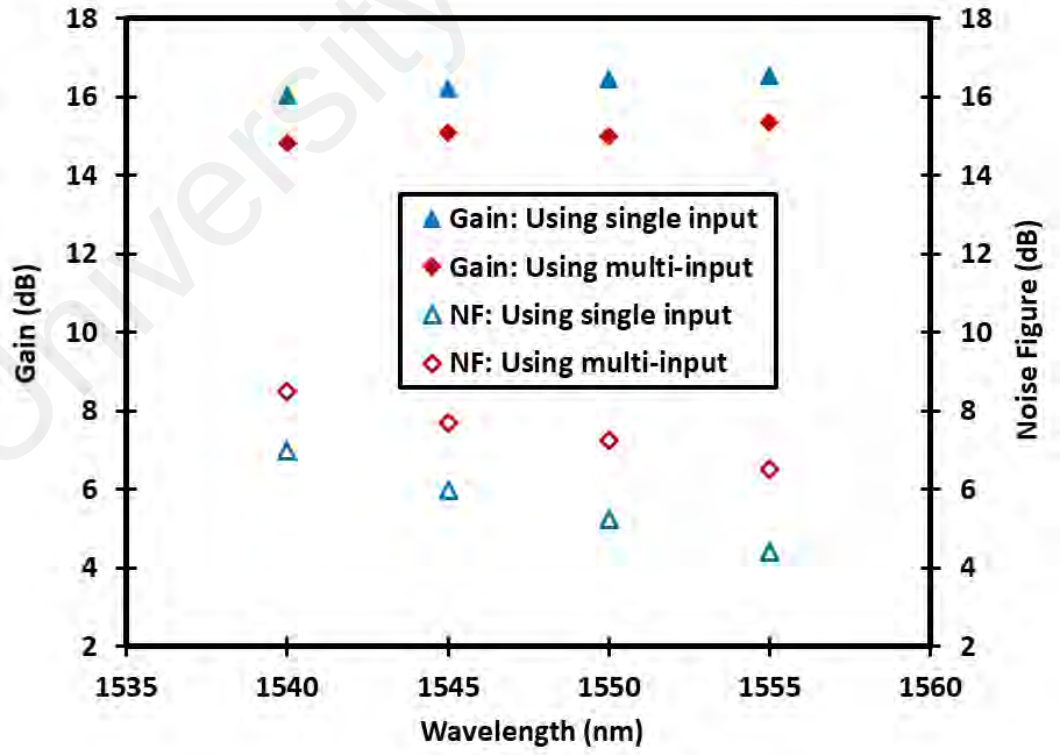

Figure 3.25: The comparison performance between HB-EDFA using multi-input source and that using single input source for double pass configuration.

3.8 Summary

A compact optical amplifier with a flat-gain characteristic at C-band region was demonstrated using short lengths of the new HB-EDF as the gain medium. The HB-EDF was fabricated using MCVD process in conjunction with SD technique. The fiber has an Erbium ions concentration of 12500 wt. ppm, which was realized due to the co-doping with Hafnium and Aluminum ions. The proposed amplifier was investigated for both single and double pass configurations. It was found that the 0.5 m long HB-EDF is the optimum length for the C-band region.

For single pass HB-EDFA at input signal power of -10 dBm, a flat gain of 12.4 dB was realized with a gain ripple of less than 1.4 dB, along the 45 nm wavelength region from 1525 to 1570 nm. Within the flat gain region, the noise figure was less than 4.6 dB. However, for the double pass HB-EDFA at input signal power of -30 dBm, a flat gain of 30.8 dB was realized with a gain ripple of less than 1.3 dB, along the 30 nm wavelength region from 1530 to 1560 nm. Within the flat gain region, the noise figure was less than 7 dB. Besides, at input signal power of -10 dBm, a flat gain of 15.9 dB was realized with a gain ripple of less than 1.4 dB, along the 45 nm wavelength region from 1525 to 1570 nm. Within the flat gain region, the noise figure was less than 8.1 dB. On the other hand, the shorter length of 0.2 m long HB-EDF also achieved an efficient performance with flat gain characteristics. For instance, at input signal power of -10 dBm, a flat gain of 11.8 dB was realized with a gain ripple of less than 1.1 dB, along the 40 nm wavelength region from 1525 to 1565 nm. Within the flat gain region, the noise figure was less than 8.8 dB. The comparison between single and double pass HB-EDFA showed that the double pass HB-EDFA offers a better gain spectrum. The performance of double pass HB-EDFA was investigated for both 980 nm and 1480 nm wavelengths pumping. It was obvious that the double pass HB-EDFA that pumping with 980 nm wavelength achieves a better amplification performance especially at C-band region, as compared to that pumping with

1480 nm wavelength. The amplification performance of the HB-EDFA was compared with the previous EDFAs, such as the commercial Si-EDFA and the conventional Zr-EDFA. The comparison showed that the proposed HB-EDFA obtains a more efficient gain and lower noise figure as compared to that of Si-EDFA and Zr-EDFA. Furthermore, the proposed HB-EDFA used a shorter gain medium length than that of Si-EDFA.

The performances of single and double pass HB-EDFA were also investigated using home-made multi-input wavelengths source to examine the flat gain characteristics. A flat output peaks powers of around 1.9 dBm and 5 dBm were realized for the single and double pass HB-EDFA, respectively. The performance of the HB-EDFA using multi-input wavelengths source was compared to the one that using single input wavelength, for both single and double pass configurations. The comparisons showed a relatively lower gain and higher noise figure are obtained with HB-EDFA that using multi-input wavelengths source.

CHAPTER 4: WIDEBAND HAFNIA-BISMUTH ERBIUM CO-DOPED FIBER AMPLIFIER AND ASE SOURCE USING SERIES AND PARALLEL CONFIGURTIONS

4.1 Introduction

The massive expansion of optical communication systems in recent years has resulted in a huge demand for efficient optical fiber amplifiers with a wideband operating region and flat-gain characteristics, to cover the whole range of dense wavelength division multiplexing (DWDM) spectrum (Firstov et al., 2017; Pradhan & Mandloi, 2018). In addition to conventional band (C-band) which is start from 1530 nm to 1565 nm, the optical amplification in long wavelength band (L-band) permits the capacity of DWDMs to be upgraded with an additional 40 nm bandwidth (1565–1605 nm) (Durak & Altuncu, 2017). The wideband erbium doped fiber amplifier (EDFA) is commonly constructed utilizing dual stages in series or parallel structures, with different lengths of the erbium doped fibers (EDFs) (Abdullah et al., 2018; Ali et al., 2014). This is due to the amplification in the L-band region which requires longer EDFs to obtain the same attainable gain in the C-band region.

Previously, a wideband bismuth-erbium doped fiber amplifier (Bi-EDFA) utilizing dual stages in series structure was introduced (Cheng et al., 2011). Unfortunately, a high noise figures were observed as compared to the achieved gain. The average gain was about 7 dB while the noise figure fluctuates from 6 dB to 10 dB. In addition, Bi-EDFs have a problem in splicing with standard single mode fibers (SMFs) by utilizing a standard splicing machine. In another studies, a wideband optical amplifier using a silica erbium doped fibers (Si-EDFs) as a gain medium was proposed, in parallel (Hamida et al., 2012) and series (Latiff et al., 2013) configurations. However, the total length of the

Si-EDFs used was 10.5 m which is very long. Besides, the gain ripple was high in parallel amplifier and thus, this amplifier could not achieve flat gain over the wideband operation region.

In this chapter, a new wideband and flat gain hafnia-bismuth erbium co-doped fiber amplifier (HB-EDFA) is demonstrated and developed, by utilizing two short lengths of HB-EDF sections to fulfill amplification in C- and L-band telecommunication regions. The proposed two-stage amplifier is investigated for both series and parallel structures in conjunction with double-pass scheme. The performance of the amplifier is explored for two different lengths of the HB-EDFs, as well as various pump powers to determine the optimum design. The proposed series amplifier is examined in both backward and forward pumping schemes. On the other hand, a broadband amplified spontaneous emission (ASE) light source is also investigated and achieved using two pieces of HB-EDF in series and parallel structures. The proposed ASE source covers both of C- and L-bands wavelength region.

4.2 Wideband HB-EDFA using parallel configuration

The schematic diagram of the two-stage double-pass HB-EDFA in conjunction with parallel configuration, is depicted in Figure 4.1. The amplifier employs two pieces of HB-EDF in parallel to provide amplification for both C and L-bands wavelengths region. The first stage HB-EDF is forward pumped by using a 980 nm laser diode (LD1) to operate in C-band, while the second stage HB-EDF, which was designed for L-band operation is forward pumped by using a 1480 nm laser diode (LD2). This is because the 1480 nm pumping achieves a higher optical power conversion efficiency (PCE) in the L-band region, as compared to that of 980 nm pumping. A wavelength division multiplexing (WDM) is used in each stage to combine the pump laser and the input signal together. A

coarse wavelength division multiplexing (CWDM) filter is utilized to separate/ combine both C and L-band signals into/from C and L-band HB-EDFAs, respectively. Three optical circulators are utilized at the input and output ports of the amplifier to permit double propagation of the signal in the erbium fibers.

At the input port, an optical circulator is utilized to deliver the input signal into the CWDM, and to extract the double amplified signal to the optical spectrum analyzer (OSA). At the output ports of each stage, an optical circulator is utilized as a broadband loop mirror for reflecting the amplified signal into the erbium fiber. The broadband loop mirror is constructed by joining port 3 with port 1 so that the signal from port 2 is routed back into the same port. A tunable laser source (TLS) is used as a signal source while an OSA is utilized to test the gain and noise figure characteristics. A programmable optical attenuator (POA) is used to get the exact input signal power to the amplifier. All the experiments were carried out at room temperature, ~25 °C.

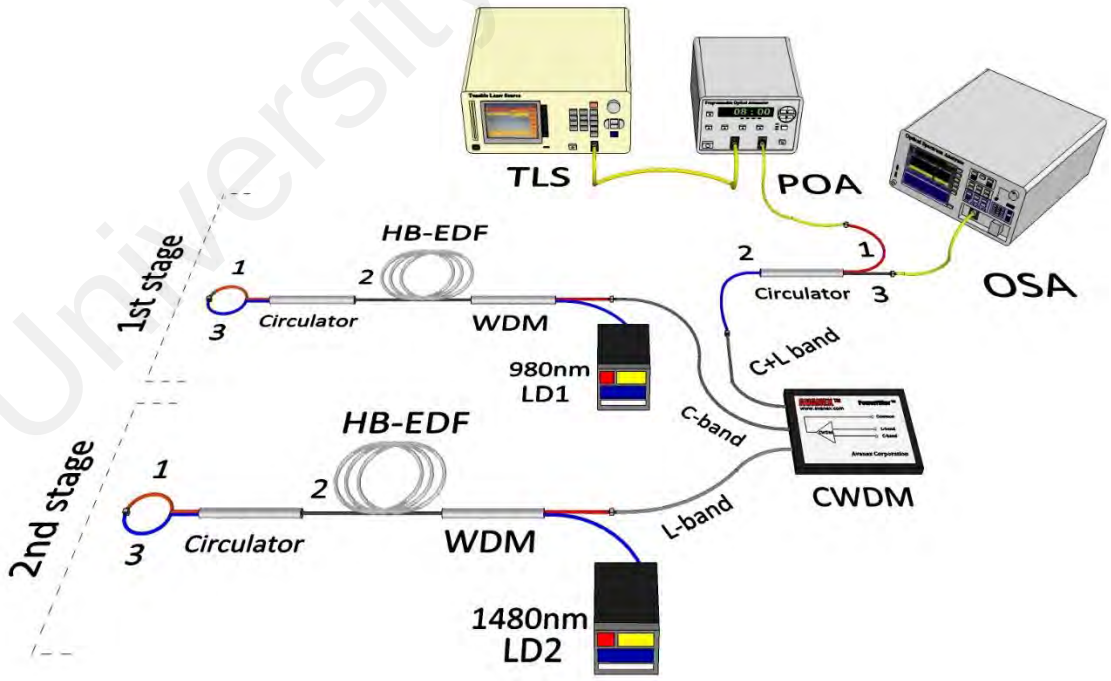

Figure 4.1: Two-stage double-pass HB-EDFA in conjunction with parallel configuration.

As mentioned in the previous chapter, the optimum length of the HB-EDF for C-band wavelengths region was 0.5 m long HB-EDF. However, the short length of about 0.2 m long HB-EDF also achieved an efficient amplification performance. Thereby, two wideband HB-EDFA is investigated using various lengths of the HB-EDFs in parallel configuration to achieve the best performance.

4.2.1 Parallel HB-EDFA with total erbium fiber length of 2 meters

In this amplifier, the HB-EDFs are adjusted at 50 cm and 150 cm long respectively, for amplification in C and L-bands so that the total length is 2 m. Figures 4.2 and 4.3 illustrate the performance of the parallel HB-EDFA at various L-band pump powers, for input signal powers of -30 dBm and -10 dBm, respectively. In the experiment, the LD1 power is fixed at the maximum power of 170 mW. Nevertheless, the LD2 power which controls the L-band gain, is varied from 110 mW to 140 mw and then to 170 mW. It is obvious that the variation of the LD2 power gives the same effect on both input signal powers.

It can be observed that the L-band gain spectrum rises as the LD2 power increases. However, the increment in the gain spectrum declines when the LD2 power increases from 140 to 170 mW, due to the saturation effect. For instance, at wavelength of 1580 nm and -30 dBm input signal power, the gain increases from 14.4 dB to 18.2 dB and 19.7 dB as the LD2 power changes from 110 mW to 140 mW and then to 170 mW respectively. The L-band noise figure is relatively higher when the LD2 power is fixed at 110 mW. This is due to the lower gain and higher loss related to the lower LD2 power. On the other hand, no significant changes in the gain and noise figure spectra is observed at C-band region. This is owing to the LD1 power which is fixed, and the LD2 power variation that affects only on the L-band region.

It is found that the optimum laser diodes powers to achieve higher gain and lower noise figure characteristics over a wideband operation region, are 170 mW for both LD1 and LD2. At input signal power of -30 dBm with the optimum LDs powers, the gain fluctuates from 11 to 30.1 dB along the wavelength span of 85 nm from 1525 to 1610 nm. Besides that, the noise figure of less than 7.8 dB is obtained within this 85 nm wavelength region. However, at input signal power of -10 dBm, the gain fluctuates from 11 to 16.4 dB along the wavelength span of 80 nm from 1525 to 1605 nm. Within this 80 nm wavelength span, the noise figure values vary from 5.4 to 8.7 dB.

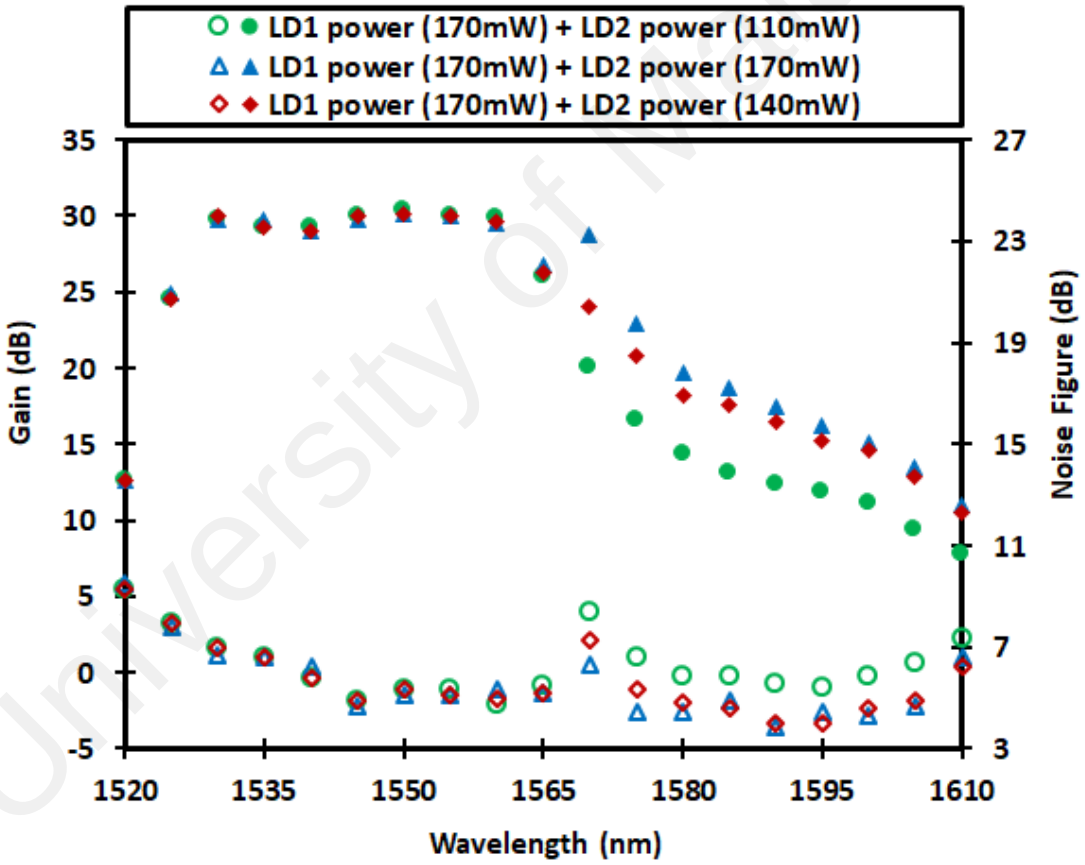

Figure 4.2: Measured gain (solid symbol) and noise figure (hollow symbol) spectra of the parallel HB-EDFA using a total 2 m long of the active fiber, at various LD2 powers when the input signal power is set at -30 dBm.

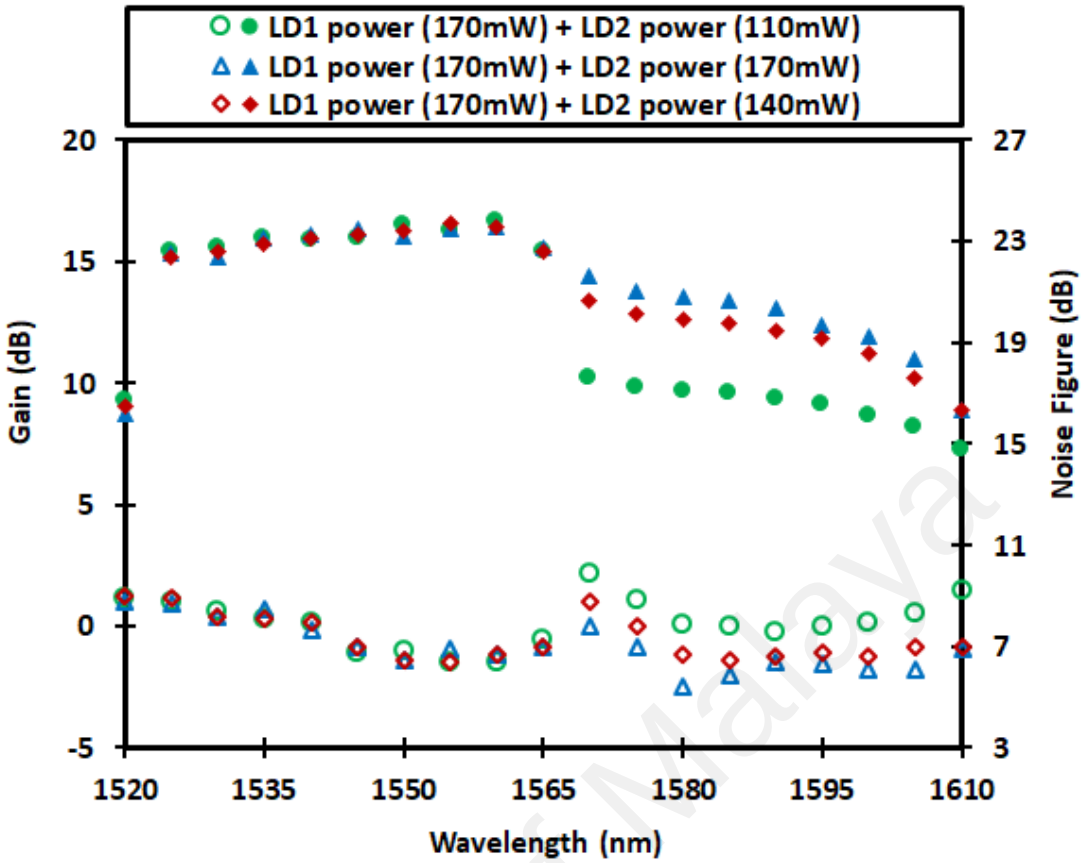

Figure 4.3: Measured gain (solid symbol) and noise figure (hollow symbol) spectra of the parallel HB-EDFA using a total 2 m long of the active fiber, at various LD2 powers when the input signal power is set at -10 dBm.

4.2.2 Parallel HB-EDFA with total erbium fiber length of 1.72 meters

The above experiment was repeated at slightly shorter length of total active fiber. In this amplifier, the HB-EDFs are adjusted at 22 cm and 150 cm long respectively, for amplification in C and L-bands so that the total length is 1.72 m. Figures 4.4 and 4.5 illustrate the performance of the parallel HB-EDFA at various L-band pump powers, for input signal powers of -30 dBm and -10 dBm, respectively. In the experiment, the LD1 power is fixed at the maximum power of 170 mW. Nevertheless, the LD2 power which controls the L-band gain, is varied from 110 mW to 170 mW. It is clearly observed that the L-band gain rises as the LD2 power increases before it is saturated as the pump power

is increased above 140 mW. Therefore, it is believed that the optimum laser diodes powers to achieve higher and flatter gain spectrum over a wideband operation region, are 170 mW and 140 mW for LD1 and LD2, respectively. At input signal power of -30 dBm with the optimum LDs powers, the gain fluctuates from 10.5 to 24 dB along the wavelength span of 90 nm from 1520 to 1610 nm. On the other hand, the noise figure of less than 10.1 dB is obtained within the wavelength region from 1520 to 1610 nm.

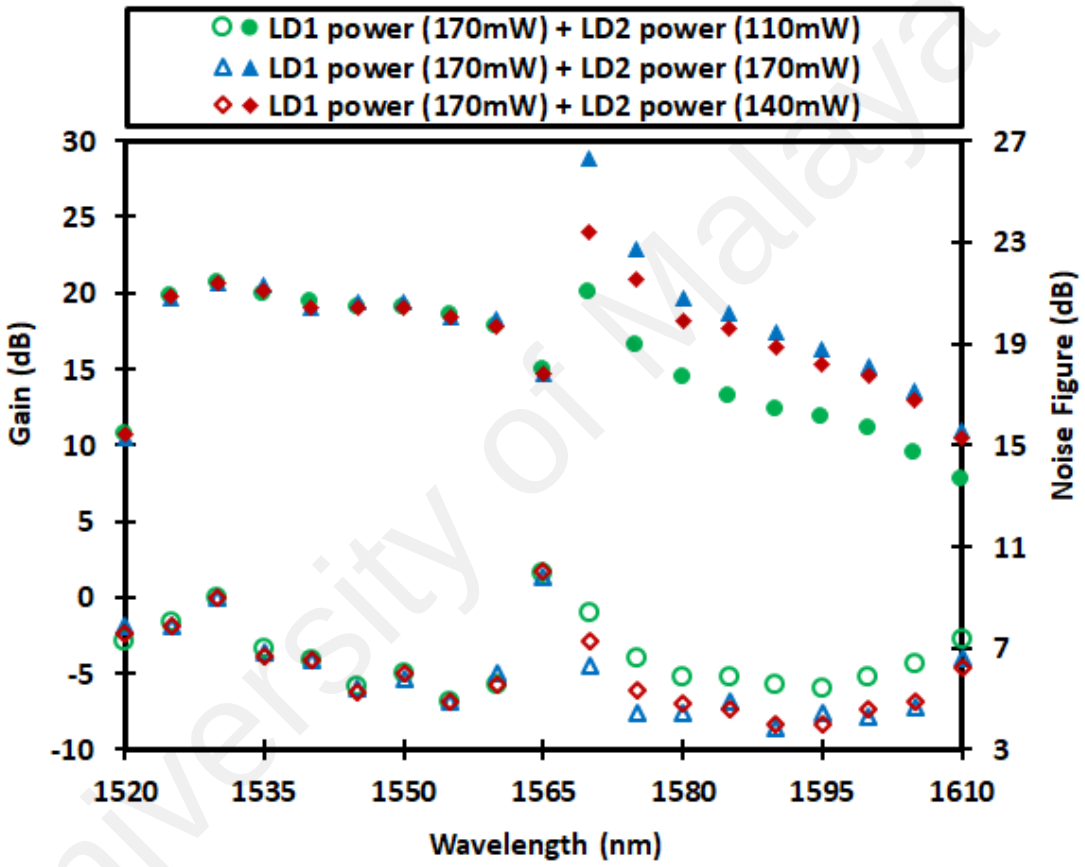

Figure 4.4: Measured gain (solid symbol) and noise figure (hollow symbol) spectra of the parallel HB-EDFA using a total 1.72 m long of the active fiber, at various LD2 powers when the input signal power is set at -30 dBm.

At input signal power of -10 dBm, a flat gain of 12.1 dB is realized with a gain ripple of less than 2 dB, along the wideband wavelength region of 80 nm from 1525 to 1605 nm. Within the flat gain region, the noise figure values vary from 6 to 11.8 dB. It

can be inferred that the noise figure is higher at shorter wavelength span and it reduces gradually when it goes to longer wavelength span. This is attributed to the decrement in the erbium absorption to emission cross section as it goes from shorter to longer wavelength span. Furthermore, the higher noise figure is obtained at 1565 nm wavelength. This is due to two reasons; the lower gain and higher loss characteristics at the tail of C-band region owing to the short erbium fiber of 22 cm long HB-EDF, as well as the insertion loss of CWDM which is high when the amplification medium shifts from 22 to 150 cm.

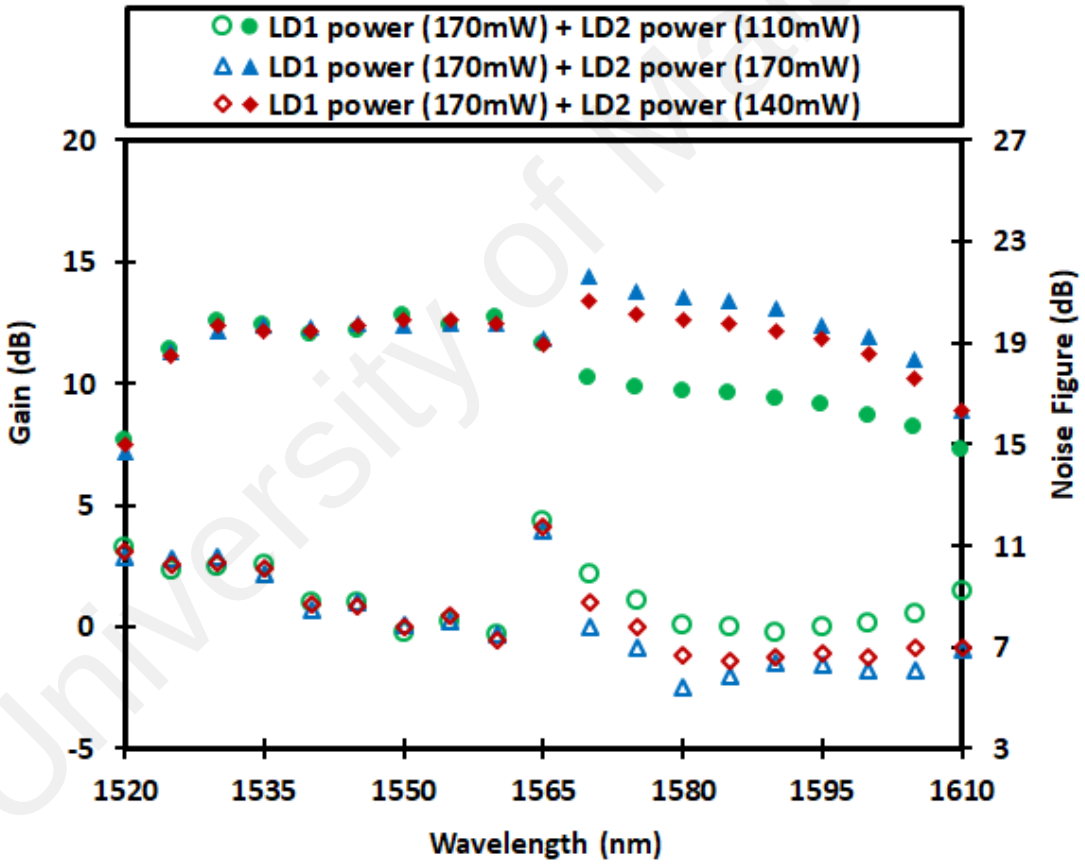

Figure 4.5: Measured gain (solid symbol) and noise figure (hollow symbol) spectra of the parallel HB-EDFA using a total 1.72 m long of the active fiber, at various LD2 powers when the input signal power is set at -10 dBm.

4.2.3 Performance comparison of the proposed parallel HB-EDFAs

The performance of the proposed parallel HB-EDFA that using 2 m long HB-EDF is compared to that using 1.72 m long HB-EDF. It is found that both amplifiers are obtaining an efficient amplification with wideband operation region from 1520 to 1610 nm. The use of 2 m long HB-EDF achieves a higher gain and lower noise figure as compared to that of 1.72 m. However, the use of 1.72 m long HB-EDF provides a flat gain characteristic along the wideband wavelength span of 80 nm from 1525 to 1605 nm. The result indicates that the use of 1.72 m long HB-EDF is preferable in parallel configuration. Unfortunately, the noise figures at 1525 nm, 1530 nm and 1565 nm wavelengths are higher with a shorter active fiber. Further investigations aimed at improving the noise figures are required. Table 4.1 summarizes the performance comparison of the proposed parallel HB-EDFA for two different total length of the active fiber; 2 m and 1.72 m long HB-EDF.

Table 4.1: The performance comparison of the proposed parallel HB-EDFAs.

Merit	**Parallel HB-EDFA using 1.72 m long HB-EDF**	**Parallel HB-EDFA using 2.0 m long HB-EDF**
Erbium fiber lengths	Total length: 1.72 m. 22 cm for C-band region. 150 cm for L-band region.	Total length: 2 m. 50 cm for C-band region. 150 cm for L-band region.
Optimum LDs powers	LD1 power: 170 mW. LD2 power: 140 mW.	LD1 power: 170 mW. LD2 power: 170 mW.

Table 4.1, continued.

Merit	Parallel HB-EDFA using 1.72 m long HB-EDF	Parallel HB-EDFA using 2.0 m long HB-EDF
Wideband amplification	At input signal power of -30 dBm • The gain fluctuates from 10.5 to 24 dB along the wavelength span of 90 nm. • The NF is less than 10.1 dB. At input signal power of -10 dBm • A flat gain of 12.1 dB with a gain ripple of ± 2 dB, along the wavelength span of 80 nm is realized. • The NF values vary from 6 to 11.8 dB.	At input signal power of -30 dBm • The gain fluctuates from 11 to 30.1 dB along the wavelength span of 85 nm. • The NF is less than 7.8 dB. At input signal power of -10 dBm • The gain fluctuates from 11 to 16.4 dB along the wavelength span of 80 nm. • The NF values vary from 5.4 to 8.7 dB.

4.3 Wideband HB-EDFA using series configuration

In series configuration, the amplification characteristic at each stage is affected on the other stage. Due to that, the performance of the series HB-EDFA is investigated for different pumping schemes; forward and backward pumping. The schematic diagrams of the two series stages HB-EDFA with forward and backward pumping are depicted in Figures 4.6 and 4.7, respectively. Both structures consist of CWDM filter, three optical circulators as well as two pieces of HB-EDF sections. The optical fiber circulator (C1) is

used to transfer the input signal inside the first stage, and to pull out the returned output signal to the OSA. In the experiment, a novel structure utilizing a CWDM filter, instead of C-band fiber Bragg grating (FBG), is proposed. The CWDM is placed in between the two stages to separate and combine the C- and L-band signals. The optical circulator (C2) is used to reflect the C-band signal, which passes then over the CWDM to the first stage for double amplification. The L-band signal undergoes single amplification firstly by the first and second stages. The optical circulator (C3) is used to reflect the L-band signal to undergo double amplification in both stages. A TLS is used as a signal source while an OSA is utilized to test the gain and noise figure characteristics. A programmable optical attenuator (POA) is utilized to provide an accurate input power to the amplifier. All the experiments were carried out at room temperature, ~25 °C. The performance of the proposed series HB-EDFA is investigated for two different lengths of the HB-EDFs, whereas the total lengths of HB-EDF used are 2 m and 1.72 m.

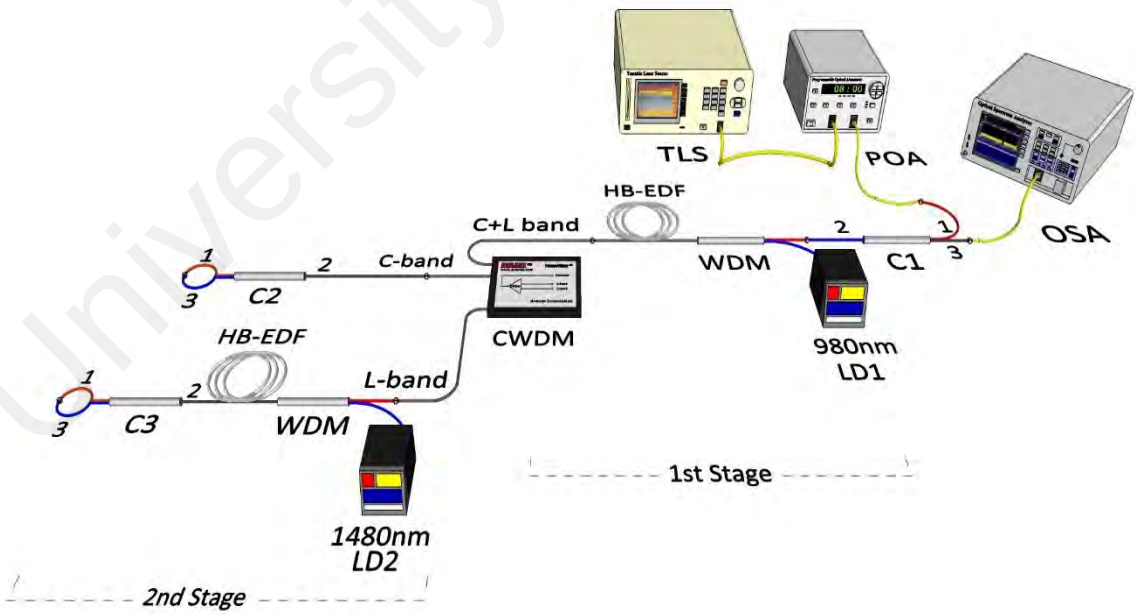

Figure 4.6: Two-stage double-pass HB-EDFA in conjunction with series configuration using forward pumping.

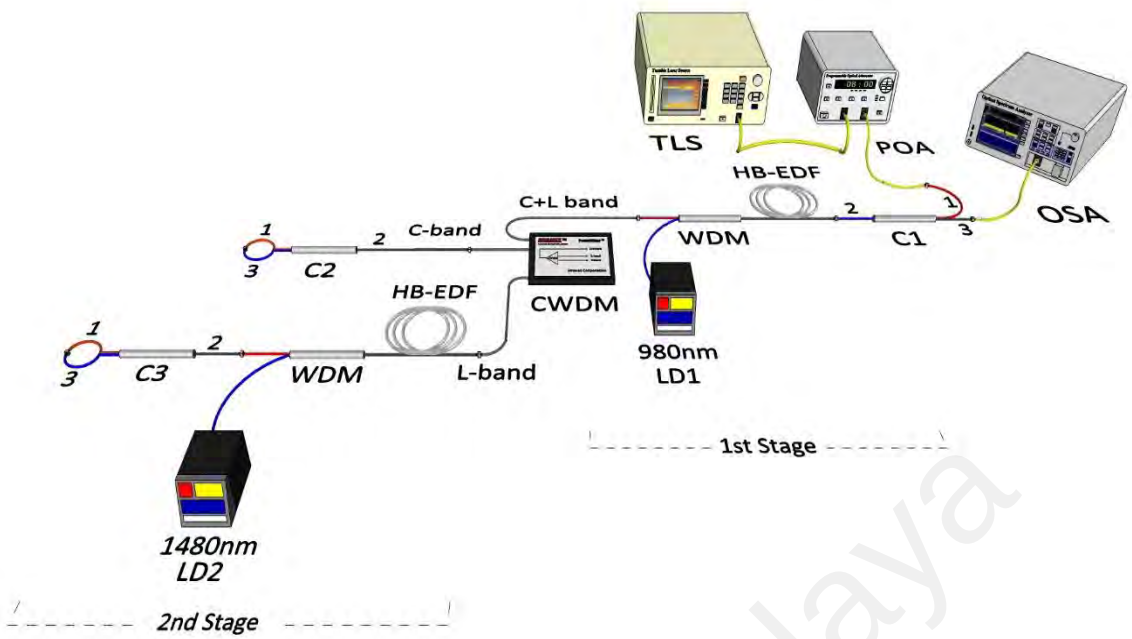

Figure 4.7: Two-stage double-pass HB-EDFA in conjunction with series configuration using backward pumping.

4.3.1 Forward pumping for 1.72 m long HB-EDF

In this amplifier, the HB-EDFs are adjusted at 22 cm and 150 cm long respectively, for amplification in C and L-bands so that the total length is 1.72 m. Same to the parallel HB-EDFA, the C-band HB-EDF is forward pumped by using a 980 nm LD1. However, the L-band HB-EDF is forward pumped by using a 1480 nm LD2. Figures 4.8 and 4.9 illustrate the performance of the forward pumping-based series HB-EDFA at various L-band pump powers, for input signal powers of -30 dBm and -10 dBm, respectively. In the experiment, the LD1 power is fixed at the maximum power of 170 mW. Nevertheless, the LD2 power which controls the L-band gain, is varied from 110 mW to 140 mW and then to 170 mW. Similar to the parallel type of amplifier, the variation of the LD2 power gives the same effect on both input signal powers.

Overall, it can be inferred that the optimum laser diodes powers to achieve even better performance in term of gain, noise figures and amplification bandwidth are 170 mW and 110 mW for LD1 and LD2, respectively. At input signal power of -30 dBm with the optimum LDs powers, the gain fluctuates from 10 to 20.4 dB along the wavelength span of 55 nm from 1525 to 1580 nm. Besides that, the noise figure is less than 12.1 dB within this 55 nm wavelength region. However, at input signal power of -10 dBm, the gain fluctuates from 9.5 to 11.4 dB along the wavelength span of 50 nm from 1525 to 1575 nm. Within this 50 nm wavelength span, the noise figure is less than 12.8 dB. It can be observed that the gain suddenly increases beyond 1565 nm, for all LD2 powers. This is due to the change in the amplification medium from 22 cm to 150 cm long HB-EDF.

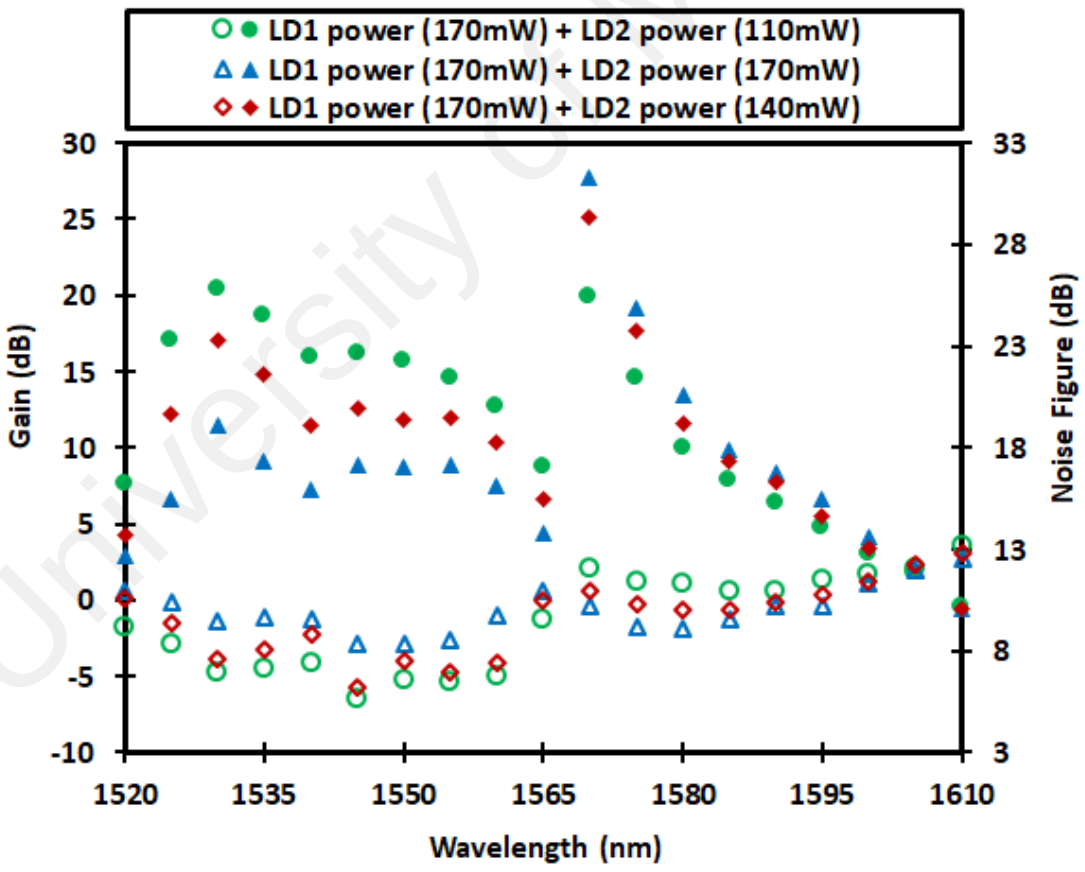

Figure 4.8: Measured gain (solid symbol) and noise figure (hollow symbol) spectra of the forward pumping-based series HB-EDFA using 1.72 m long of the total active fiber, at various LD2 powers when the input signal power is set at -30 dBm.

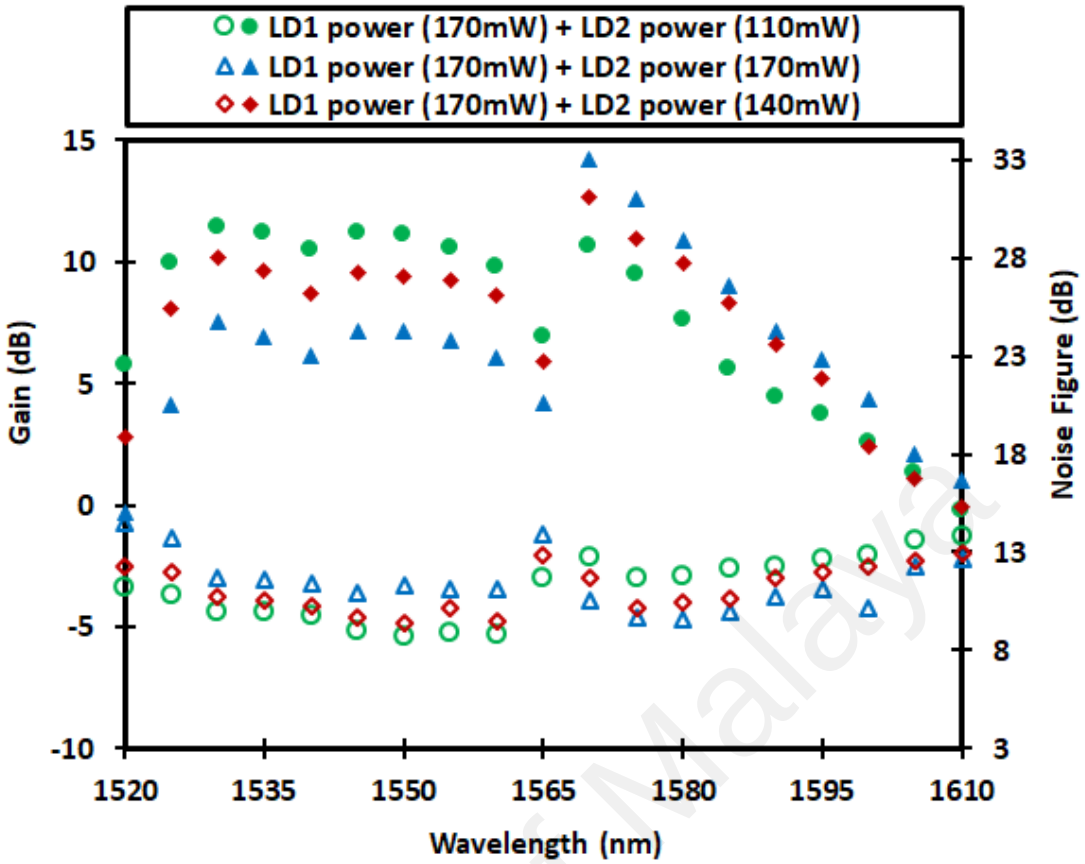

Figure 4.9: Measured gain (solid symbol) and noise figure (hollow symbol) spectra of the forward pumping-based series HB-EDFA using 1.72 m long of the total active fiber, at various LD2 powers when the input signal power is set at -10 dBm.

It can be seen in Figures 4.8 and 4.9 that the L-band gain spectrum rises as the LD2 power increases. However, the increment in the gain spectrum declines when the LD2 power increases from 140 to 170 mW. This is most probably owing to the gain saturation effect. Meanwhile, the C-band gain spectrum descends when LD2 power increases above 110 mW, although LD1 power is fixed. This is due to the high backward ASE noise effect from the second stage at the input port of the first stage amplifier, which reduces the population inversion, and hence reduces the C-band gain spectrum. On the other hand, the L-band noise figure spectrum decreases as LD2 power increases. This is owing to the higher gain and lower loss resulting from higher LD2 power. Besides that, the C-band

noise figure spectrum is increased as LD2 power increased, due to the increment of ASE noise effect.

4.3.2 Backward pumping for 1.72 m long HB-EDF

In this amplifier configuration, the HB-EDFs are also adjusted at 22 cm and 150 cm long respectively, for amplification in C and L-bands so that the total length is 1.72 m. The shorter HB-EDF is backward pumped by using a 980 nm LD1, while the longer HB-EDF is backward pumped by using a 1480 nm LD2. Figures 4.10 and 4.11 show the gain and noise figure spectra of the backward pumping-based series HB-EDFA at various L-band pump powers, for input signal powers of -30 dBm and -10 dBm, respectively. In the experiment, the LD1 power is fixed at 170 mW while the LD2 power which controls the L-band gain, is varied from 110 mW to 140 mW and then to 170 mW. It is clearly shown that the variation of the LD2 power changes the gain and noise figure performances of the amplifier for both input signal powers. The gain at L-band region increases as the LD2 power increases before it saturates as the LD2 power exceeds 140 mW. Meanwhile, the C-band gain spectrum descends when LD2 power increases above 110 mW, although LD1 power is fixed. This is due to the effect of high forward ASE from the second stage which reduces the population inversion, and hence reduces the C-band gain spectrum. On the other hand, the L-band noise figure spectrum decreases as LD2 power increases. This is owing to the higher gain and lower loss resulting from higher LD2 power. Besides that, the C-band noise figure spectrum is increased as LD2 power increased, due to the increment of ASE noise effect. Overall, it can be inferred that the optimum laser diodes powers to achieve even better performance in term of gain, noise figures and bandwidth are 170 mW and 110 mW for LD1 and LD2, respectively.

At input signal power of -30 dBm with the optimum LDs powers, the gain fluctuates from 10.1 to 21.6 dB along the wavelength span of 75 nm from 1520 to 1595 nm. It can be observed that the gain suddenly increases beyond 1565 nm. This is attributed to the change in the input signal from C-band to L-band wavelength and thus, the signal is amplified in both first and second stages. On the other hand, the noise figure is less than 10.5 dB within the wavelength region from 1520 to 1600 nm. At high input signal power of -10 dBm, a flat gain of 11.7 dB is realized with a gain ripple of less than 2 dB, along the wavelength region of 65 nm from 1525 to 1590 nm. Within the flat gain region, the noise figure values vary from 6.7 to 11.2 dB.

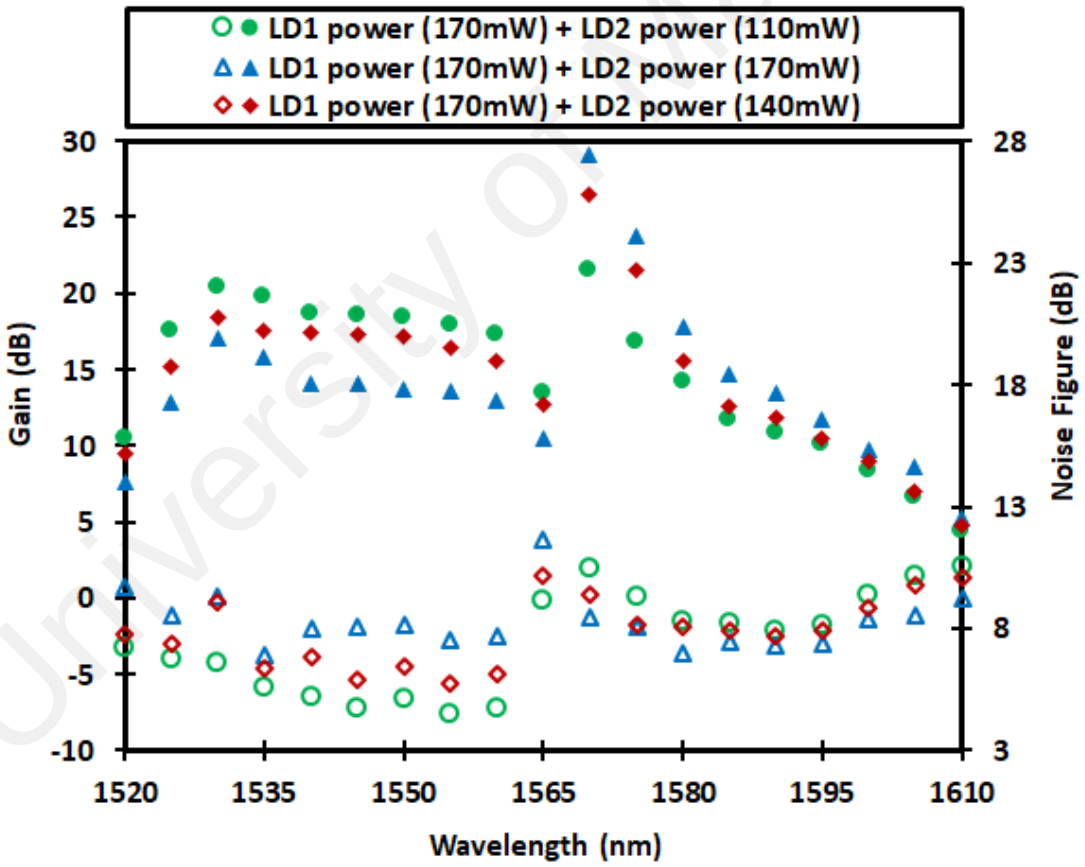

Figure 4.10: Measured gain (solid symbol) and noise figure (hollow symbol) spectra of the backward pumping-based series HB-EDFA using 1.72 m long of the total active fiber, at various LD2 powers when the input signal power is set at -30 dBm.

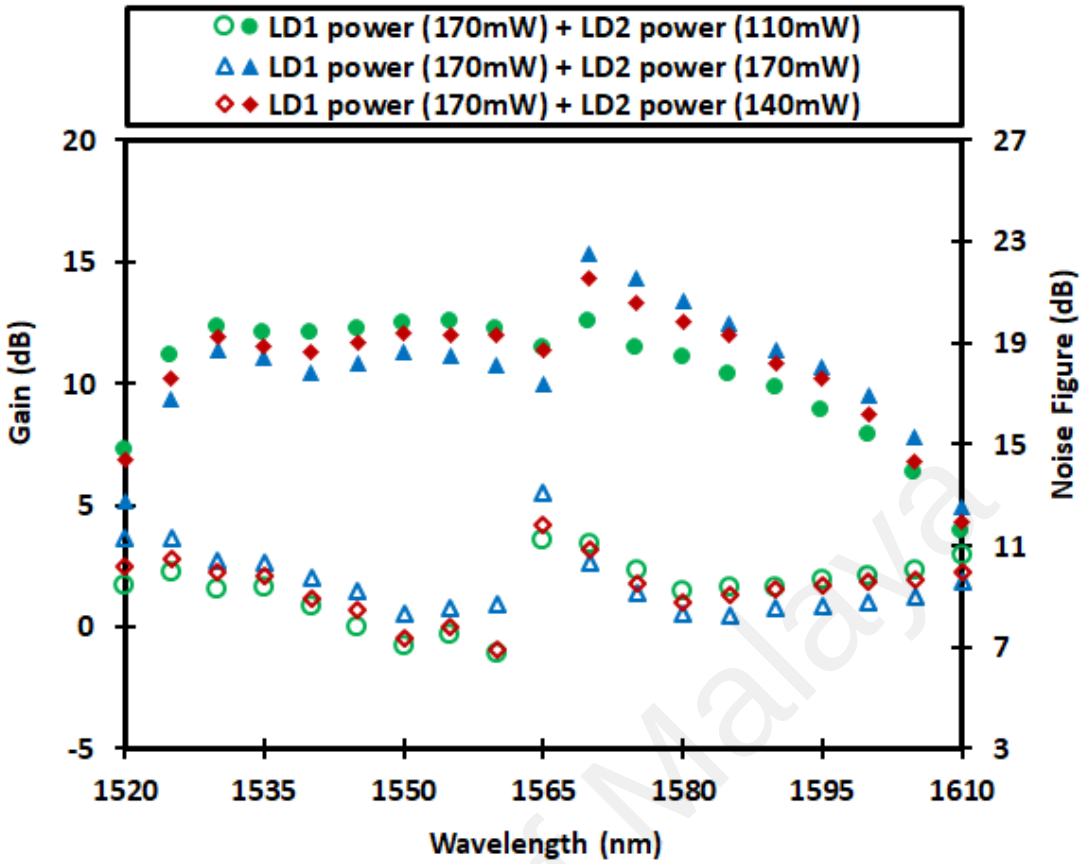

Figure 4.11: Measured gain (solid symbol) and noise figure (hollow symbol) spectra of the backward pumping-based series HB-EDFA using 1.72 m long of the total active fiber, at various LD2 powers when the input signal power is set at -10 dBm.

4.3.3 Comparison performance of forward and backward pumping

The performance comparison between forward and backward pumping for series HB-EDFA is investigated, at the optimum LDs powers when the length of the HB-EDFs are fixed at 22 cm and 150 cm in the first and second stage, respectively. Figures 4.12 and 4.13 show the amplification performance comparisons at input signal power of -30 dBm and -10 dBm, respectively. The comparisons show that the backward pumping amplifier obtains a higher gain and lower noise figure than that of the forward pumping

amplifier. This is attributed to the saturation effect of ASE, which is weaker with the backward pumping.

With backward pumping amplifier at -30 dBm input signal power, an average gain enhancement of around 2.5 dB and 4.1 dB are observed along the C-band and L-band wavelength regions, respectively. However, at input signal power of -10 dBm, an average gain enhancement of around 1.7 dB and 4.1 dB are observed along the C-band and L-band wavelength regions, respectively. Furthermore, the backward pumping amplifier shows a more efficient wideband and flatter gain spectrum as compared to that of forward pumping amplifier. On the other hand, a lower noise figure is obtained with backward pumping amplifier.

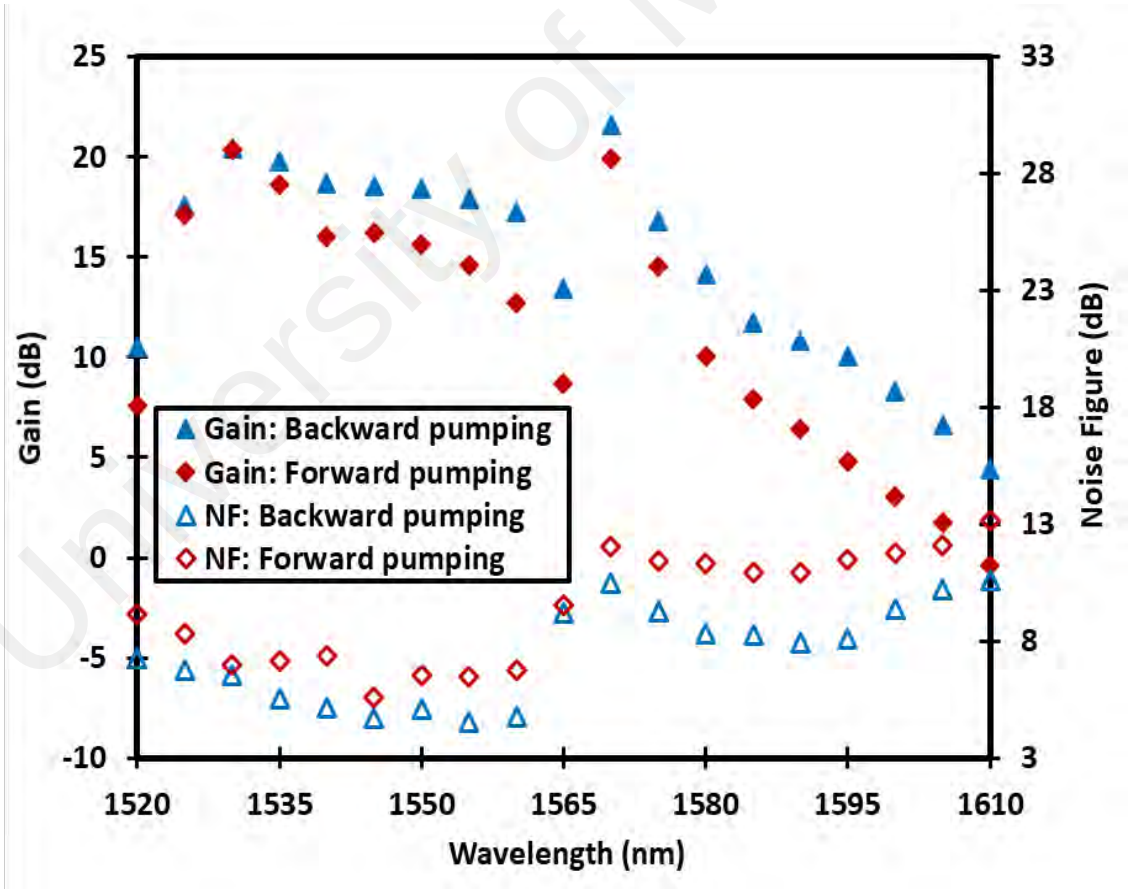

Figure 4.12: Comparison of the gain and noise figure characteristics between the forward and backward pumping-based series HB-EDFAs at input power of -30 dBm.

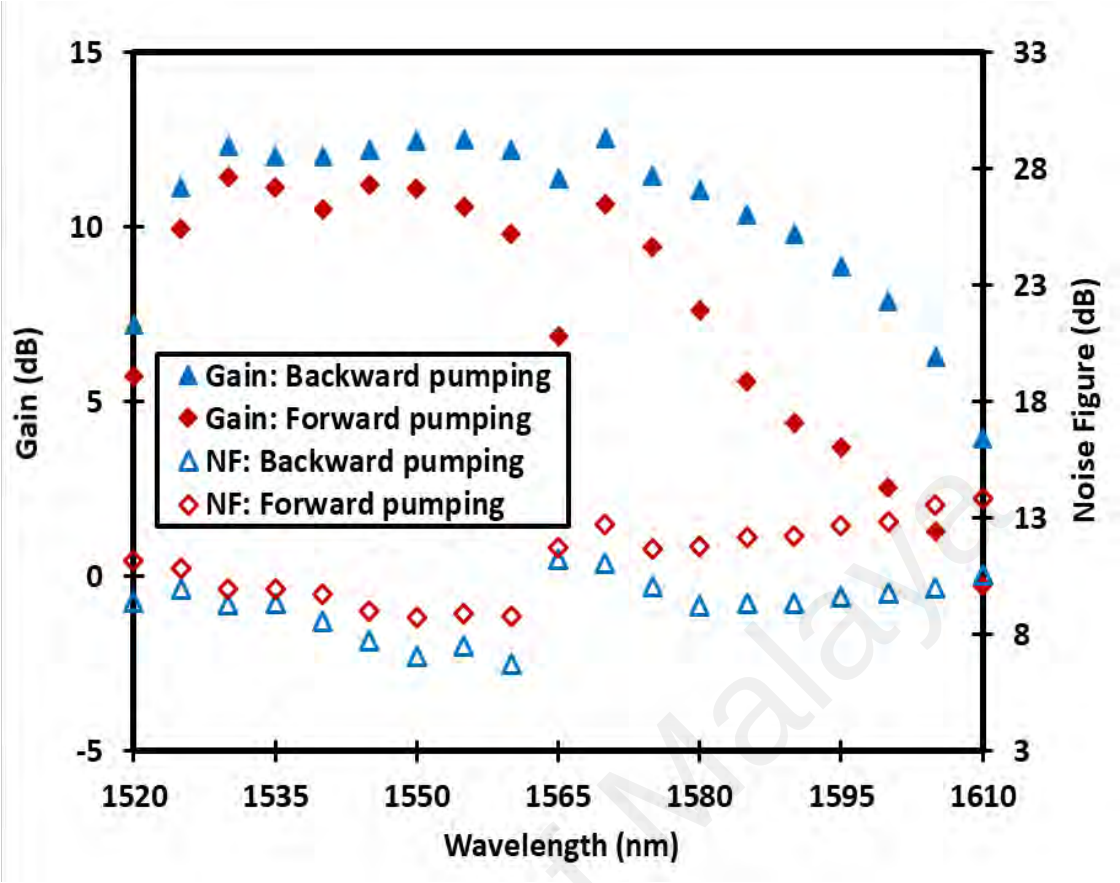

Figure 4.13: Comparison of the gain and noise figure characteristics between the forward and backward pumping-based series HB-EDFAs at input power of -10 dBm.

4.3.4 Backward pumping for 2 m long HB-EDF

Since the backward pumping of the series HB-EDFA displays a preferable performance, this technique is adopted to accomplish a wideband HB-EDFA using another length of HB-EDF. In the experiment, the HB-EDFs are also adjusted at 50 cm and 150 cm long respectively, for amplification in C and L-bands so that the total length is 2 m. The C-band HB-EDF is backward pumped by using a 980 nm LD1, while the L-band HB-EDF is backward pumped by using a 1480 nm LD2. Figures 4.14 and 4.15 present the performance of the backward pumping-based series HB-EDFA at various L-band pump powers, for input signal powers of -30 dBm and -10 dBm, respectively. In the

experiment, the LD1 power is fixed at 170 mW while the LD2 power which controls the L-band gain, is varied from 110 mW to 170 mW. It is obvious that the optimum laser diodes powers to achieve even better performance in term of gain, noise figures and bandwidth are 170 mW and 140 mW for LD1 and LD2, respectively. At input signal power of -30 dBm with the optimum LDs powers, the gain fluctuates from 10.9 to 30 dB along the wavelength span of 85 nm from 1520 to 1605 nm. Besides that, the noise figure is less than 9 dB within this 85 nm wavelength region. However, at high input signal power of -10 dBm, a flat gain of 14.6 dB is realized with a gain ripple of less than 2 dB, along the wavelength region of 65 nm from 1530 to 1595 nm. Within the flat gain region, the noise figure values vary from 6.8 to 10.2 dB.

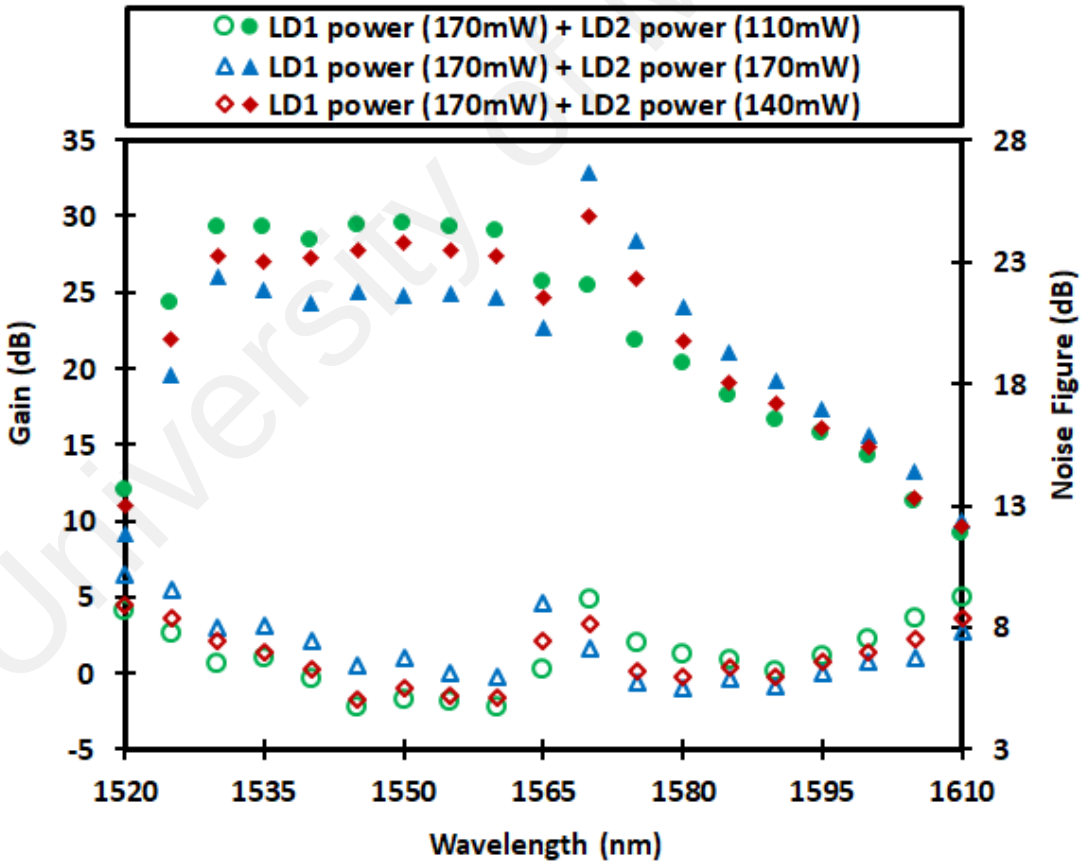

Figure 4.14: Measured gain (solid symbol) and noise figure (hollow symbol) spectra of the backward pumping-based series HB-EDFA using 2 m long of the total active fiber, at various LD2 powers when the input signal power is set at -30 dBm.

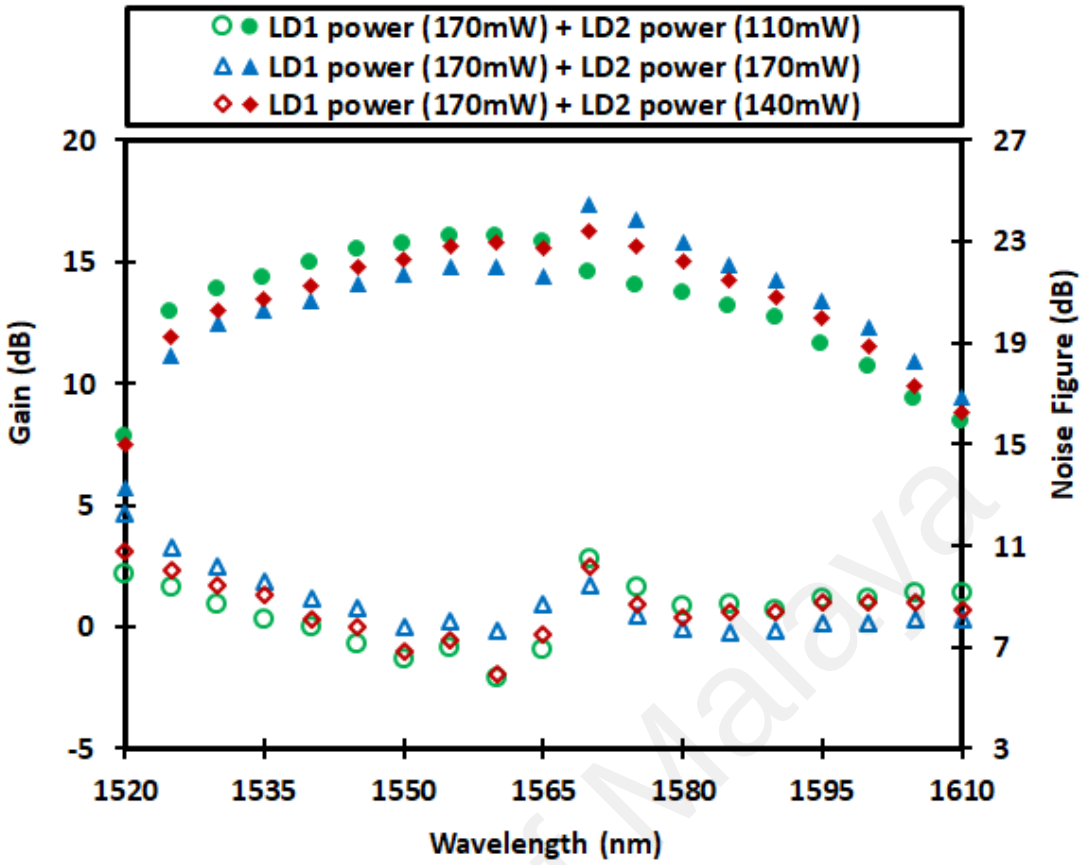

Figure 4.15: Measured gain (solid symbol) and noise figure (hollow symbol) spectra of the backward pumping-based series HB-EDFA using 2 m long of the total active fiber, at various LD2 powers when the input signal power is set at -10 dBm.

Similar to the backward pumping-based series HB-EDFA configured with 1.72 long HB-EDF, L-band gain spectrum of the amplifier rises as the LD2 power increases as shown in Figures 4.14 and 4.15. However, this increment rate drastically declines when the LD2 power increases from 140 to 170 mW. The C-band gain spectrum is also observed to descend when LD2 power increases above 110 mW. On the other hand, the L-band noise figure spectrum decreases as LD2 power increases. However, the C-band noise figure spectrum is increased as LD2 power increased. Finally, the performance comparison of the proposed backward pumping-based series HB-EDFA with two

different total HB-EDF lengths is summarized in Table 4.2. The comparison shows both amplifiers obtain an efficient amplification with wideband operation region from 1520 to 1610 nm. The series HB-EDFA that using 2 m long HB-EDF achieves a higher gain, lower noise figure and broader wavelength amplification as well. However, the series HB-EDFA with 1.72 m long HB-EDF requires lower LDs power to operate due to lower Erbium concentration.

Table 4.2: The performance comparison of the proposed series HB-EDFAs that using backward pumping technique.

Merit	**Series HB-EDFA using 1.72 m long HB-EDF**	**Series HB-EDFA using 2.0 m long HB-EDF**
Erbium fiber lengths	Total length: 1.72 m. 22 cm for C-band region. 150 cm for L-band region.	Total length: 2 m. 50 cm for C-band region. 150 cm for L-band region.
Optimum LDs powers	LD1 power: 170 mW. LD2 power: 110 mW.	LD1 power: 170 mW. LD2 power: 140 mW.
Wideband amplification	At input signal power of -30 dBm • The gain fluctuates from 10.1 to 21.6 dB along the wavelength span of 75 nm. • The NF is less than 10.5 dB.	At input signal power of -30 dBm • The gain fluctuates from 10.9 to 30 dB along the wavelength span of 85 nm. • The NF is less than 9.0 dB.

Table 4.2, continued.

Merit	Series HB-EDFA using 1.72 m long HB-EDF	Series HB-EDFA using 2.0 m long HB-EDF
Wideband amplification	At input signal power of -10 dBm • A flat gain of 11.7 dB with a gain ripple of ± 2 dB, along the wavelength span of 65 nm is realized. • The NF values vary from 6.7 to 11.2 dB.	At input signal power of -10 dBm • A flat gain of 14.6 dB with a gain ripple of ± 2 dB, along the wavelength span of 65 nm is realized. • The NF values vary from 6.8 to 10.2 dB.

4.4 Broadband amplified spontaneous emission (ASE) source

An efficient broadband ASE light source is also investigated and achieved using two sections of HB-EDF in series and parallel structures. The proposed ASE source covers both of C- and L-telecommunication bands. The ASE is produced by spontaneous emission due to the population inversion when the erbium fiber is pumped. In this work, the previous configurations of parallel and series HB-EDFA is utilized to produce a broadband ASE by taking off the TLS and POA. In the experiment, the power of both LDs is fixed at the maximum of 170 mW for each configuration. The ASE source is also demonstrated for two different lengths of the HB-EDFs, which are 1.72 m (22 cm + 150cm) and 2 m (50cm + 150cm).

Figure 4.16 shows the ASE spectra which are obtained from series and parallel configurations, when the total length of the HB-EDF is 1.72 m. It is found that the highest C-band ASE spectrum is obtained with parallel configuration. However, the highest L-

band ASE spectrum is obtained with backward pumping-based series configuration. With forward and backward series configurations, two peaks laser is observed at 1568 nm wavelength. This is due to the spurious reflection in the cavity, which suppresses the ASE level around it and affects the gain level at this wavelength region. To eliminate this laser, the power of LD2 should be decreased. Overall, a relatively broad and reasonable ASE light spectrum is achieved at the parallel configuration. The ASE power achieved varies from -55 dBm to -37 dBm within wavelength region from 1525 nm to 1600 nm.

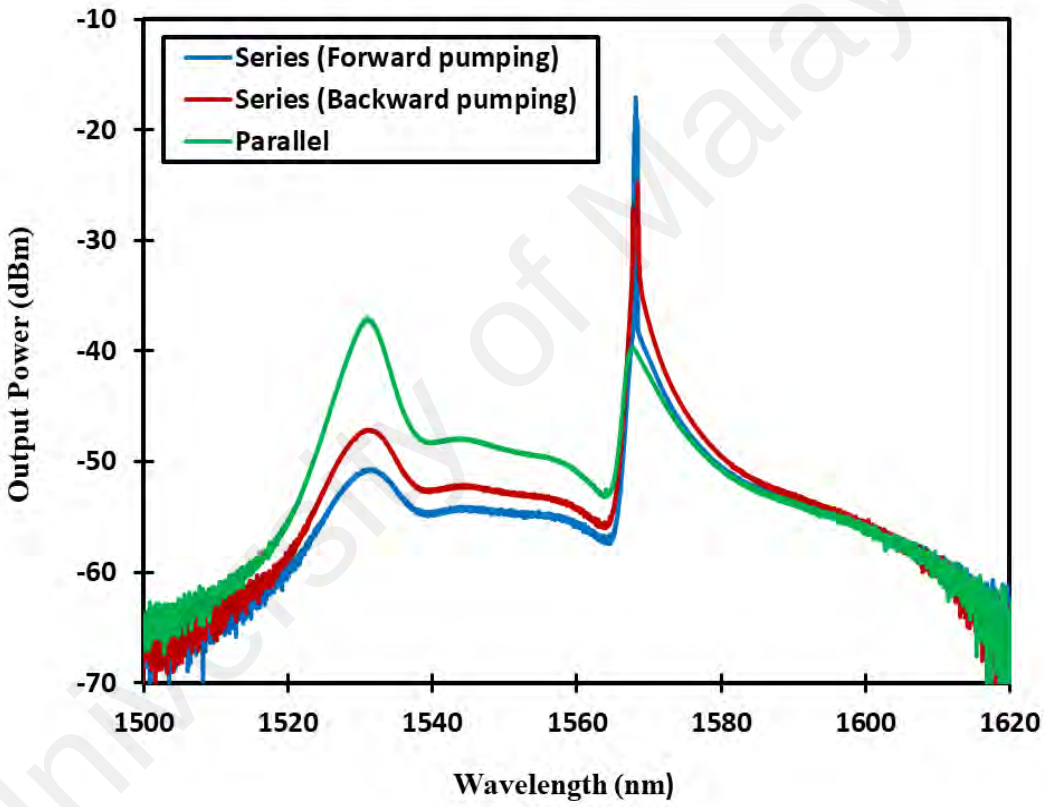

Figure 4.16: Broadband ASE spectra when the total length of the HB-EDF is 1.72 m.

Figure 4.17 shows the ASE spectra which are obtained from series and parallel configurations, when the total length of the HB-EDF is 2 m. It is obvious that the highest C-band and L-band ASE spectra are obtained with parallel and backward pumping-based series configurations, respectively. A peak laser is also observed at 1568 nm wavelength

with forward pumping-based series configuration. Overall, a broad and reasonable ASE light spectrum is achieved at the backward pumping-based series configuration. The ASE power achieved varies from -51 dBm to -24 dBm within wavelength region from 1520 nm to 1600 nm.

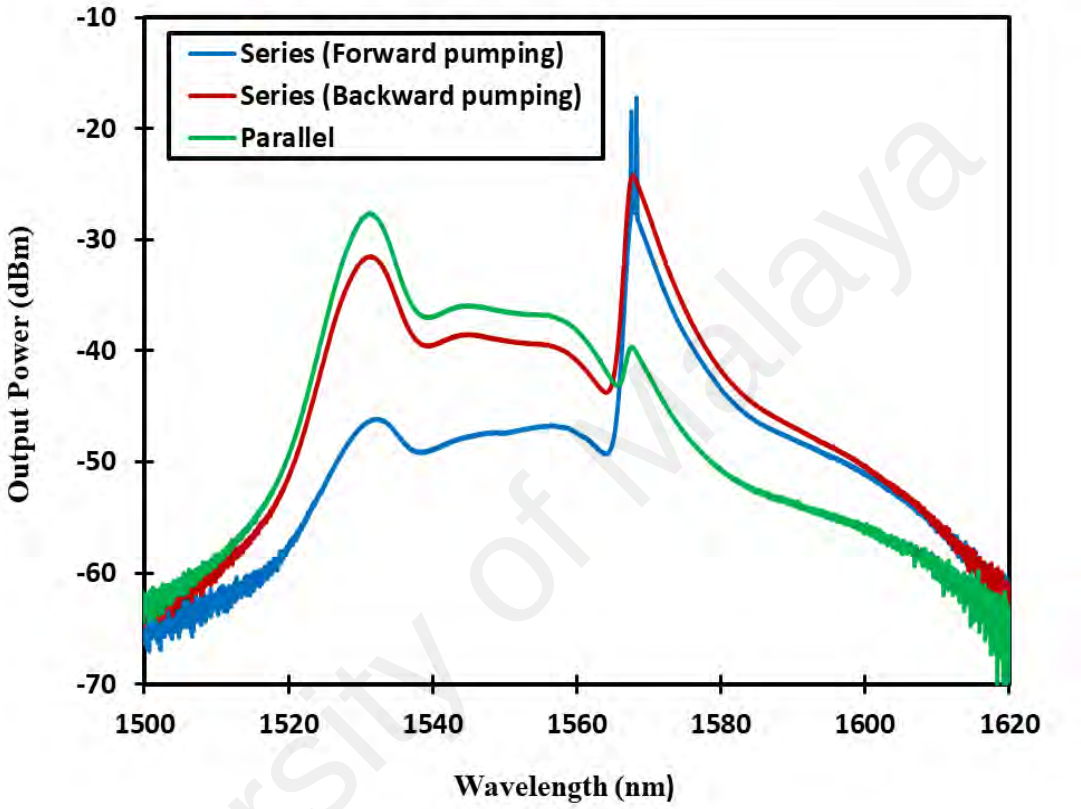

Figure 4.17: Broadband ASE spectra when the total length of the HB-EDF is 2 m.

4.5 Summary

In this chapter, a compact wideband HB-EDFA and ASE source were experimentally demonstrated and developed, utilizing a newly fabricated HB-EDF as a gain medium. The proposed amplifier was investigated by utilizing two short lengths of HB-EDF sections to fulfill amplification in C- and L-telecommunication bands. The wideband HB-EDFA was achieved using two stages in both series and parallel structures

in conjunction with double-pass scheme. The performance of the amplifier was investigated for two different lengths of the HB-EDFs, as well as various pump powers to determine the optimum design. During the experiments, first, the HB-EDFs were adjusted at 50 cm and 150 cm long respectively, for amplification in C and L-bands so that the total length is 2 m. Second, the HB-EDFs were adjusted at 22 cm and 150 cm long respectively, for amplification in C and L-bands so that the total length is 1.72 m. On the other hand, the LD1 power was fixed at the maximum power of 170 mW. Nevertheless, the LD2 power which controls the L-band gain, was varied from 110 mW to 140 mW and 170 mW. For comparison purpose, the series HB-EDF was examined in both backward and forward pumping schemes.

It can be concluded that both parallel and backward pumping-based series HB-EDFAs obtain a wideband operation within 1520 nm to 1610 nm. Besides, a flat gain characteristic was achieved throughout C- and L- bands wavelengths region. For instance, in parallel HB-EDFA that using 1.72 m long HB-EDF, a flat gain of 12.1 dB was realized with a gain ripple of less than 2 dB, along the wideband wavelength region of 80 nm from 1525 to 1605 nm. Within the flat gain region, the noise figure values varied from 6 to 11.8 dB. However, in backward pumping-based series HB-EDFA that using 2 m long HB-EDF, a flat gain of 14.6 dB was realized with a gain ripple of less than 2 dB, along the wavelength region of 65 nm from 1530 to 1595 nm. Within the flat gain region, the noise figure values varied from 6.8 to 10.2 dB. It can be inferred that the backward pumping-based series HB-EDFA achieves higher flat gain with lower noise figure. However, the flat gain region was larger with parallel HB-EDFA than that with backward pumping-based series HB-EDFA. Table 4.3 summarize the amplification performance of the proposed parallel and backward pumping-based series HB-EDFAs.

Finally, a broadband amplified spontaneous emission (ASE) light source was also investigated and achieved using two pieces of HB-EDF in series and parallel structures.

The proposed ASE source covers both of C- and L-bands wavelength region. The ASE source was also demonstrated for two different lengths of the HB-EDFs, which are 1.72 m (22 cm + 150cm) and 2 m (50cm + 150cm).

Table 4.3: The amplification performance of the parallel and backward pumping-based series HB-EDFAs.

Type	At -10 dBm input signal power	At -30 dBm input signal power
Parallel HB-EDFA using 1.72 m long HB-EDF **LD1: 170 mW** **LD2: 140 mW**	• A flat gain of 12.1 dB with a gain ripple of ± 2 dB, along the wavelength span of 80 nm is realized. • The NF values vary from 6 to 11.8 dB.	• The gain fluctuates from 10.5 to 24 dB along the wavelength span of 90 nm. • The NF is less than 10.1 dB.
Parallel HB-EDFA using 2.0 m long HB-EDF **LD1: 170 mW** **LD2: 170 mW**	• The gain fluctuates from 11 to 16.4 dB along the wavelength span of 80 nm. • The NF values vary from 5.4 to 8.7 dB.	• The gain fluctuates from 11 to 30.1 dB along the wavelength span of 85 nm. • The NF is less than 7.8 dB.
Series HB-EDFA using 1.72 m long HB-EDF **LD1: 170 mW** **LD2: 110 mW**	• A flat gain of 11.7 dB with a gain ripple of ± 2 dB, along the wavelength span of 65 nm is realized. • The NF values vary from 6.7 to 11.2 dB.	• The gain fluctuates from 10.1 to 21.6 dB along the wavelength span of 75 nm. • The NF is less than 10.5 dB.

Table 4.3, continued.

Type	At -10 dBm input signal power	At -30 dBm input signal power
Series HB-EDFA using 2.0 m long HB-EDF **LD1: 170 mW** **LD2: 140 mW**	• A flat gain of 14.6 dB with a gain ripple of ± 2 dB, along the wavelength span of 65 nm is realized. • The NF values vary from 6.8 to 10.2 dB.	• The gain fluctuates from 10.9 to 30 dB along the wavelength span of 85 nm. • The NF is less than 9 dB.

CHAPTER 5: WIDEBAND ERBIUM DOPED FIBER AMPLIFIER AND ASE SOURCE USING HYBRID ACTIVE FIBERS AS THE GAIN MEDIUM

5.1 Introduction

The quest for covering the full range of dense wavelength division multiplexing (DWDM) system has encouraged a search for new optical fiber amplifiers with high gain, flat gain and low noise figure characteristics over a wideband operation span (Durak & Altuncu, 2018). A hybrid erbium doped fiber amplifier (EDFA) was previously proposed to enhance the DWDM communication system by improving the amplifier performances such as; the bandwidth, gain level, noise figure, and pump conversion efficiency (PCE) (Abass et al., 2018; Singh & Kaler, 2015). In general, two main topologies were normally used in designing the hybrid fiber amplifiers; series and parallel. The series type of hybrid EDFA consists of two amplification stages in single path, with two different erbium doped fibers (EDFs) (Ali et al., 2015). In this amplifier, the amplified output signal after the first EDF is considered as the input signal for the second stage of EDF. On the other hand, the parallel type of hybrid EDFA consists of two parallel stages, in which the input signal is separated into two different wavelength bands (Harun et al., 2011). In this amplifier, the C-band signal is amplified only in the first stage, while the L-band signal is amplified only in the second stage.

Previously, Hamida et al. (2012) proposed and demonstrated a wideband hybrid EDFA utilizing two stages in series structure, by using a combination of bismuth-based erbium doped fiber (Bi-EDF) and silica-based erbium-doped fiber (Si-EDF) as the gain medium. Unfortunately, this amplifier has produced a relatively high noise figure as compared to the achieved gain. Furthermore, the total length of the EDFs used was 9 m

which is considered very long. Besides, Bi-EDFs have a problem in splicing with standard SMFs by utilizing a standard splicing machine. In another study, the combination of zirconia-erbium doped fiber (Zr-EDF) and Si-EDF were used in series and parallel structures to achieve a wideband hybrid EDFA (Hamida et al., 2016). However, the total length of EDF used in this amplifier was relatively longer (11 m). Besides, the series amplifier could not achieve flat gain over the wideband operation region. The employment of a large number of separated stages in the hybrid amplifiers is unbeneficial both economically and technically (Firstov et al., 2017; Harun et al., 2011). Therefore, minimizing the size of optic components is one of the key factors in designing an efficient hybrid EDFAs.

In this chapter, a new wideband and flat gain hybrid EDFA is proposed and demonstrated, by employing a recently developed hafnia-bismuth erbium co-doped fiber (HB-EDF) and Zr-EDF as the gain medium. The proposed amplifier comprises of a 0.5 m long HB-EDF and 4 m long Zr-EDF as a hybrid active fiber to fulfill amplification in C- and L-telecommunication bands, respectively. The proposed amplifier is investigated for both series and parallel structures in conjunction with double-pass scheme. In addition, the series amplifier is examined in both backward and forward pumping schemes. A new pumping distribution technique is also proposed to demonstrate not only an efficient amplification performance, but also a cost reduction since only one laser diode is utilized to pump two stages. This is a new technique can be used to improve the conventional forward, backward and dual pumping for the multi-stage amplifiers. At the end of this chapter, a broadband amplified spontaneous emission (ASE) light source is also proposed and demonstrated by using the hybrid active fibers in series and parallel structures. The proposed ASE source covers both C- and L-band wavelength regions.

5.2 The L-band amplification with Zr-EDF

In the proposed hybrid EDFA, a hafnia-bismuth erbium co-doped fiber (HB-EDF) and zirconia erbium co-doped fiber (Zr-EDF) are used to allow a wideband amplification. The HB-EDF and Zr-EDF cover the amplification in C- and L-telecommunication bands, respectively. Consequently, the double-pass Zr-EDFA is also investigated to optimize the required Zr-EDF length for amplification in L-band region. The Zr-EDF was obtained from a fiber perform, which was fabricated in a ternary class host, zirconia-yttria-aluminum co-doped silica fiber using modified chemical vapor deposition (MCVD) in conjunction with solution doping (SD) process. The Zr-EDF was drawn from the over cladded preform utilizing a standard fiber drawing technique at a temperature of 2000 °C. The fabricated Zr-EDF has an absorption loss of 14.5 dB/m at 980 nm, which can be translated to the erbium ion concentration of 2800 wt. ppm. The optical fiber specifications of the Zr-EDF and HB-EDF are given in Table 5.1.

The double pass Zr-EDFA setup is shown in Figure 5.1. A 980 nm laser diode is used to forward pumped the Zr-EDF via a 980/1550 nm WDM coupler. Two optical circulators are utilized at the input and output ports of the amplifier to permit double propagation of the signal in the erbium fiber. At the input port, an optical circulator is utilized to launch the input signal into the WDM, and to extract the doubly amplified signal to the optical spectrum analyzer (OSA). At the output port, the optical circulator functioned as a broadband loop mirror for reflecting the amplified signal into the erbium fiber. The broadband loop mirror is constructed by joining port 3 with port 1 of the circulator so that the signal from port 2 is routed back into the same port. The performance of double pass Zr-EDFA is investigated for three different doped fiber lengths, 2 m, 4 m and 6 m. In the experiment, the input signal power is controlled by the programmable optical attenuator (POA). The gain and noise figure of the double-pass amplifier are investigated using a tunable laser source (TLS) in conjunction with an OSA.

Table 5.1: The optical fiber specification of the HB-EDF as compared to the conventional Zr-EDF.

Merit	HB-EDF	Zr-EDF
Fibers preform	Hafnium-bismuth-erbium co-doped yttria-aluminum silica fiber	Zirconia-yttria–aluminum–erbium co-doped silica fiber
Erbium ion concentration	12500 wt. ppm	2800 wt. ppm
Absorption loss	100 dB/m at 980 nm	14.5 dB/m at 980 nm
Fiber Diameter	123.94 µm	125 µm
Numerical Aperture	0.21	0.17

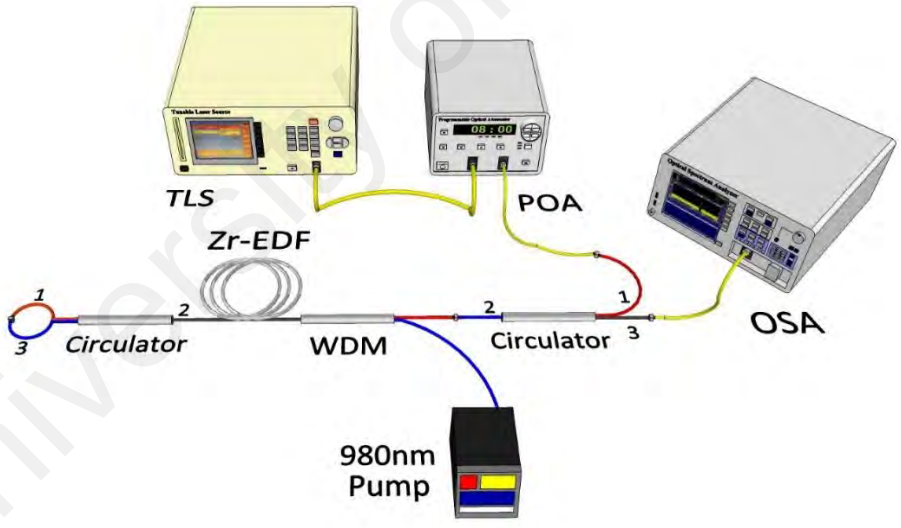

Figure 5.1: Experimental setup of the double pass L-band Zr-EDFA.

Figures 5.2 and 5.3 show the gain and the noise figure spectra of the double pass Zr-EDFA for the input signal powers of -30 dBm and -10 dBm, respectively. These measured results were obtained under the pumping power of 140 mW. At the input signal power of -30 dBm, it is found that the 4 m long Zr-EDF provides the best amplification

performance especially in the L-band region. At 4 m long Zr-EDF, the amplifier's gain varies from 17.7 to 34.3 dB within a wavelength range from 1565 to 1600 nm. The corresponding noise figures are less than 6 dB within the same wavelength region. Meanwhile, the 4 m long Zr-EDF also achieved the best amplification performance for -10 dBm input signal power. At 4 m long Zr-EDF, a flat gain of 16 dB is realized with a gain ripple of less than 1.5 dB, along the 45 nm wavelength region from 1555 to 1600 nm. Within the flat gain region, the noise figure is less than 8.5 dB. For both input signal powers, it can be observed that the amplifier's gain of the 2 m long Zr-EDF declines gradually at the wavelengths above 1565 nm. This is due to the length of the active fiber which is short and not compatible for L-band wavelengths region. However, a low gain and high noise figure are obtained with 6 m long Zr-EDF. This is attributed to insufficient pump power to support the population inversion with a longer active fiber.

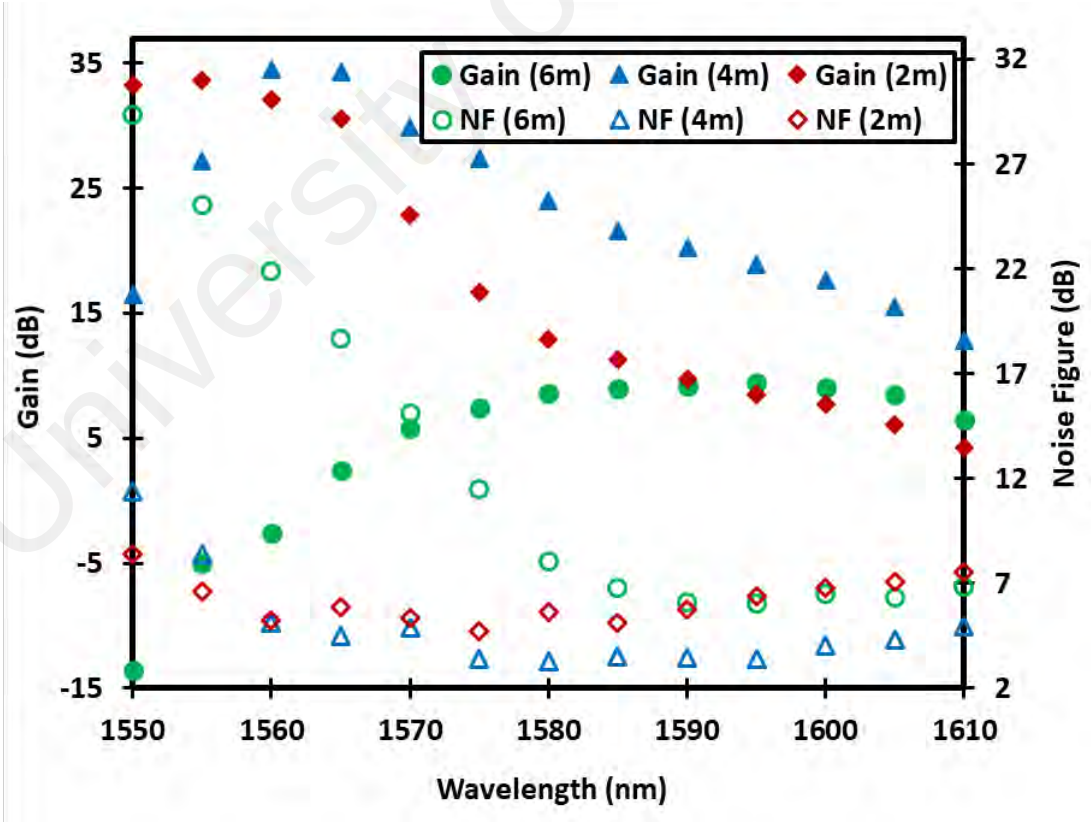

Figure 5.2: Gain and noise figure spectrums of the double pass Zr-EDFA at input signal power of -30 dBm.

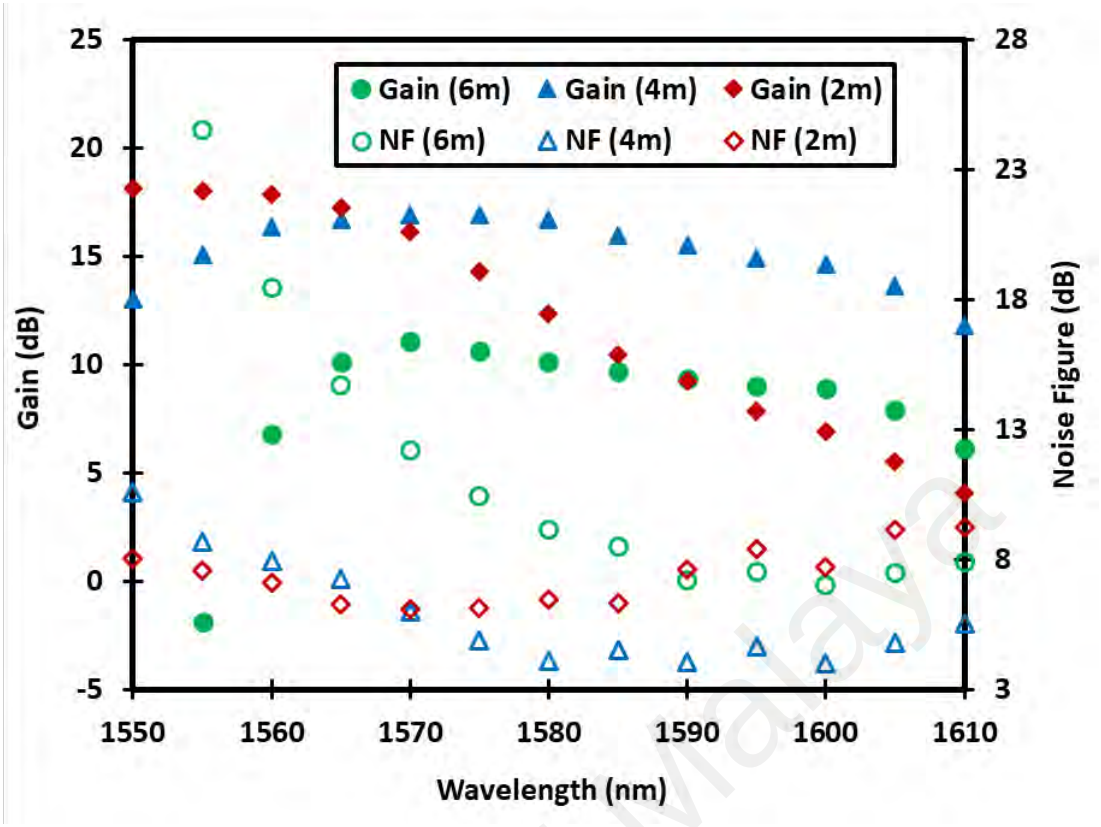

Figure 5.3: Gain and noise figure spectrums of the double pass Zr-EDFA at input signal power of -10 dBm.

5.3 The ASE spectrum of HB-EDF and Zr-EDF

In this section, the ASE spectra are investigated for both HB-EDF and Zr-EDF, which were obtained based on double-pass configuration of Figure 5.1. Figure 5.4 shows the ASE light spectrum at the optimized length of 0.5 and 4 m for HB-EDF and Zr-EDF, respectively. In the experiment, the 980 nm pump power is fixed at 140 mW for each investigated case. It is shown that the double-pass HB-EDF and Zr-EDF amplifier spectra peak at 1530 nm and 1565, respectively. This is attributed to the HB-EDF and Zr-EDF lengths, which are optimized for operation in the C- and L-band regions, respectively. It is also shown that the Zr-EDF gives an average power of 9 dB higher than its HB-EDF counterpart at L-band region. As we employ a long piece of active fiber, the operating

wavelength of the amplifier shifts to the L-band region due to a quasi-two-level absorption effect. As a conclusion, the 4 m long Zr-EDF achieved a high and broad ASE level at the L-band region, which in turn show the possibility to yield an efficient amplification at the long wavelengths. In addition, the 4 m long Zr-EDF proved that it is the optimum length among different lengths investigated. For these reasons, this fiber is combined with the HB-EDF as hybrid active fibers to achieve a wideband amplification.

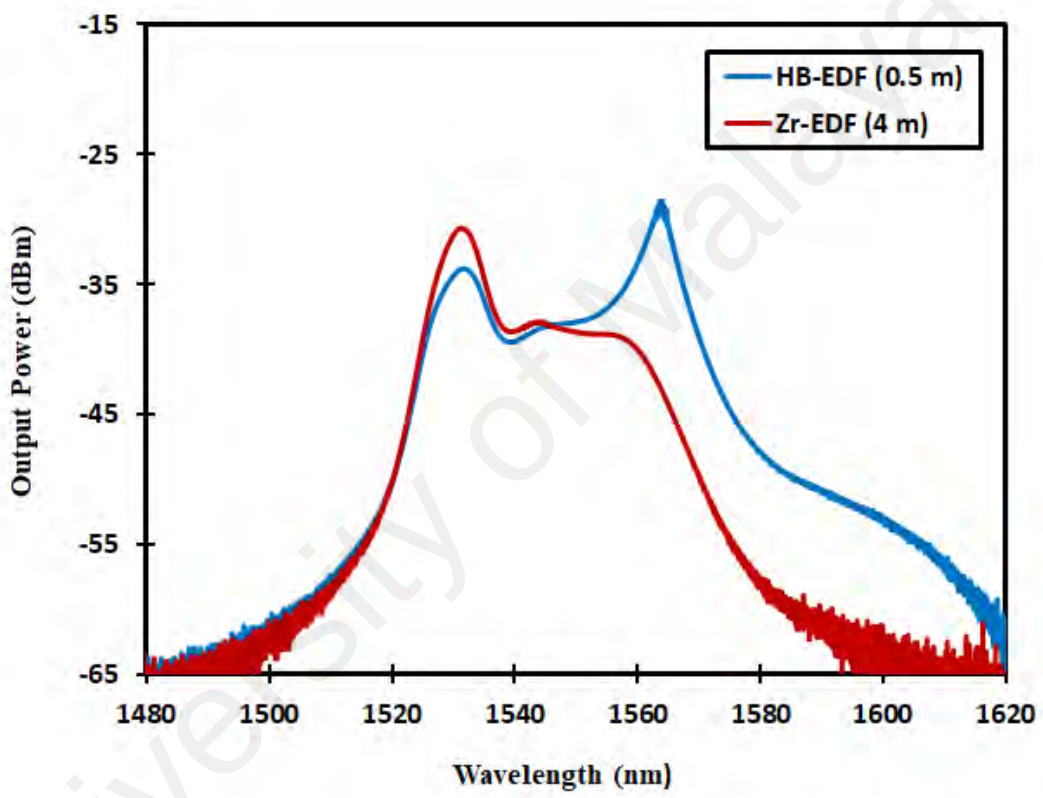

Figure 5.4: The ASE spectrum from double-pass HB-EDF and double-pass Zr-EDF under pump power of 140 mW.

5.4 Wideband EDFA using hybrid active fibers in parallel

The schematic diagram of the two-stage double-pass EDFA in conjunction with parallel configuration, is depicted in Figure 5.5. A 0.5 m long HB-EDF and 4 m long Zr-EDF are utilized as hybrid active fiber to produce amplification at C-band and L-band

region, respectively. Each stage is forward pumped by 980 nm laser diode (LD) via wavelength division multiplexer (WDM). A coarse wavelength division multiplexing (CWDM) filter is utilized to separate/ combine both C and L-band signals into/from C and L-band stages, respectively. At the input port, an optical circulator is utilized to deliver the input signal into the CWDM, and to extract the doubly amplified signal to the OSA. At the end of each stage, an optical circulator is used as a reflector so that the test signal is allowed to propagate twice in the active fiber. The amplified signal is allowed to reflect into the active fiber by joining port 3 with port 1 for the circulator. This allows the light from port 2 to be routed back into the same port. A TLS is used as a signal source while an OSA is utilized to test the gain and noise figure characteristics. A POA is utilized to provide an accurate input power to the amplifier. All the experiments were carried out at room temperature, ~25 °C.

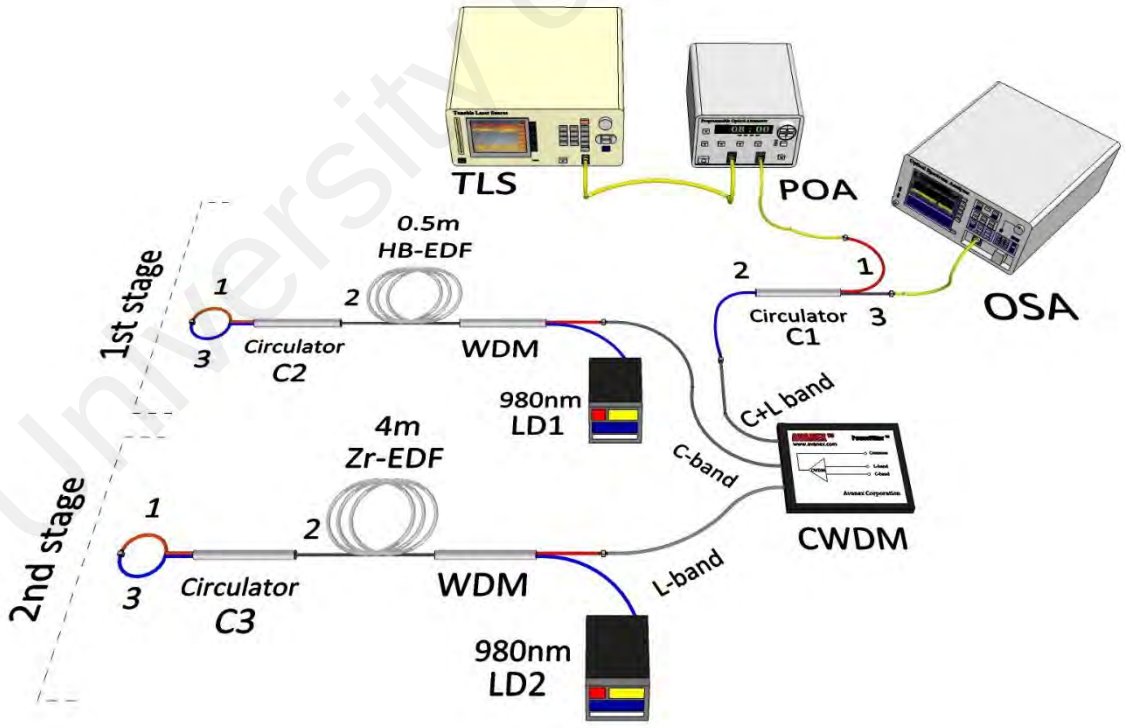

Figure 5.5: Two-stage double-pass hybrid EDFA in conjunction with parallel configuration.

During the experiment, the HB-EDF and Zr-EDF are pumped at 170 mW and 140 mW pump power, respectively. Figure 5.6 shows the gain and noise figure performances across wideband wavelength region for input signal powers of -30 dBm and -10 dBm. As shown in the figure, the proposed hybrid amplifier achieves a wideband operation in both input signal powers, which is operating in wavelength region from 1525 to1610 nm. For input signal power of -30 dBm, the gain fluctuates from 12 to 28.9 dB along the wavelength span of 90 nm from 1520 to 1610 nm. Furthermore, a flat gain of 28.1 dB is realized with a gain ripple of less than 1.6 dB, along the wavelength region of 45 nm from 1530 to 1275 nm. Within the flat gain region, the noise figure is less than 7.3 dB. At -10 dBm input signal, a flat gain of 15.6 dB is realized with a gain ripple of less than 1 dB, along the wideband wavelength region of 75 nm from 1525 to 1600 nm. Within the flat gain region, the noise figure values vary from 4.1 to 8.7 dB.

It can be inferred that the higher flat gain was observed at low input signal power of -30 dBm. However, the lower flat gain was observed at high input signal power of -10 dBm. This is due to the influence of the population inversion which is larger at low input signals powers, whereas the high input signals powers suppress the population inversion and hence reduce the attainable gain.

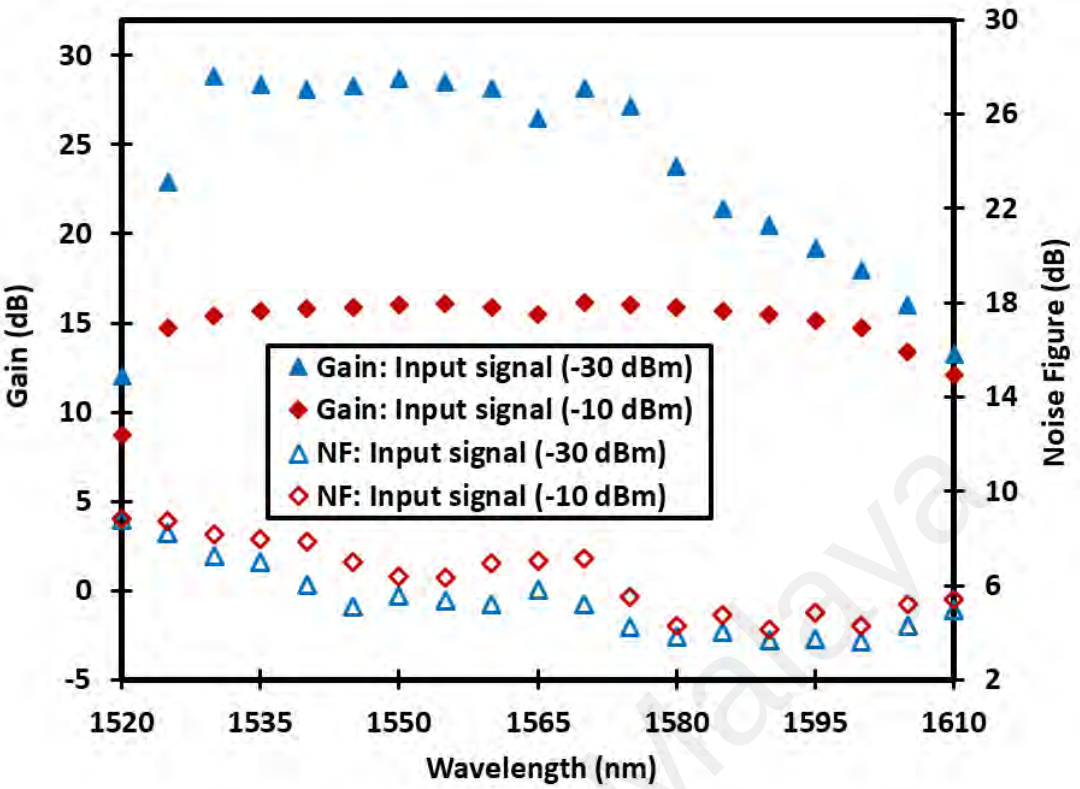

Figure 5.6: Gain and noise figure spectra of the parallel hybrid EDFA at input signal powers of -30 dBm and -10 dBm.

The performance of the proposed parallel hybrid amplifier is compared with an amplifier configured with the same gain medium for both stages. The HB-EDFs and Zr-EDFs have erbium concentration of 12500 ppm and 2800 ppm, respectively. For fair comparison with the proposed amplifier, the lengths of the HB-EDFs are fixed at 0.5 m and 0.9 m for C- and L-band stages, respectively. However, the lengths of the Zr-EDFs are fixed at 2.3 m and 4 m for C- and L-band stages, respectively so that the total amount of erbium ions in the fibers of each amplifier is similar. Figures 5.7 and 5.8 show the comparison of the gain and noise figure performances among the amplifiers for input signal powers of -30 dBm and -10 dBm, respectively. The comparison performance is investigated at LDs powers of 170 mW and 140 mW for LD1 and LD2, respectively. At

input signal power of -30 dBm, the proposed amplifier with hybrid gain medium achieves an efficient flat gain and lower noise figure compared to Zr-EDFA at C-band region. For instance, the gain improvement of more than 8 dB is obtained at wavelength of 1535 nm. This is attributed to the population inversion which is higher in shorter length of HB-EDF. The proposed amplifier also achieved higher gain and lower noise figure values compared to HB-EDFA at L-band region. This is due to the significantly higher erbium ion concentration in the HB-EDF and thus the available pump power is insufficient to provide population inversion with a longer active fiber. At -10 dBm input signal power, the proposed amplifier with hybrid gain medium achieves an efficient wideband and flat-gain as well as lower noise figure compared to Zr-EDFA and HB-EDFA.

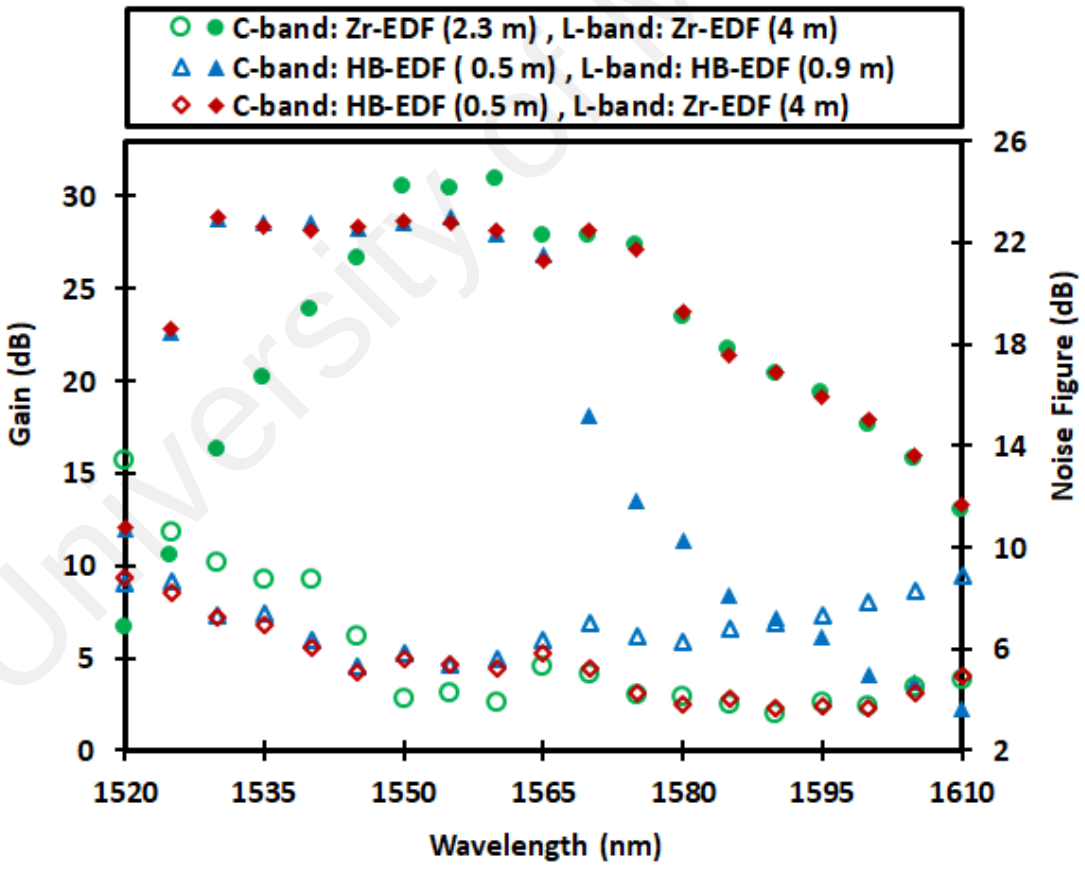

Figure 5.7: Gain (solid symbol) and noise figure (hollow symbol) performances of the parallel hybrid EDFA and the parallel EDFAs with same fibers, at input signal power of -30 dBm.

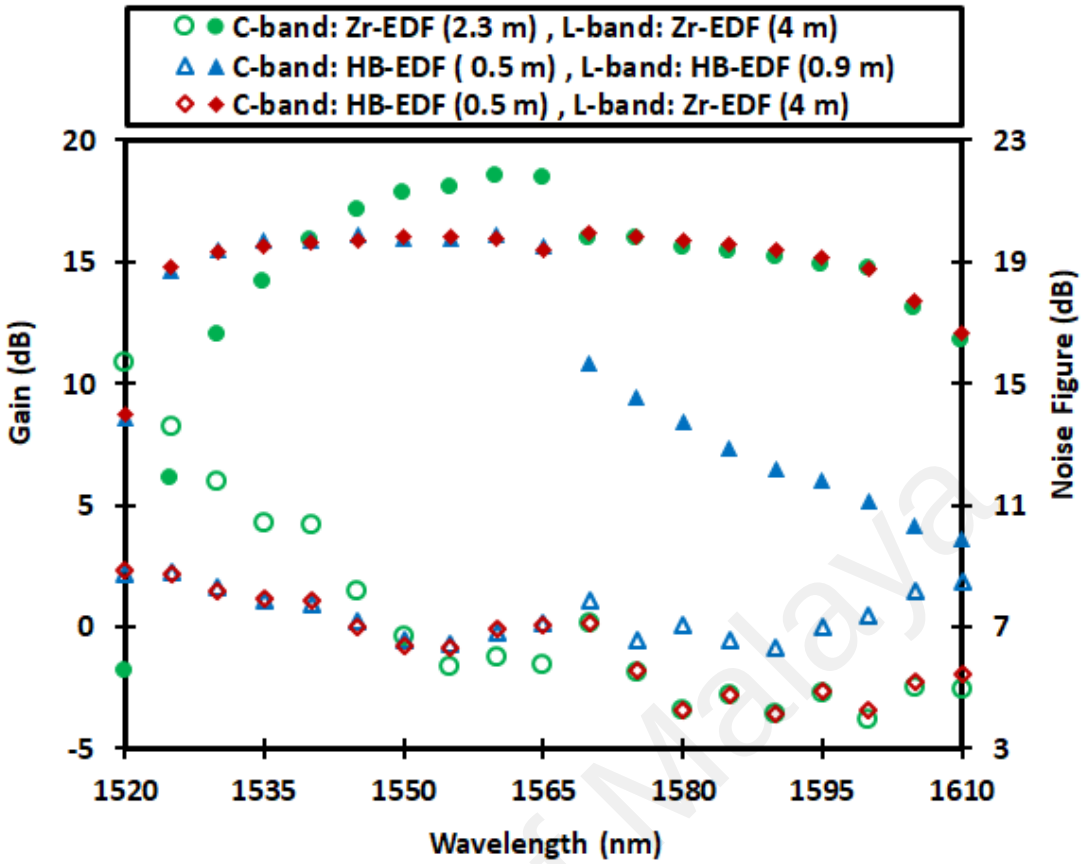

Figure 5.8: Gain (solid symbol) and noise figure (hollow symbol) performances of the parallel hybrid EDFA and the parallel EDFAs with same fibers, at input signal power of -10 dBm.

5.4.1 The optimization of the laser diodes powers

The LD2 power of the second stage (see Figure 5.5), which controls the L-band gains, is varied as shown in Figure 5.9 and Figure 5.10 for the input signal power of -30 dBm and -10 dBm, respectively. In the experiment, the LD1 power is fixed at the maximum power of 170 mW. Nevertheless, the LD2 power which controls the L-band gain, is varied from 110 mW to 140 mW and then to 170 mW. It can be observed that the L-band gain spectrum rises as the LD2 power increases for both input signal powers. However, the increment in the gain spectrum is slight, owing to the saturation effect. For

instance, at 1590 nm input wavelength and -30 dBm input signal power, the gain increases from 18.3 dB to 20.5 dB and 21.2 dB as the LD2 power changes from 110 mW to 140 mW and 170 mW respectively. The L-band noise figure is relatively higher when the LD2 power is fixed at 110 mW. This is due to the lower gain and higher loss related to the lower LD2 power. On the other hand, the gain and noise figure characteristics are almost unchanged at C-band region for both input signal powers of -30 and -10 dBm. This is due to the LD1 power of the first stage, which is fixed at 170 mW. It is found that the optimum laser diodes powers to achieve flat gain characteristics over a wideband operation region, are 170 mW and 140 mW for LD1 and LD2, respectively.

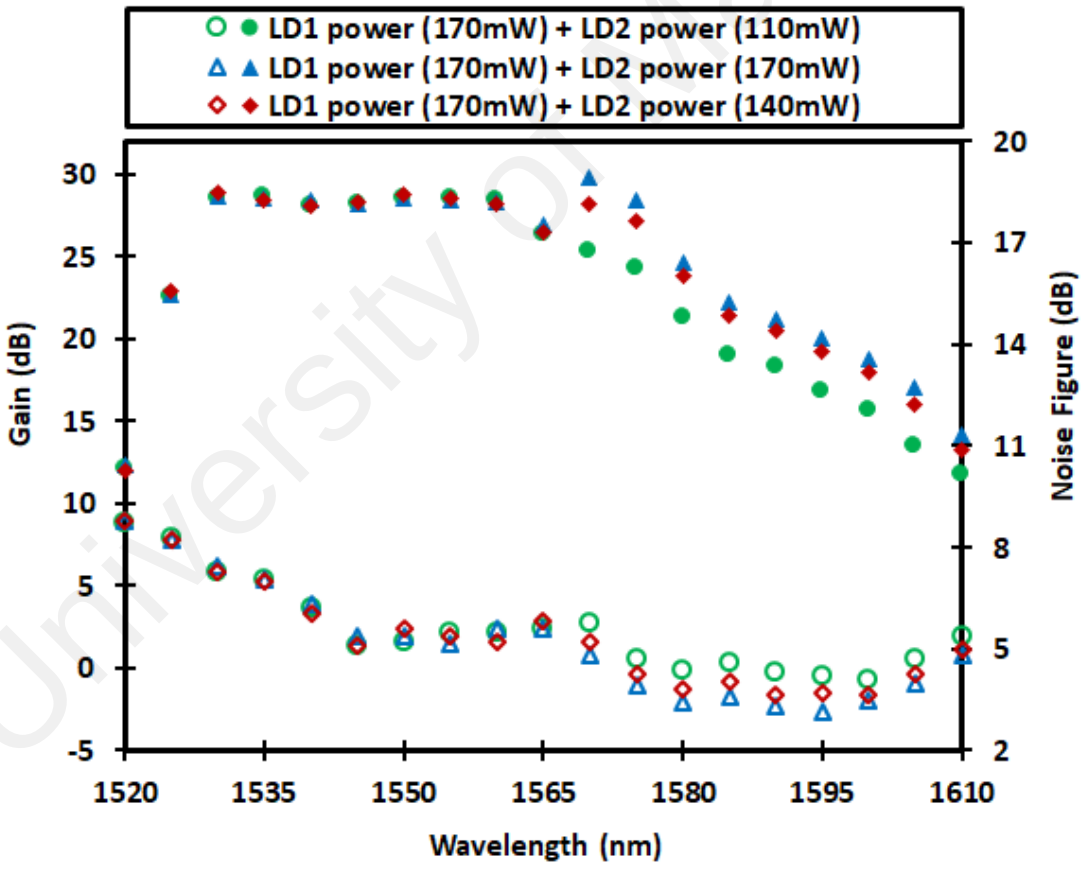

Figure 5.9: Measured gain (solid symbol) and noise figure (hollow symbol) spectrums of the parallel hybrid EDFA at various LD2 powers for input signal power of -30 dBm.

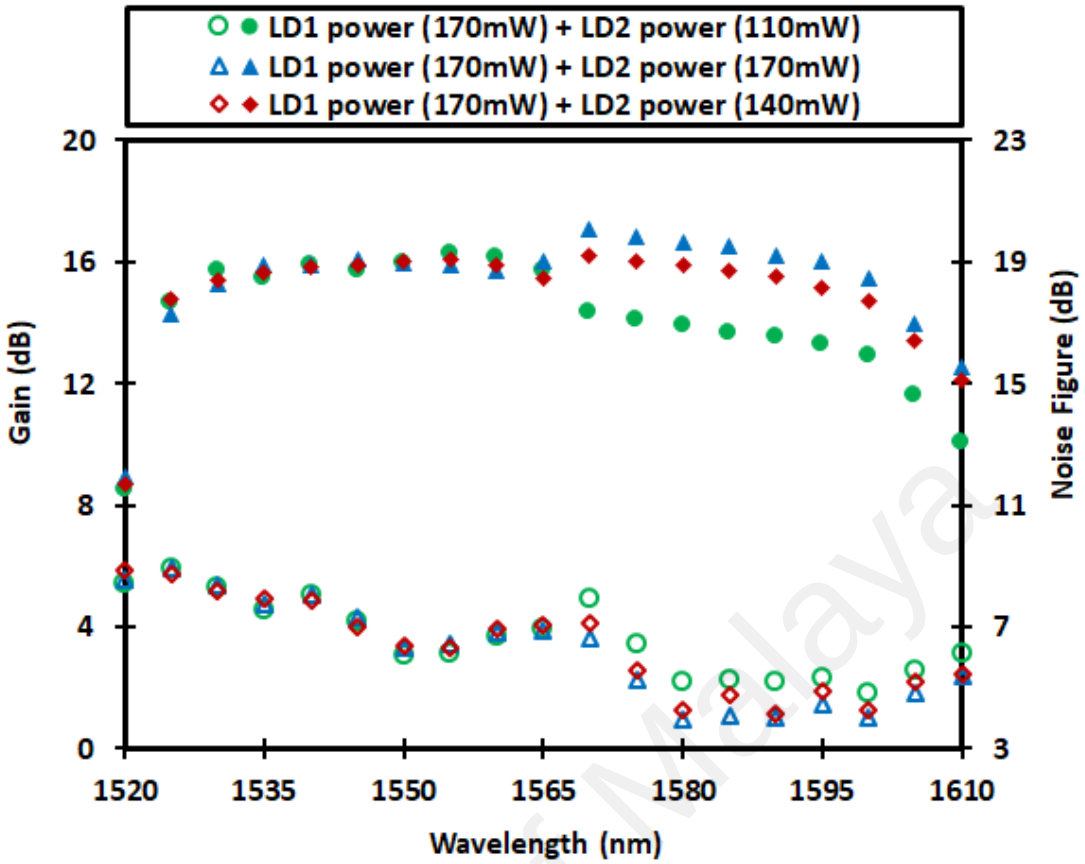

Figure 5.10: Measured gain (solid symbol) and noise figure (hollow symbol) spectrums of the parallel hybrid EDFA at various LD2 powers for input signal power of -10 dBm.

5.4.2 Pumping distribution technique

The system overall cost and complexity is the main disadvantages of the hybrid fibers amplifier. In this regard, it is important to design a wideband EDFA that realize not only the functional requirements but also the economically viable. Consequently, a novel structure of parallel hybrid EDFA is introduced using pumping distribution technique as shown in Figure 5.11. Using the pumping distribution technique, the proposed amplifier demonstrates not only an efficient performance, but also a cost reduction since only one laser diode is utilized to pump two stages. A single 980 nm LD with power of 310 mW, is used to pump both HB-EDF and Zr-EDF according to the distribution ratio. An optical fiber coupler operating at 980 nm wavelength is spliced at the output end of the LD.

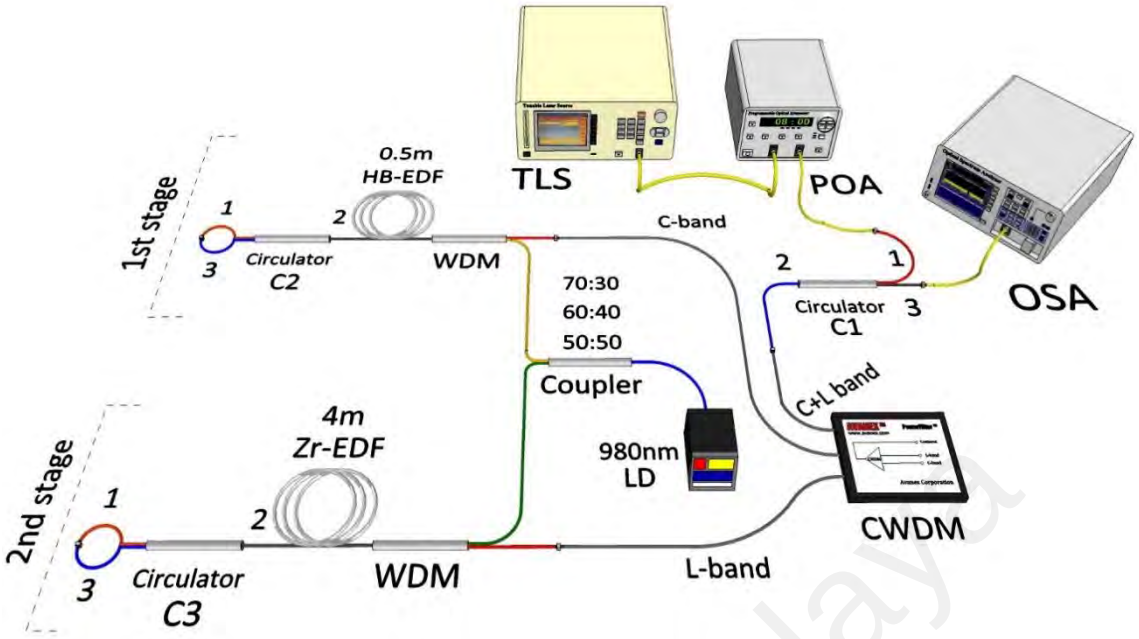

Figure 5.11: Two-stage parallel hybrid EDFA using pumping distribution technique.

During the experiment, the performance of the proposed parallel hybrid EDFA is investigated for three different cases, using three different couplers with splitting ratio of 70/30, 60/40 and 50/50. Therefore, 70%, 60% and 50% of LD power which are around 217 mW, 186 mW and 155 mW, respectively are distributed to pump the HB-EDF in the first stage. However, the remaining powers are distributed to pump the Zr-EDF in the second stage. Table 5.2 illustrates the distribution ratio of the LD power for the proposed parallel hybrid EDFA. Figures 5.12 and 5.13 show the effect of LD power distribution ratio on the amplification performance of the parallel hybrid EDFA, at input signal powers of -30 dBm and -10 dBm, respectively. It is obvious that the replacing of the optical coupler gives the same effect on both input signal powers. For C-band wavelength region, it is found that the higher gain and lower noise figure are obtained when the 70/30 output coupler is connected. Meanwhile, connecting of this coupler achieves a lower gain and higher noise figure at L-band wavelength region. This is attributed to the distribution ratio of the LD power, where the pump power for the HB-EDF is enough while the pump power for the Zr-EDF is insufficient. Likewise, a higher gain and lower noise figure are

obtained at L-band wavelength region when the 50/50 output coupler is connected. It is found that the 60/40 output coupler achieves an efficient performance for both C- and L-band wavelength regions. Furthermore, a flatter gain is achieved with using the 60/40 output coupler. At -10 dBm input signal, a flat gain of 15.3 dB is realized with a gain ripple of less than 1.5 dB, along the wideband wavelength region of 75 nm from 1525 to 1600 nm. Within the flat gain region, the noise figure values vary from 4.9 to 8.3 dB.

Table 5.2: The distribution ratio of the LD power for the parallel hybrid EDFA.

Coupler distribution ratio	Power distributed to first stage	Power distributed to second stage
70/30	217 mW	93 mW
60/40	186 mW	124 mW
50/50	155 mW	155 mW

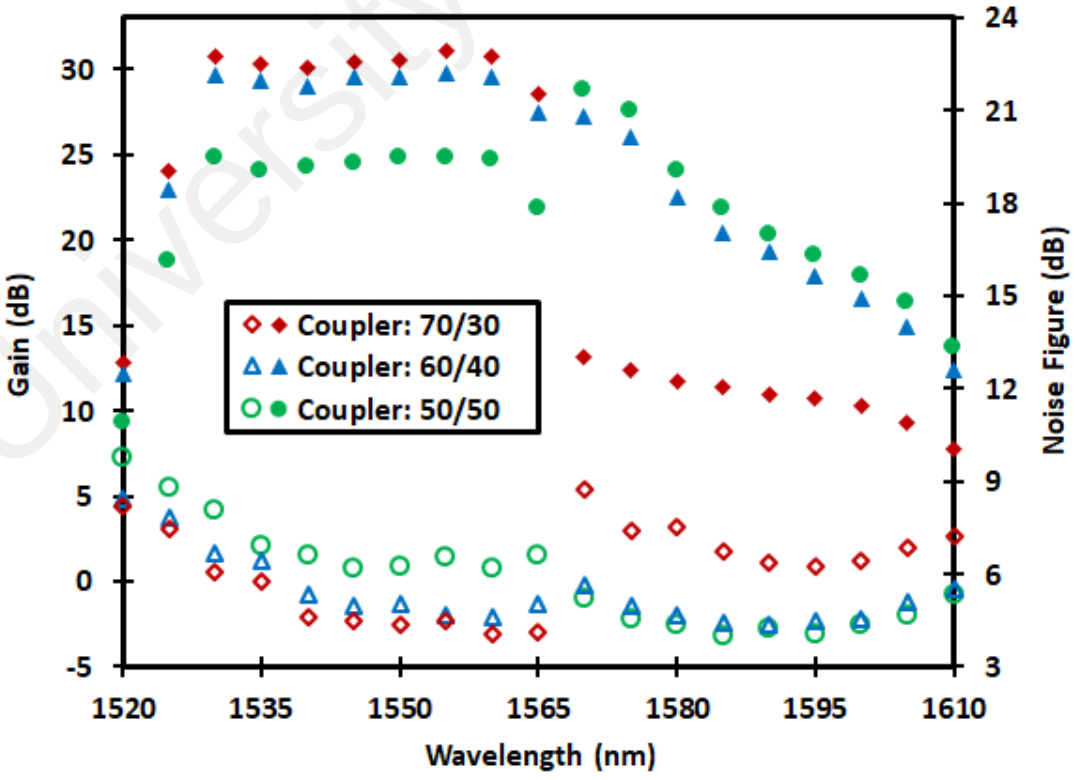

Figure 5.12: The effect of LD power distribution ratio on gain (solid symbol) and noise figure (hollow symbol) of the parallel hybrid EDFA, at input signal power of -30 dBm.

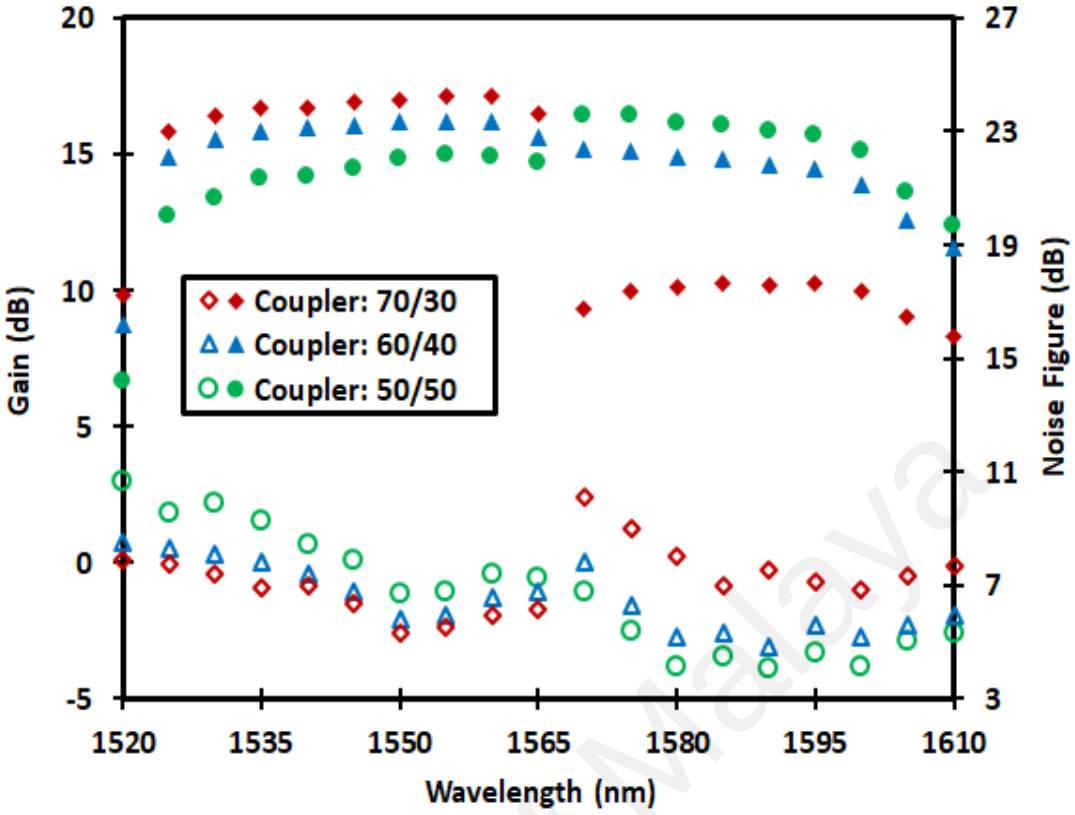

Figure 5.13: The effect of LD power distribution ratio on gain (solid symbol) and noise figure (hollow symbol) of the parallel hybrid EDFA, at input signal power of -10 dBm.

Figures 5.14 and 5.15 compare the performance of parallel hybrid EDFA configured with one LD, and that configured with two LDs scheme, for two input signal powers of -30 dBm and -10 dBm. The optimum optical coupler with splitting ratio of 60/40 is used for the parallel hybrid EDFA pumping with one LD. It can be observed that the gain and noise figure characteristics obtained by the EDFA pumping with one LD, show a similar performance as compared to the EDFA that pumping with two LDs, for both input signal powers. However, at the EDFA pumping with one LD, a very small higher gain and lower gain are obtained for C-band and L-band wavelength regions, respectively. This is due to the distribution ratio.

At input signal power of −30 dBm, the average gain increment is 0.8 dB in the C-band region, while the average gain decrement is 1.1 dB in the L-band region. The gain increment in the C-band region is owing to the coupling ratio, where the 60% of the total optimum power is around 186 mW, which is higher than the power at LD1 for the EDFA pumping with two LDs. Likewise, for the gain decrement in the L-band region, where the 40% of the total optimum power is around 124 mW, which is lower than the power at LD2 for the EDFA pumping with two LDs. At input signal power of −10 dBm, the average gain increment is 0.2 dB in the C-band region, while the average gain decrement is 0.8 dB in the L-band region. Overall, the proposed parallel hybrid EDFA using pumping distribution technique demonstrates an efficient performance as well as a cost reduction as only one LD is utilized to pump two stages.

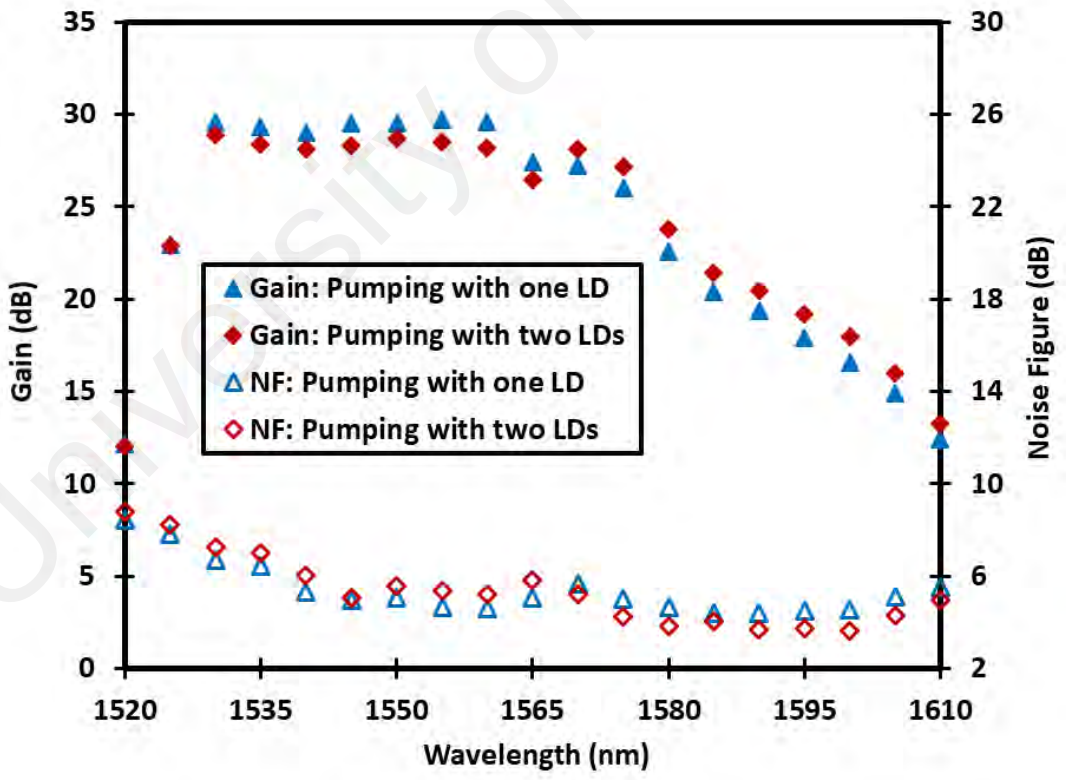

Figure 5.14: Comparison of the gain and noise figure performances between the parallel hybrid EDFA pumping with one LD and that pumping with two LDs at input signal powers of -30 dBm.

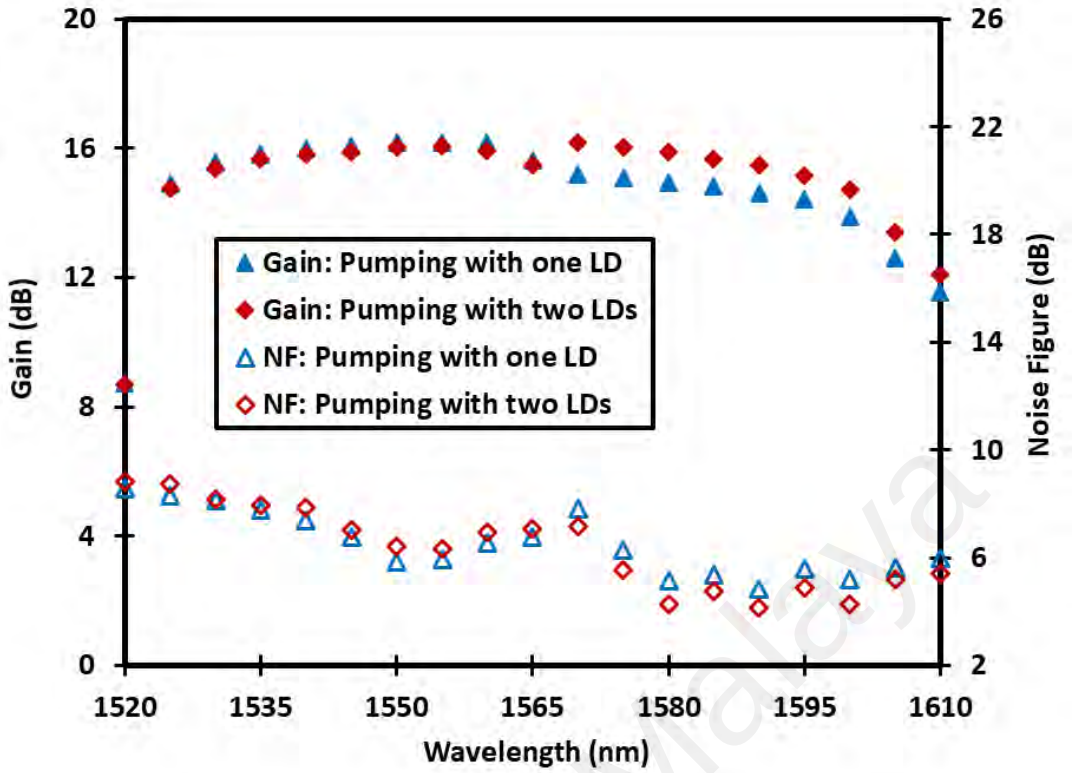

Figure 5.15: Comparison of the gain and noise figure performances between the parallel hybrid EDFA pumping with one LD and that pumping with two LDs at input signal powers of -10 dBm.

5.5 Wideband EDFA using hybrid active fibers in series

The schematic diagrams of the two series hybrid EDFA with forward and backward pumping are depicted in Figure 5.16 (a) and (b), respectively. Both structures consist of CWDM filter, three optical circulators as well as two pieces of EDF sections. A length of 0.5m HB-EDF and 4m Zr-EDF are utilized to produce C-band and L-band amplifications, respectively. The erbium fibers are fixed at the optimum lengths, which are determined in parallel hybrid EDFA. Two 980 nm single mode laser diodes (LDs) are applied to core pump both EDFs via 980/1550 nm WDM. The optical fiber circulator (C1) is used to transfer the input signal inside the first stage, and to pull out the returned output signal to the OSA. In the experiment, a novel structure utilizing a CWDM filter, instead of C-band FBG, is proposed. The CWDM is placed in the middle of the two stages to separate and

combine the C- and L-band signals. The optical circulator (C2) is used to reflect the C-band signal, which passes then over the CWDM to the first stage for double amplification. The L-band signal undergoes single amplification firstly by the first and second stages. The optical circulator (C3) is used to reflect the L-band signal to undergo double amplification in both stages. A TLS is used as a signal source while an OSA is utilized to test the gain and noise figure characteristics. A POA is utilized to provide an accurate input power to the amplifier.

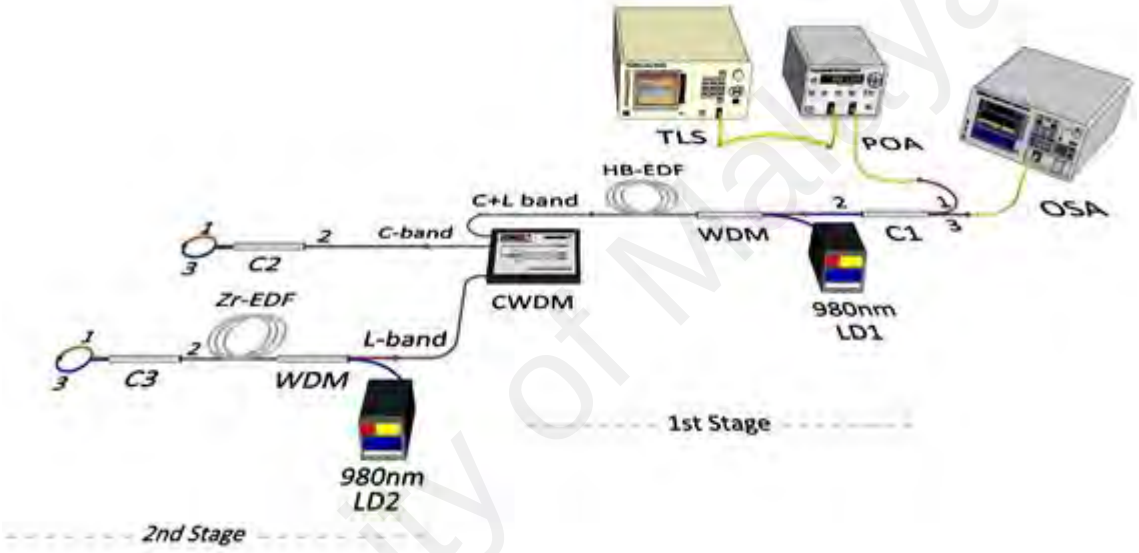

(a)

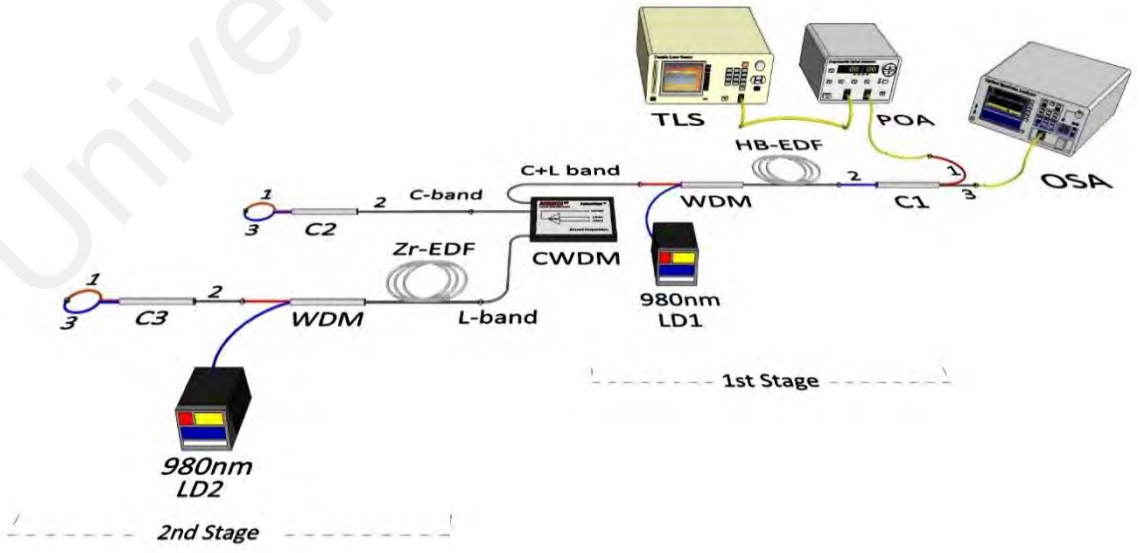

(b)

Figure 5.16: Two-stage series hybrid EDFA using (a) forward pumping, and (b) backward pumping.

Figure 5.17 compares the practically measured gain and noise figure of the series hybrid EDFA, between forward and backward pumping, at low input signal power of -30 dBm. The pump power of LD1 and LD2 are adjusted at 170 mW and 90 mW, respectively. As shown in the figure, both forward and backward pumped amplifiers achieve a wideband amplification throughout a wavelength span from 1520 nm to 1610 nm. However, the backward pumping amplifier obtains a higher gain and lower noise figure than that of the forward pumping amplifier. This is attributed to the saturation effect of ASE, that is weaker with the backward pumping. With backward pumping amplifier, an average gain enhancement of around 3.3 dB and 1.5 dB are observed along the C-band and L-band wavelength regions, respectively. Besides that, a flat gain of 23.8 dB is realized with a gain ripple of less than 1.3 dB, along the 45 nm wavelength region from 1530 to 1575 nm. On other hand, a relatively lower noise figure below 7.8 dB, is found with backward pumping.

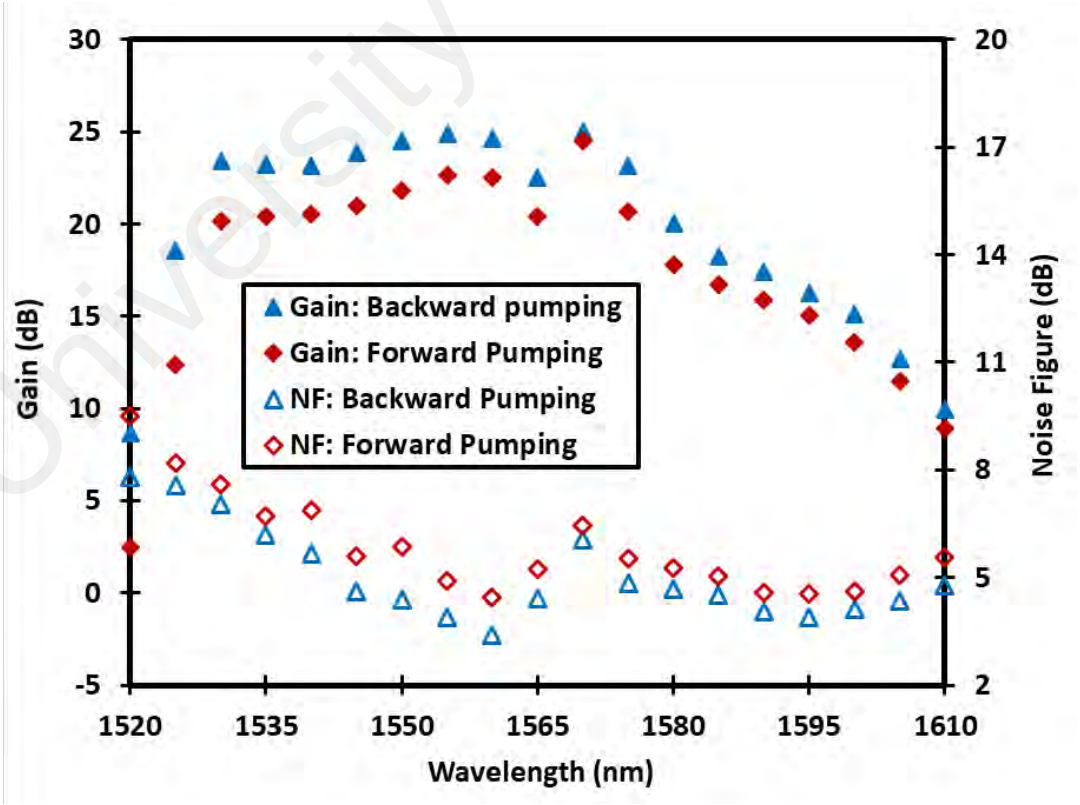

Figure 5.17: Comparison of the gain and noise figure characteristics between the forward and backward pumping-based series hybrid EDFA at input power of -30 dBm.

The gain and noise figure characteristics are, as well tested at high input signal level of -10 dBm, as apparent in Figure 5.18. It shows that the backward pumping amplifier achieves an almost comparable performance with the forward pumping amplifier. This is due to the total pump to ASE conversion which is smaller at high input signal power, leading to a reduction of population inversion and in turn a reduction of the gain in the backward pumped amplifier. Meanwhile, it can be observed that the backward pumping amplifier obtains slightly higher gain and lower noise figure at wavelengths that are below 1540 nm. With backward pumping amplifier, a flat gain of 12 dB is realized with a gain ripple of less than 2 dB, along the 70 nm wavelength region from 1530 to 1600 nm. Within the flat gain region, the noise figure values vary from 5 to 9 dB. It is obvious that the noise figure is higher at the shorter wavelength span as compared to that in the longer wavelength span. The is attributed to the erbium absorption-to-emission cross section which decreases at longer wavelength region.

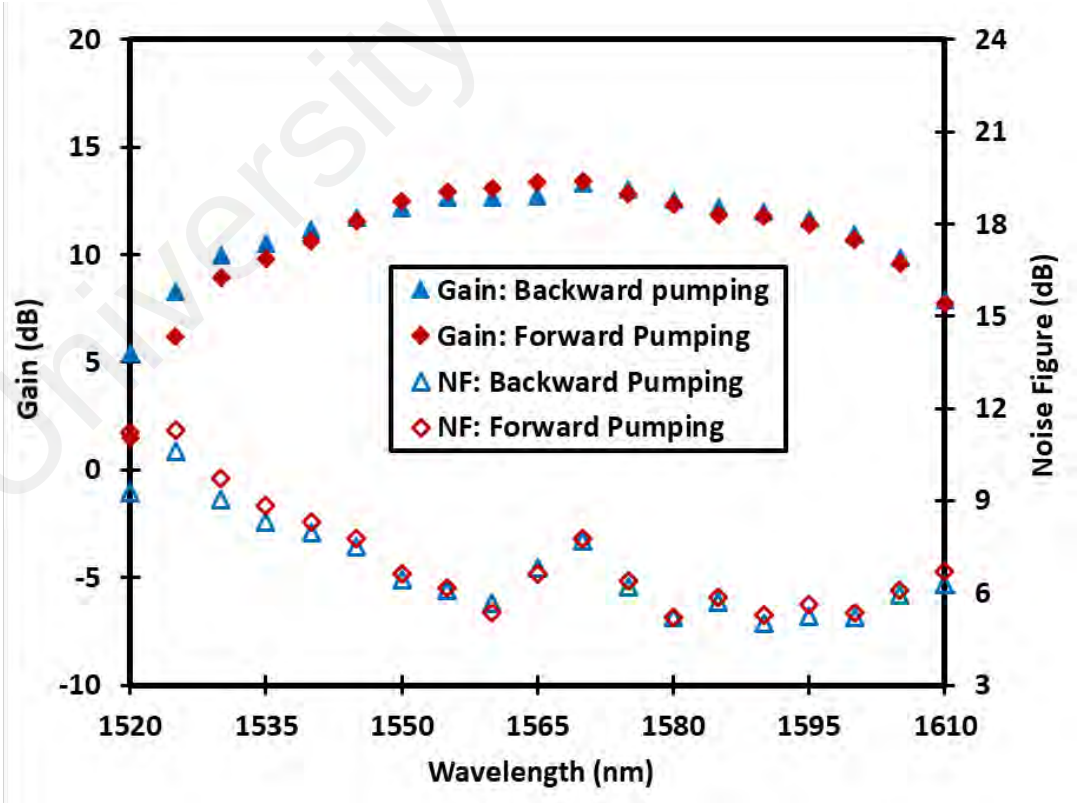

Figure 5.18: Comparison of the gain and noise figure characteristics between the forward and backward pumping-based series hybrid EDFA at input power of -10 dBm.

5.5.1 The optimization of the laser diodes powers

Since the backward pumping of the series hybrid EDFA displays a preferable performance, this technique is adopted and used to obtain a higher attainable flat gain as well as lower noise figure over the wide bandwidth. The gain and noise figure characteristics are examined at various backward pumping powers as depicted in Figure 5.19 and Figure 5.20, for input signal powers of -30 dBm and -10 dBm, respectively. In the experiment, LD1 power is set at 170 mW while LD2 power is varied from 60 mW to 90 mW and then to 120 mW. After that, LD1 power is adjusted to the maximum value of 220 mW while LD2 is fixed at 100 mW.

It is obvious that the variation of the laser diodes powers gives the same effect on both input signal powers. As illustrated in the Figures, the L-band gain spectra enhances as LD2 power increases. Nevertheless, the enhancement in the L-band gain spectra descends when LD2 power increases above 90 mW. This is most probably owing to the gain saturation effect. Meanwhile, the C-band gain spectrum descends when LD2 power increases above 90 mW, although LD1 power is fixed. This is due to the high forward ASE effect from the second stage which reduces the population inversion, and hence reduces the C-band gain spectra. On other hand, the L-band noise figure spectra decreases as LD2 power increases. This is owing to the higher gain and lower loss resulting from higher LD2 power. Besides that, a high noise figure spectra is noticed at C-band region when LD2 power is fixed at 120 mW, due to the high ASE noise.

Overall, it can be inferred that the optimum laser diodes powers to achieve higher flat gain and lower noise figures are 220 mW and 100 mW for LD1 and LD2, respectively. For instance, at input signal level of -30 dBm, a flat gain of 28.4 dB is realized with a gain ripple of less than 1.5 dB, along the 45 nm wavelength region from 1530 to 1575 nm. Within the flat gain region, the noise figure is less than 6 dB. Whereas at input signal

level of -10 dBm, a flat gain of 14.6 dB is realized with a gain ripple of less than 1.8 dB, along the 70 nm wavelength region from 1530 to 1600 nm. Within the flat gain region, the noise figure values vary from 4.3 to 7.9 dB.

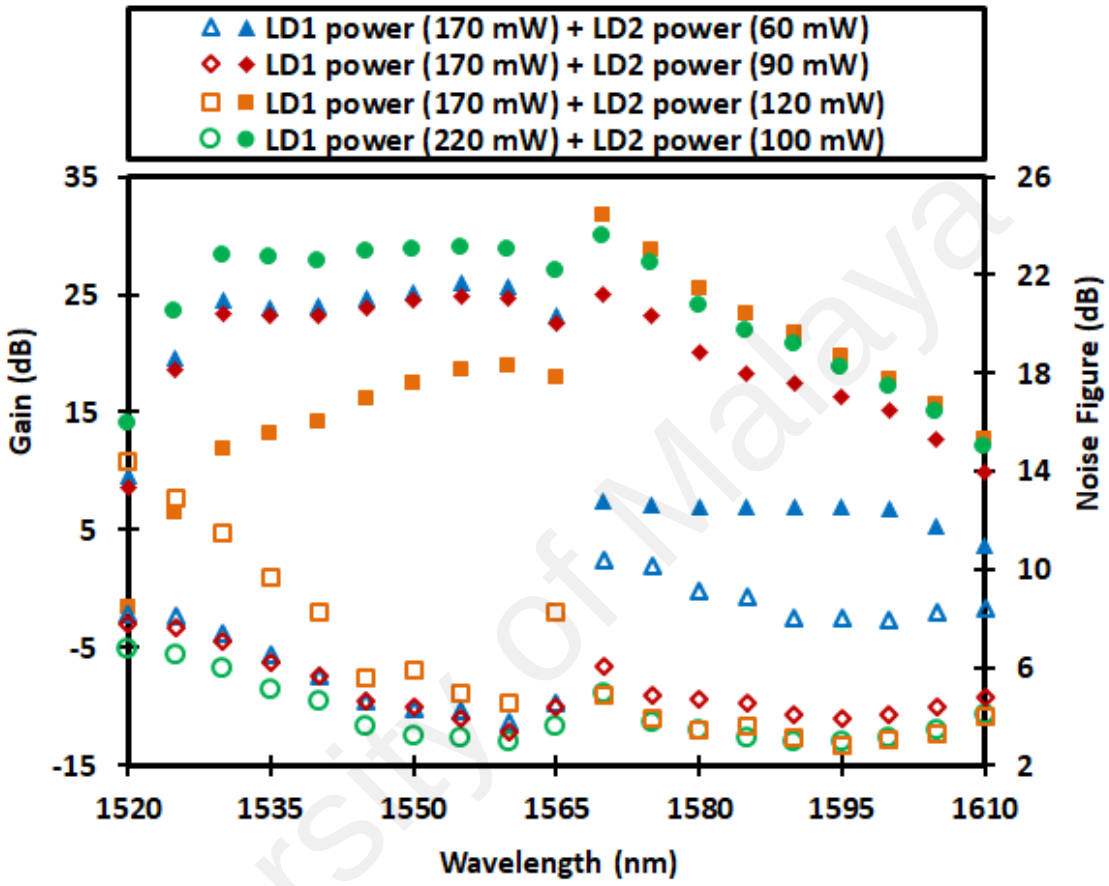

Figure 5.19: Measured gain (solid symbol) and noise figure (hollow symbol) spectra of the backward pumping-based series hybrid EDFA at various laser diode powers for input signal powers of -30 dBm.

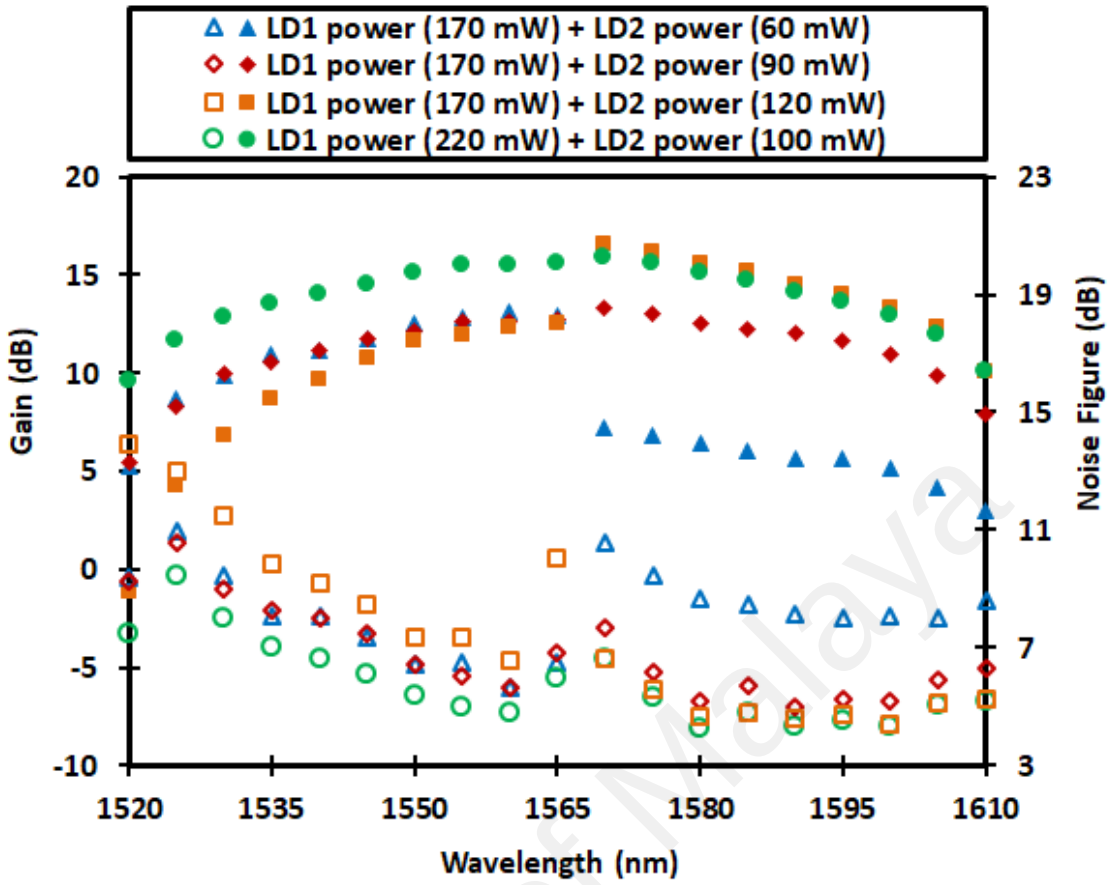

Figure 5.20: Measured gain (solid symbol) and noise figure (hollow symbol) spectra of the backward pumping-based series hybrid EDFA at various laser diode powers for input signal powers of -10 dBm.

5.5.2 Backward pumping distribution technique

For the proposed backward pumping-based series hybrid EDFA, it is found that the total optimum power from combining LD1 and LD2 powers is 320 mW. Therefore, the ratio of LD1 power to the total power is around 69% whereas the ratio of LD2 power to the total power is around 31%. Consequently, a novel structure of series hybrid EDFA is introduced using backward pumping distribution technique as depicted in Figure 5.21. A single 980 nm LD is utilized to pump the EDFs in both stages according to the distribution ratio. An optical fiber coupler operating at 980 nm wavelength with splitting ratio of 70/30

is spliced at the output end of the LD. A 70% of LD power which is around 224 mW, is distributed to pump the HB-EDF in the first stage. Meanwhile, the remaining power which is around 96 mW, is distributed through 30% coupler output to pump the Zr-EDF in the second stage.

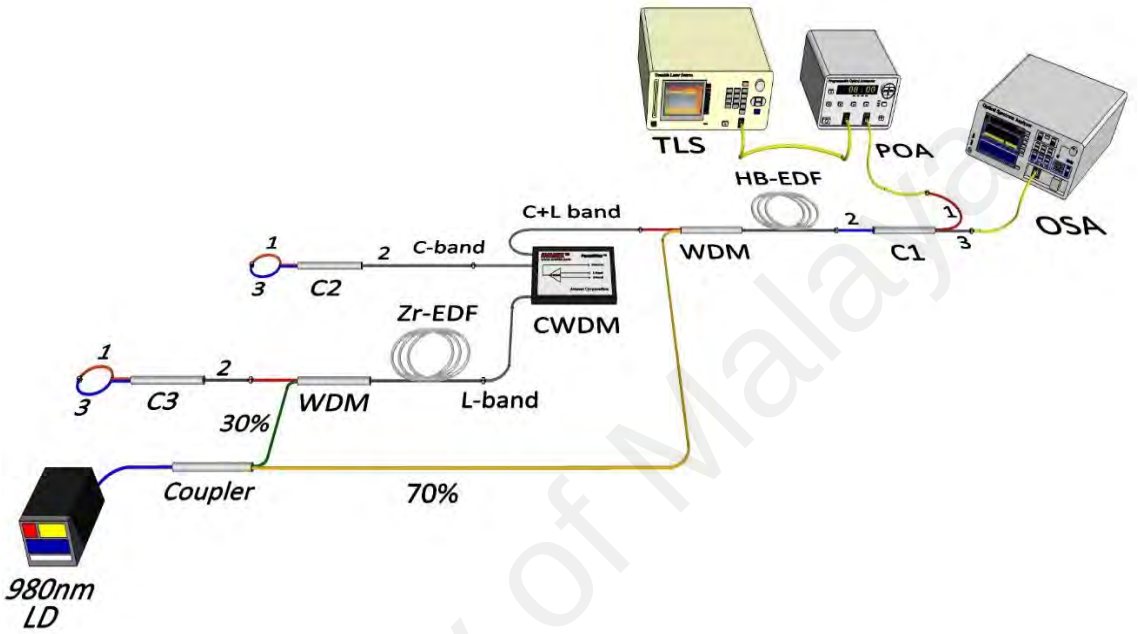

Figure 5.21: The series hybrid EDFA structure using backward pumping distribution technique.

Figures 5.22 and 5.23 show the performance comparison of series hybrid EDFA configured with one LD, and that configured with two LDs scheme, for two input signal powers of -30 dBm and -10 dBm, respectively. It can be observed that the gain and noise figure characteristics obtained by the EDFA pumping with one LD, show a similar performance as compared to the EDFA that pumping with two LDs, for both input signal powers. However, a very small gain decrement is obtained with a single LD pumping due to the coupling loss in the coupler. At input signal power of -30 dBm, the average gain decrements are 0.3 dB and 0.6 dB in the C-band and L-band regions, respectively. The

gain decrement is higher in the L-band region owing to the coupling ratio, where the 30% of the total optimum power is around 96 mW, which is lower than the optimum power at LD2 for the EDFA pumping with two LDs. At input signal power of -10 dBm, the average gain decrement is 0.5 dB within the gain flatness region. Overall, the proposed EDFA using backward pumping distribution technique demonstrates an efficient performance as well as a cost reduction as only one LD is utilized to pump two stages.

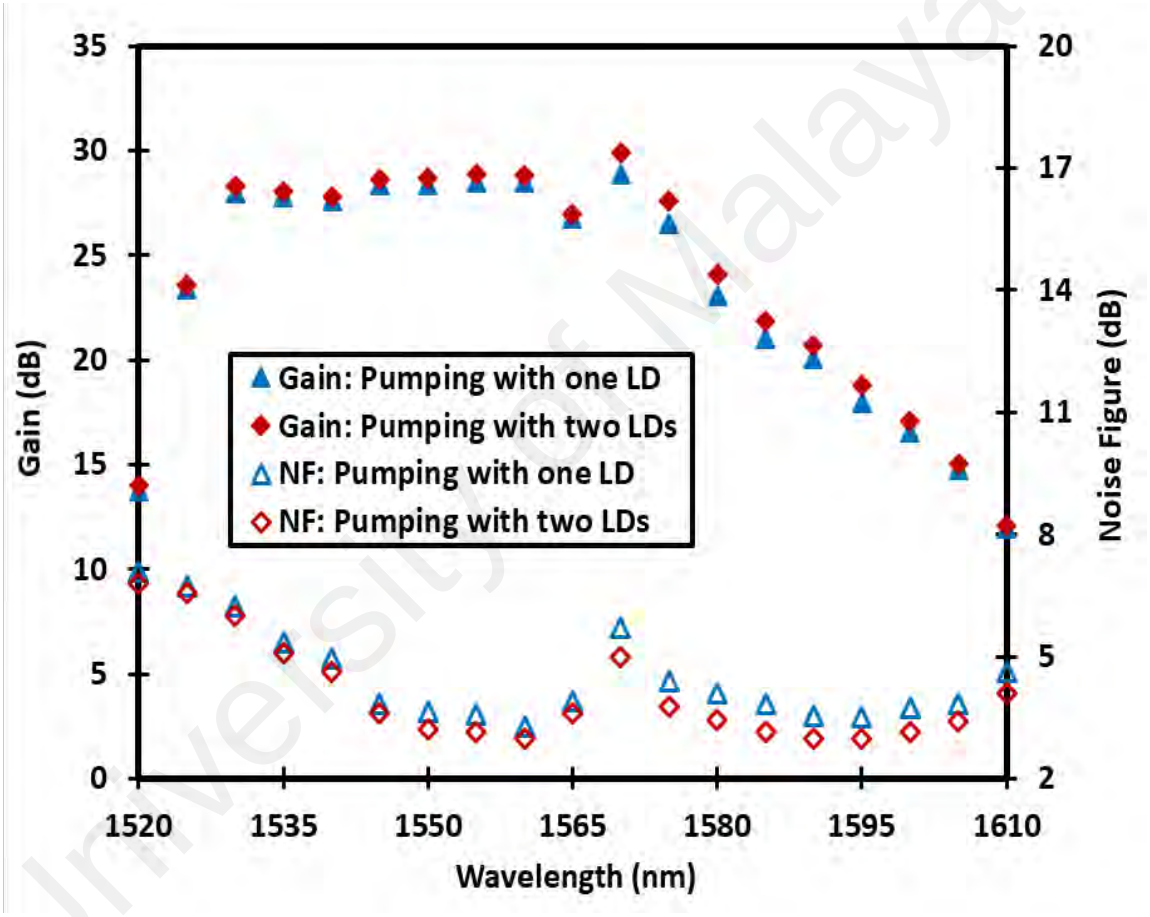

Figure 5.22: Comparison of the gain and noise figure performances between the series hybrid EDFA pumping with one LD and that pumping with two LDs, at input signal power of -30 dBm.

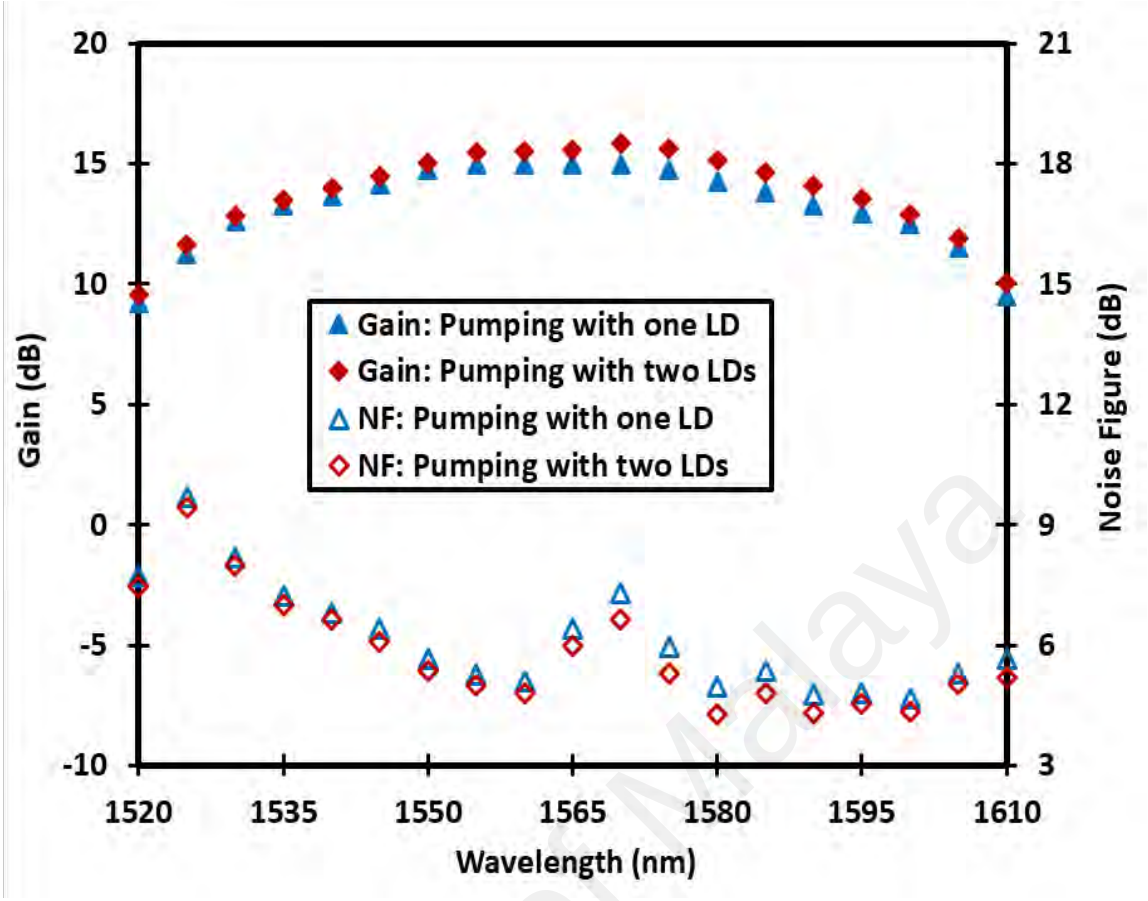

Figure 5.23: Comparison of the gain and noise figure performances between the series hybrid EDFA pumping with one LD and that pumping with two LDs, at input signal power of -10 dBm.

5.6 Parallel and series hybrid EDFA comparison

The comparison performance between the parallel and backward pumping-based series hybrid EDFA, is illustrated in Table 5.3. It is found that both amplifiers obtain an efficient wideband operation within 1520 nm to 1610 nm. At input signal power of -30 dBm, a slightly higher gain and lower noise figure are obtained with series amplifier. However, at input signal power of -10 dBm, the parallel hybrid EDFA achieved a higher flat gain, lower gin ripple and wider bandwidth. In addition, the total pumping power is lower for parallel amplifier. Overall, the parallel amplifier has a better performance than

the series amplifier. In parallel EDFA, each C- and L-band stages work independently as compared to that in series EDFA. As a result, the parallel hybrid EDFA prevents the pump of the L-band stage to effect on the C-band stage. In addition, the L-band signals go directly for amplifying in the L-band stage without passing the C-band stage, and thus minimize the effect on the gain flatness.

Table 5.3: The comparison performance between the parallel hybrid EDFA and the series hybrid EDFA that using backward pumping scheme.

Merit	**Parallel hybrid EDFA**	**Series hybrid EDFA**
Total hybrid fiber length	4.5 m	4.5 m
Pumping direction	Forward	Backward
Total pumping power	310 mW	320 mW
Amplification at input signal power of -30 dBm	Flat Gain: 28.1 dB Gain ripple: ± 1.6 dB Bandwidth: 45 nm NF: < 7.3 dB	Flat Gain: 28.4 Gain ripple: ± 1.5 dB Bandwidth: 45 nm NF: < 6 dB
Amplification at input signal power of -10 dBm	Flat Gain: 15.6 dB Gain ripple: ± 1 dB Bandwidth: 75 nm NF: varies from 4.1 to 8.7 dB	Flat Gain of 14.6 dB Gain ripple: ± 1.8 dB Bandwidth: 70 nm NF: varies from 4.3 to 7.9 dB.

5.7 Broadband ASE source using hybrid active fibers

An efficient broadband ASE light source is also investigated and achieved using the hybrid active fibers in series and parallel structures. In this work, a 0.5 m long HB-EDF and 4 m long Zr-EDF are utilized as hybrid active fiber to produce a broadband ASE light source. The ASE is produced by spontaneous emission due to the population inversion when the erbium fiber is pumped. So that, the previous configurations of parallel, forward series and backward series hybrid EDFA is utilized to produce a broadband ASE by taking off the TLS and POA. In the experiment, the LDs powers are fixed at the optimum powers which are determined in the design of the amplifier. Therefore, the LD1 and LD2 powers are fixed at 170 mW and 140 mW, respectively for parallel configuration. However, the LD1 and LD2 powers are fixed at 220 mW and 100 mW, respectively for series configuration.

Figure 5.24 shows the ASE spectra which is obtained from series and parallel configurations, when the total length of the hybrid active fiber is 4.5 m. It is found that the highest C-band ASE spectrum is obtained with parallel configuration. However, the highest L-band ASE spectrum is obtained with backward pumping-based series configuration. With forward pumping-based series configurations, a peak laser is observed at 1567 nm wavelength. This is due to the spurious reflection in the cavity, which suppresses the ASE level around it and affects the gain level at this wavelength region. To eliminate this laser, the power of LD2 should be decreased. Overall, a broader and higher ASE light spectrum is achieved at the backward pumping-based series configuration. The ASE power achieved varies from -50 dBm to -23 dBm within wavelength region from 1520 nm to 1600 nm.

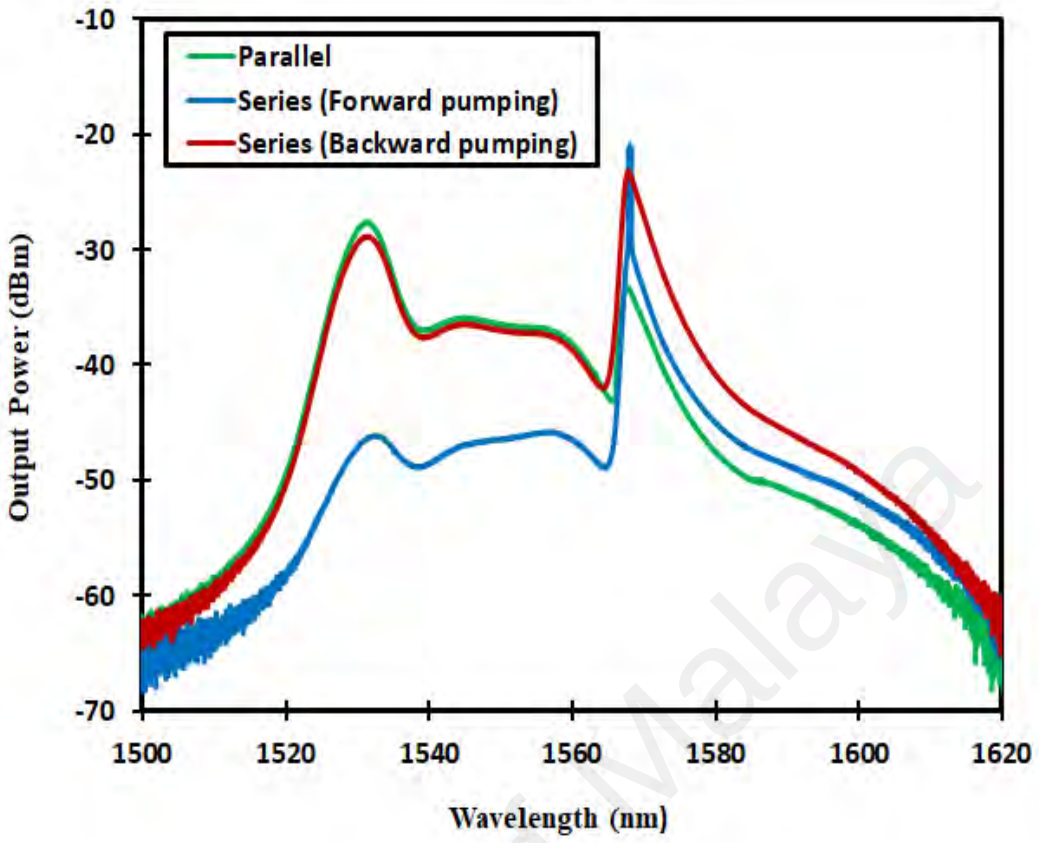

Figure 5.24: Broadband ASE spectra for parallel, forward series and backward series configurations using hybrid active fibers.

5.8 Summary

An efficient wideband and flat gain EDFA was successfully developed and demonstrated experimentally, utilizing two-stage configuration. The proposed amplifier comprises of a 0.5 m long HB-EDF and 4 m long Zr-EDF as a hybrid active fiber to fulfill amplification in C- and L-telecommunication bands, respectively. The performance of the proposed EDFA was investigated for parallel, and series configurations. The performance of these amplifiers was investigated for various pump powers to determine the optimum design. It can be concluded that both parallel and backward pumping-based series HB-EDFAs obtained a wideband operation within 1520 nm to 1610 nm, at the

optimum LDs powers. Besides, a flat gain characteristic was achieved throughout C- and L- bands wavelengths region. For parallel hybrid EDFA, at input signal power of -30 dBm, the gain fluctuated from 12 to 28.9 dB along the wavelength span of 90 nm from 1520 to 1610 nm. Furthermore, a flat gain of 28.1 dB was realized with a gain ripple of less than 1.6 dB, along the wavelength region of 45 nm from 1530 to 1275 nm. Within the flat gain region, the noise figure was less than 7.3 dB. At -10 dBm input signal, a flat gain of 15.6 dB was realized with a gain ripple of less than 1 dB, along the wideband wavelength region of 75 nm from 1525 to 1600 nm. Within the flat gain region, the noise figure values varied from 4.1 to 8.7 dB.

It can be concluded that the backward pumping amplifier performed better than the forward pumping amplifier. With backward pumping-based series hybrid EDFA, at input signal level of -30 dBm, a flat gain of 28.4 dB was realized with a gain ripple of less than 1.5 dB, along the 45 nm wavelength region from 1530 to 1575 nm. Within the flat gain region, the noise figure was less than 6 dB. Whereas at input signal level of -10 dBm, a flat gain of 14.6 dB was realized with a gain ripple of less than 1.8 dB, along the 70 nm wavelength region from 1530 to 1600 nm. Within the flat gain region, the noise figure values varied from 4.3 to 7.9 dB.

Using the pumping distribution technique, the proposed parallel and series hybrid EDFA demonstrated not only an efficient performance, but also a cost reduction since only one laser diode was utilized to pump both stages. This is a new technique can be used to improve the conventional forward, backward and dual pumping for the multi-stage amplifiers. Finally, a broadband amplified spontaneous emission (ASE) light emission was also demonstrated using the hybrid active fibers in series and parallel structures. The broader and higher ASE light spectrum was achieved at the backward pumping-based series configuration. The proposed ASE source covers both C- and L-band wavelength regions.

CHAPTER 6: CONCLUSIONS AND FUTURE WORKS

6.1 Conclusions

This thesis has presented a novel research work on hafnia-bismuth erbium co-doped fiber (HB-EDF) for both amplifier and ASE source applications. The HB-EDF was recently developed and fabricated using modified and chemical vapor deposition (MCVD) process in conjunction with solution doping (SD) technique. This fiber has a high Erbium ions concentration of 12500 wt. ppm, which was realized due to the co-doping with Hafnium and Aluminum ions, that minimize the ion clustering effect. On the other hand, the HB-EDF could be easily spliced with a standard SMF, due to the similarity in their melting temperature. Due to these features, the HB-EDF was expected to be useful for developing efficient and compact optical amplifier and ASE source devices.

Firstly, a compact optical amplifier with a flat-gain characteristic at C-band region was demonstrated in Chapter 3, by using short lengths of the new HB-EDF as the gain medium. The proposed amplifier was investigated for both single and double pass configurations. It was found that the double pass HB-EDF amplifier (HB-EDFA) offers a better gain spectrum as compared to that of single pass HB-EDFA. Besides, it was observed that the 0.5 m long HB-EDF is the optimum length for the C-band region. At input signal power of -30 dBm, a flat gain of 30.8 dB was realized with a gain ripple of less than 1.3 dB, along the 30 nm wavelength region from 1530 to 1560 nm. Within the flat gain region, the noise figure was less than 7 dB. However, at input signal power of -10 dBm, a flat gain of 15.9 dB was realized with a gain ripple of less than 1.4 dB, along the 45 nm wavelength region from 1525 to 1570 nm. Within the flat gain region, the noise figure was less than 8.1 dB. The performance of double pass HB-EDFA was then investigated for both 980 nm and 1480 nm wavelengths pumping. It was found that the

double pass HB-EDFA that pumping with 980 nm wavelength achieves a better amplification performance especially at C-band region, as compared to that pumping with 1480 nm wavelength.

The amplification performance of the HB-EDFA was compared with the conventional Erbium doped fiber amplifiers (EDFAs), such as the commercial silica erbium doped fiber amplifier (Si-EDFA) and the conventional zirconia erbium co-doped fiber amplifier (Zr-EDFA). It was observed that the proposed HB-EDFA obtains a more efficient gain and lower noise figure as compared to that of Si-EDFA and Zr-EDFA. Furthermore, the proposed HB-EDFA used a shorter gain medium length than that of Si-EDFA. The performance of the proposed HB-EDFA using single input wavelength source was compared to the one that using multi-input wavelengths, for both single and double pass configurations. The comparisons showed a relatively lower gain and higher noise figure were obtained with HB-EDFA that using multi-input wavelengths source. These results indicate that a new amplifier based on HB-EDF has been successfully demonstrated using a shorter length of active fiber.

The following chapters proposed different amplifiers and ASE sources working throughout a wideband operation to cover both C- and L-telecommunication bands. A wideband HB-EDFA and ASE source were demonstrated and developed in Chapter 4, utilizing two short lengths of HB-EDF sections. The wideband HB-EDFA was achieved by using two stages in both series and parallel structures in conjunction with double-pass scheme. The series HB-EDF was examined in both backward and forward pumping schemes. It was found that the backward pumping-based series amplifier obtains a higher gain and lower noise figure than that of the forward pumping-based series amplifier. On the other hand, it can be concluded that both parallel and backward pumping-based series HB-EDFAs obtain a wideband operation within 1520 nm to 1610 nm. Besides, a flat gain characteristic was achieved throughout C- and L- bands wavelengths region. For instance,

in parallel HB-EDFA that using 1.72 m long HB-EDF, a flat gain of 12.1 dB was realized with a gain ripple of less than 2 dB, along the wideband wavelength region of 80 nm from 1525 to 1605 nm. Within the flat gain region, the noise figure values varied from 6 to 11.8 dB. However, in backward pumping-based series HB-EDFA that using 2 m long HB-EDF, a flat gain of 14.6 dB was realized with a gain ripple of less than 2 dB, along the wavelength region of 65 nm from 1530 to 1595 nm. Within the flat gain region, the noise figure values varied from 6.8 to 10.2 dB. It can be inferred that the backward pumping-based series HB-EDFA achieves higher flat gain with lower noise figure. However, the flat gain region was larger with parallel HB-EDFA than that with backward pumping-based series HB-EDFA. On the other hand, a broadband ASE light source was also investigated and achieved using two pieces of HB-EDF in series and parallel structures. At the total lengths of 1.72 m long HB-EDFs, it was observed that the broad and reasonable ASE light spectrum is achieved at the parallel configuration. However, at the total lengths of 2 m long HB-EDFs, it was found that the broad and reasonable ASE light spectrum is obtained at backward pumping-based series configuration. These results indicate that a compact EDFA with flat gain characteristics over a wideband operation that covers both C- and L-telecommunication bands was successfully developed. New schemes of amplifier were also successfully proposed based on the series or parallel configurations.

Finally, an efficient hybrid EDFA and ASE source were successfully developed and demonstrated in Chapter 5. The hybrid amplifier was proposed to improve the amplification performance of the previous HB-EDFA (Chapter 4). The proposed amplifier achieved a flat gain and wideband amplification, utilizing two-stage configuration comprise a 0.5 m long HB-EDF and 4 m long Zr-EDF. The performance of the proposed EDFA was successfully investigated for parallel, and series configurations with both forward and backward pumping schemes. It can be concluded that both parallel

and backward pumping-based series HB-EDFAs obtain a wideband operation within 1520 nm to 1610 nm, at the optimum LDs powers. Besides, a flat gain characteristic was achieved throughout C- and L- bands wavelengths region. For parallel hybrid EDFA, at -10 dBm input signal, a flat gain of 15.6 dB was realized with a gain ripple of less than 1 dB, along the wideband wavelength region of 75 nm from 1525 to 1600 nm. Within the flat gain region, the noise figure values varied from 4.1 to 8.7 dB. It can be concluded that the backward pumping-based series amplifier performs a better than the forward pumping-based series amplifier. With backward pumping-based series hybrid EDFA, at input signal level of -10 dBm, a flat gain of 14.6 dB was realized with a gain ripple of less than 1.8 dB, along the 70 nm wavelength region from 1530 to 1600 nm. Within the flat gain region, the noise figure values varied from 4.3 to 7.9 dB. One of the main contributions of this chapter was the using of pumping distribution technique. By using this technique, the proposed parallel and series hybrid EDFA demonstrated not only an efficient performance, but also a cost reduction since only one laser diode was utilized to pump both stages. The proposed amplifiers were successfully realized not only the functional requirements but also the economically viable, by mitigation the complexity and devices used. A broadband ASE light was also successfully demonstrated to cover both the C- and L-band region by using the hybrid active fibers in series and parallel structures. It was observed that a broader and higher ASE light spectrum is achieved at the backward pumping-based series configuration.

6.2 Future works

This thesis has been mainly focused on the use of HB-EDFs to demonstrate an efficient amplifier in terms of compactness, gain flatness, and broadband operation. Therefore, the proposed amplifiers could be used in future dense wavelength division

multiplexing (DWDM) communication system, due to these features. However, this research work is possible to have further improvements. In this section, brief suggestions for future research works are given:

1. The core diameter of the HB-EDF is 3.71 μm which is very small as compared to that of the pigtail standard single mode fibers (SMFs). A typical SMF has a core diameter between 8 and 10.5 μm. This resulted in increasing the loss and noise figures in most of the proposed amplifiers and thus reduce the maximum performance efficiency. Moreover, the small overall fiber diameter makes the fiber easily to broken.

2. The short length of 0.5 m long HB-EDF achieved an efficient performance in the C-band region. However, the 1.5 m long HB-EDF which is the optimum length for L-band region, achieved an acceptable gain with high noise figure. Therefore, a 4 m long Zr-EDF was used for L-band region. The high noise figure of HB-EDF in the L-band region, should be solved in future work. It is very interesting to achieve a flat gain over wideband operation with low noise figure, using only 2 m long HB-EDF.

3. Improvement the performance of the proposed amplifier to achieve an ultra-wide band amplification, by covering the short band (S-band) which is ranging 1460 to 1530 nm. This could be accomplished by integrating the proposed amplifier with Raman amplifier.

4. Although the advance in optical fiber fabrication technology but still there is a lack of theoretical works. This is due to these fabricated fibers are not supported by the simulation software's. Designing and producing of a software similar to GainMaster™ that produced from the Fibercore Tech Center, could by very interesting.

5. For two-stage amplifier, the pumping distribution technique demonstrates a cost reduction since only one laser diode was utilized to pump two stages. However, further cost reduction could be achieved be reducing the optical circulators. Designing of one optical circulator for both stages having the ability to reflect any incoming signal, seems attractive in future work.

REFERENCES

Abass, A., Ali, M., & Al–Hussein, S. A. A. (2018). *Optimization of Hybrid Fiber Amplifier Utilizing Combined Serial-Parallel Configuration.* Paper presented at the IOP Conference Series: Materials Science and Engineering.

Abass, A. K., Abdul-Razak, M. J., & Salih, M. A. (2014). Gain characteristics for C-band erbium doped fiber amplifier utilizing single and double-pass configurations: A comparative study. *Engineering and Technology Journal, 32*(9 Part (A) Engineering), 2165-2173.

Abdullah, F., Jamaludin, M., Ali, M., Al-Mansoori, M., Abass, A., & Al-Mashhadani, T. (2018). *Influence of Raman Pump Direction on the Performance of Serial Hybrid Fiber Amplifier in C+ L-Band.* Paper presented at the 2018 IEEE 7th International Conference on Photonics (ICP).

Abu-Aisheh, A., & Moslehpour, S. (2010). Pre-amp EDFA ASE noise minimization for optical receiver transmission performance optimization. *Optics Communications, 283*(12), 2603-2606.

Agrawal, G. P. (2012). *Fiber-optic communication systems* (Vol. 222): John Wiley & Sons.

Ahlawat, D., Arora, P., & Kumar, S. (2019). Performance evaluation of proposed WDM optical link using EDFA and FBG combination. *Journal of Optical Communications, 40*(2), 101-107.

Akhter, F., Ibrahimy, M. I., Naji, A. W., & Siddiquei, H. R. (2012). Modeling and characterization of all possible triple pass EDFA configurations. *International Journal of Physical Sciences, 7*(18), 2656-2663.

Ali, M., Abdullah, F., Jamaludin, M. Z., Al-Mansoori, M., Abass, A., & Al-Mashhadani, T. (2015). Effect of cascading amplification stages on the performance of serial hybrid fiber amplifier. *Fiber and Integrated Optics, 34*(3), 131-144.

Ali, M. H., Abdullah, F., Jamaludin, M. Z., Al-Mansoori, M. H., Al-Mashhadani, T. F., & Abass, A. K. (2014). Simulation and experimental validation of gain-control parallel hybrid fiber amplifier. *Journal of the Optical Society of Korea, 18*(6), 657-662.

Allwood, G., Wild, G., & Hinckley, S. (2011). *Power over fibre: Material properties of homojunction photovoltaic micro-cells.* Paper presented at the 2011 Sixth IEEE International Symposium on Electronic Design, Test and Application.

Bass, M., DeCusatis, C., Enoch, J., Lakshminarayanan, V., Li, G., Macdonald, C., . . . Van Stryland, E. (2009). *Handbook of Optics, Volume V: Atmospheric Optics, Modulators, Fiber Optics, X-Ray and Neutron Optics*: McGraw-Hill, Inc.

Bebawi, J., Kandas, I., El-Osairy, M., & Aly, M. (2018). A Comprehensive Study on EDFA Characteristics: Temperature Impact. *Applied Sciences, 8*(9), 1640.

Bhusari Shraddha, N., Deshmukh Vikas, U., & Jagdale Shantanu, S. (2016). Analysis of SPM, XPM, and FWM in Fiber Optic Comunication Using OptiSystem. *IJSTE-International Journal of Science Technology & Engineering, 2*(07).

Caillaud, C., Glastre, G., Lelarge, F., Brenot, R., Bellini, S., Paret, J.-F., . . . Achouche, M. (2012). Monolithic integration of a semiconductor optical amplifier and a high-speed photodiode with low polarization dependence loss. *IEEE Photonics Technology Letters, 24*(11), 897-899.

Cardenas, J., Poitras, C. B., Robinson, J. T., Preston, K., Chen, L., & Lipson, M. (2009). Low loss etchless silicon photonic waveguides. *Optics express, 17*(6), 4752-4757.

Cheng, X., Hamida, B., Naji, A., Arof, H., Ahmad, H., & Harun, S. W. (2012). Compact and wide-band bismuth-based erbium-doped fibre amplifier based on two-stage and double-pass approaches. *IET optoelectronics, 6*(3), 127-130.

Cheng, X. S., Hamida, B. A., Naji, A. W., Ahmad, H., & Harun, S. W. (2011). 67 cm long bismuth-based erbium doped fiber amplifier with wideband operation. *Laser Physics Letters, 8*(11), 814-817.

Cheng, X. S., Parvizi, R., Ahmad, H., & Harun, S. W. (2009). Wide-band bismuth-based erbium-doped fiber amplifier with a flat-gain characteristic. *IEEE Photonics Journal, 1*(5), 259-264.

Cokrak, A. C., & Altuncu, A. (2004). Gain and noise figure performance of erbium doped fiber amplifiers (EDFA). *Istanbul University-Journal of Electrical & Electronics Engineering, 4*(2), 1111-1122.

Dhar, A., Kasik, I., Dussardier, B., Podrazky, O., & Matejec, V. (2012). Preparation and Properties of Er-Doped ZrO 2 Nanocrystalline Phase-Separated Preforms of Optical Fibers by MCVD Process. *International Journal of Applied Ceramic Technology, 9*(2), 341-348.

Digonnet, M. J., Murphy-Chutorian, E., & Falquier, D. G. (2002). Fundamental limitations of the McCumber relation applied to Er-doped silica and other amorphous-host lasers. *IEEE journal of quantum electronics, 38*(12), 1629-1637.

Dong, J., Wei, Y., Wonfor, A., Penty, R., White, I., Lousteau, J., . . . Jha, A. (2011). Dual-Pumped Tellurite Fiber Amplifier and Tunable Laser Using Er $^{3+} $/Ce $^{3+} $ Codoping Scheme. *IEEE Photonics Technology Letters, 23*(11), 736-738.

Duarte, J., Paul, M. C., Das, S., Dhar, A., Leitão, J. P., Ferreira, M. F., & Rocha, A. M. (2019). Optical amplification performance of erbium doped zirconia-yttria-alumina-baria silica fiber. *Optical Materials Express, 9*(6), 2652-2661.

Durak, F. E., & Altuncu, A. (2017). The effect of ASE reinjection configuration through FBGs on the gain and noise figure performance of L-Band EDFA. *Optics Communications, 386*, 31-36.

Durak, F. E., & Altuncu, A. (2018). All-optical gain clamping and flattening in L-Band EDFAs using lasing-controlled structure with FBG. *Optical Fiber Technology, 45*, 217-222.

Emmanuel, D., & Zervas, M. (1994). Erbium-doped fiber amplifiers: principles and applications: New York: Wiley Interscience.

Firstov, S., Khopin, V., Alyshev, S., Riumkin, K., Melkumov, M., Guryanov, A., & Dianov, E. (2016). *Bismuth-doped optical fiber amplifier and watt-level CW laser for the spectral region 1600–1800 nm.* Paper presented at the Optical Fiber Communication Conference.

Firstov, S., Riumkin, K., Khegai, A., Alyshev, S., Melkumov, M., Khopin, V., . . . Dianov, E. (2017). Wideband bismuth-and erbium-codoped optical fiber amplifier for C+ L+ U-telecommunication band. *Laser Physics Letters, 14*(11), 110001.

Ganbold, M.-E., Nagai, H., Mori, Y., Suzuki, K., Matsuura, H., Tanizawa, K., . . . Sato, K.-i. (2018). A large-scale optical circuit switch using fast wavelength-tunable and bandwidth-variable filters. *IEEE Photonics Technology Letters, 30*(16), 1439-1442.

Gangwar, R., Singh, S., & Singh, N. (2010). Gain optimization of an erbium-doped fiber amplifier and two-stage gain-flattened EDFA with 45 nm flat bandwidth in the L-band. *Optik-International Journal for Light and Electron Optics, 121*(1), 77-79.

George, H., Vira, C., Stehle, C., Meyer, J., Evers, S., Hogan, D., . . . Affatigato, M. (1999). A structural analysis of the physical properties of bismuth and lead based glasses. *Physics and chemistry of glasses, 40*(6), 326-332.

Giles, C. R., & Desurvire, E. (1991). Modeling erbium-doped fiber amplifiers. *Journal of Lightwave Technology, 9*(2), 271-283.

Goel, N. K., Pickrell, G., & Stolen, R. (2014). An optical amplifier having 5 cm long silica-clad erbium doped phosphate glass fiber fabricated by "core-suction" technique. *Optical Fiber Technology, 20*(4), 325-327.

Hamida, B., Azooz, S., Jasim, A., Eltaif, T., Khan, S., Ahmad, H., & Harun, S. W. (2016). Flat-gain wide-band erbium doped fiber amplifier with hybrid gain medium. *Optik, 127*(5), 2481-2484.

Hamida, B., Cheng, X., Harun, S. W., Naji, A., Arof, H., Khan, S., . . . Ahmad, H. (2012). Wideband and compact erbium-doped fiber amplifier using parallel double-pass configuration. *Microwave and Optical Technology Letters, 54*(3), 629-631.

Hamida, B. A., Azooz, S., Jasim, A. A., Eltaif, T., Ahmad, H., Khan, S., & Harun, S. W. (2015). Flat-gain wide-band erbium doped fiber amplifier by combining two difference doped fibers. *Journal of the European Optical Society-Rapid publications, 10*.

Hamida, B. A., Cheng, X. S., Naji, A. W., Ahmad, H., Al-Khateeb, W., Khan, S., & Harun, S. W. (2012). Optical amplifier with flat-gain and wideband operation

utilizing highly concentrated erbium-doped fibers. *Journal of Nonlinear Optical Physics & Materials, 21*(01), 1250005.

Hamzah, A., Azrin, N., & Saris, N. (2018). Flat-gain and Wideband EDFA by using Dual Stage Amplifier Technique. *Journal of Telecommunication, Electronic and Computer Engineering (JTEC), 10*(2-6), 25-29.

Hamzah, A., Rosli, N., Ambran, S., Aid, S., & Harun, S. (2017). Investigation on Double Pass Amplification by employing Zr-EDF as a gain medium with different types of reflectors. *Journal of Telecommunication, Electronic and Computer Engineering (JTEC), 9*(3-8), 11-15.

Harun, S. W., Parvizi, R., Cheng, X., Parvizi, A., Emami, S., Arof, H., & Ahmad, H. (2010). Experimental and theoretical studies on a double-pass C-band bismuth-based erbium-doped fiber amplifier. *Optics & Laser Technology, 42*(5), 790-793.

Harun, S. W., Paul, M. C., Huri, N., Hamzah, A., Das, S., Pal, M., . . . Kalita, M. P. (2011). Double-pass erbium-doped zirconia fiber amplifier for wide-band and flat-gain operations. *Optics & Laser Technology, 43*(7), 1279-1281.

Hui, R., & O'Sullivan, M. (2009). Chapter 3 - Characterization of Optical Devices. In R. Hui & M. O'Sullivan (Eds.), *Fiber Optic Measurement Techniques* (pp. 259-363). Boston: Academic Press.

Huri, N., Hamzah, A., Arof, H., Ahmad, H., & Harun, S. W. (2011). Hybrid flat gain C-band optical amplifier with Zr-based erbium-doped fiber and semiconductor optical amplifier. *Laser physics, 21*(1), 202-204.

Jurado-Navas, A., Tatarczak, A., Lu, X., Olmos, J. J. V., Garrido-Balsells, J. M., & Monroy, I. T. (2015). 850-nm hybrid fiber/free-space optical communications using orbital angular momentum modes. *Optics express, 23*(26), 33721-33732.

Kaler, R., & Kaler, R. (2011). Gain and Noise figure performance of erbium doped fiber amplifiers (EDFAs) and Compact EDFAs. *Optik-International Journal for Light and Electron Optics, 122*(5), 440-443.

Kao, K., & Hockham, G. A. (1966). *Dielectric-fibre surface waveguides for optical frequencies.* Paper presented at the Proceedings of the Institution of Electrical Engineers.

Kapron, F., Keck, D. B., & Maurer, R. D. (1970). Radiation losses in glass optical waveguides. *Applied Physics Letters, 17*(10), 423-425.

Kaushal, H., & Kaddoum, G. (2016). Optical communication in space: challenges and mitigation techniques. *IEEE communications surveys & tutorials, 19*(1), 57-96.

Kir'yanov, A., Barmenkov, Y., Minkovich, V., Das, S., Dutta, D., Dhar, A., . . . Tapero, K. (2018). Effect of electron irradiation on the optical properties of bismuth doped hafnia-yttria-alumina-silicate fiber. *Optical Materials Express, 8*(9), 2550-2558.

Kir'yanov, A., Siddiki, S., Barmenkov, Y., Das, S., Dutta, D., Dhar, A., . . . Didenko, S. (2017). Hafnia-yttria-alumina-silica based optical fibers with diminished mid-IR (> 2 μm) loss. *Optical Materials Express, 7*(7), 2511-2518.

Kir'yanov, A., Siddiki, S., Barmenkov, Y., Dutta, D., Dhar, A., Das, S., & Paul, M. C. (2017). Bismuth-doped hafnia-yttria-alumina-silica based fiber: spectral characterization in NIR to mid-IR. *Optical Materials Express, 7*(10), 3548-3560.

Kumar, C., & Goyal, R. (2019). Experimental Evaluation of HOA in Terms of Flat Gain in C-Band for Super Dense Optical Communication System. *Wireless Personal Communications*, 1-8.

Kumar, G., & Kumar, S. (2019). Flat gain C+ L band using optical amplifiers for 200× 14 Gbps DWDM system. *Optical and Quantum Electronics, 51*(1), 34.

Kumar, N., & Ramachandran, K. (2013). Mach–Zehnder interferometer concatenated fiber loop mirror based gain equalization filter for an EDFA. *Optics Communications, 289*, 92-96.

Ladaci, A., Girard, S., Mescia, L., Robin, T., Cadier, B., Laurent, A., . . . Ouerdane, Y. (2018). Validity of the McCumber Theory at High Temperatures in Erbium and Ytterbium-Doped Aluminosilicate Fibers. *IEEE journal of quantum electronics, 54*(4), 1-7.

Latiff, A., Zakaria, Z., Jaafar, A., Rafis, H., & Gannapathy, V. (2013). Comparative Study on Single-And Double-Pass Configurations for Serial Dual-Stage High Concentration EDFA. *Int. J. of Research in Eng. and Tech, 2*(12), 139-143.

Leon, M., Lancry, M., Ollier, N., Babu, B., Bigot, L., El Hamzaoui, H., . . . Trompier, F. (2016). Ge-and Al-related point defects generated by gamma irradiation in nanostructured erbium-doped optical fiber preforms. *Journal of Materials Science, 51*(22), 10245-10261.

Liang, T.-C., Chen, Y.-K., Su, J.-H., Tzeng, W.-H., Hu, C., Lin, Y.-T., & Lai, Y.-C. (2000). Optimum configuration and design of 1480-nm pumped L-band gain-flattened EDFA using conventional erbium-doped fiber. *Optics Communications, 183*(1-4), 51-63.

Lim, E.-L., Alam, S.-u., & Richardson, D. J. (2012). High-energy, in-band pumped erbium doped fiber amplifiers. *Optics express, 20*(17), 18803-18818.

Mahdi, M. A., & Sheih, S.-J. (2004). Gain-flattened extended L-band EDFA with 43 nm bandwidth suitable for high signal powers. *Optics Communications, 234*(1-6), 229-233.

Mahran, O., & Aly, M. H. (2016). Performance characteristics of dual-pumped hybrid EDFA/Raman optical amplifier. *Applied optics, 55*(1), 22-26.

Markom, A., Paul, M. C., Dhar, A., Das, S., Pal, M., Bhadra, S. K., . . . Harun, S. (2017). Performance comparison of enhanced Erbium–Zirconia–Yttria–Aluminum co-doped conventional erbium-doped fiber amplifiers. *Optik, 132*, 75-79.

Miniscalco, W. J. (2001). Optical and electronic properties of rare earth ions in glasses. *OPTICAL ENGINEERING-NEW YORK-MARCEL DEKKER INCORPORATED-, 71*, 17-112.

Mishra, R., Shukla, N., & Dwivedi, C. (2017). *Performance analysis and implementation of different pumping techniques on an EDFA amplifier.* Paper presented at the 2017 Third International Conference on Sensing, Signal Processing and Security (ICSSS).

Muniz-Cánovas, P., Barmenkov, Y. O., Kir'yanov, A. V., Cruz, J. L., & Andrés, M. V. (2019). ASE narrow-band noise pulsing in erbium-doped fiber amplifier and its effect on self-phase modulation. *Optics express, 27*(6), 8520-8528.

Naji, A., Hamida, B. A., Cheng, X., Mahdi, M. A., Harun, S., Khan, S., . . . Ahmad, H. (2011). Review of erbium-doped fiber amplifier. *International Journal of Physical Sciences, 6*(20), 4674-4689.

Nakandakari, M., Kuroda, K., & Yoshikuni, Y. (2017). Metastable-state lifetime of erbium ions measured in the fiber propagation direction: expansion of measurable fiber length. *Japanese Journal of Applied Physics, 56*(11), 112501.

Nakazawa, M. (2014). Evolution of EDFA from single-core to multi-core and related recent progress in optical communication. *Optical Review, 21*(6), 862-874.

Norouzi, M., Badeka, P., Chahande, P., & Briley, B. (2013). *A survey on rare earth doped optical fiber amplifiers.* Paper presented at the IEEE International Conference on Electro-Information Technology, EIT 2013.

Obaid, H. M., & Shahid, H. (2018). Novel flat-gain L-band Raman/Er-Yb co-doped fiber hybrid optical amplifier for high capacity DWDM system. *Optik, 175*, 284-289.

Ono, H., Miyamoto, Y., Mizuno, T., & Yamada, M. (2019). Gain Control in Multi-Core Erbium-Doped Fiber Amplifier With Cladding and Core Hybrid Pumping. *Journal of Lightwave Technology, 37*(13), 3365-3372.

Paul, M. C., Dhar, A., Das, S., Pal, M., Bhadra, S. K., Markom, A., . . . Harun, S. (2015). Enhanced Erbium–Zirconia–Yttria–Aluminum Co-Doped Fiber Amplifier. *IEEE Photonics Journal, 7*(5), 1-7.

Paul, M. C., Harun, S. W., Huri, N., Hamzah, A., Das, S., Pal, M., . . . Kalita, M. (2010). Performance comparison of Zr-based and Bi-based erbium-doped fiber amplifiers. *Optics letters, 35*(17), 2882-2884.

Pedro, J., & Costa, N. (2017). Optimized hybrid Raman/EDFA amplifier placement for DWDM mesh networks. *Journal of Lightwave Technology, 36*(9), 1552-1561.

Pollnau, M., & Eichhorn, M. (2017). Emission Cross Section, Füchtbauer-Ladenburg Equation, and Purcell Factor *Nano-Optics: Principles Enabling Basic Research and Applications* (pp. 387-404): Springer.

Pradhan, D., & Mishra, V. (2015). Analysis and Review of EDFA. *Int. J. Comput. Sci. Network, 6*(4).

Pradhan, D. D., & Mandloi, A. (2016). *Design Optimization of data rate 16× 40 Gbps EDFA WDM system.* Paper presented at the International Conference on Fibre Optics and Photonics.

Pradhan, D. D., & Mandloi, A. (2018). Performance Analysis of Flat Gain Wideband Raman Amplifier for S. *Advances in OptoElectronics, 2018*.

Rademacher, G., Luís, R. S., Puttnam, B. J., Eriksson, T. A., Agrell, E., Maruyama, R., . . . Wada, N. (2018). *159 Tbit/s C+ L band transmission over 1045 km 3-mode graded-index few-mode fiber.* Paper presented at the Optical Fiber Communication Conference.

Rahman, M., Latiff, A., Reddy, P., Das, S., Dhar, A., Paul, M., & Harun, S. (2019). Passively Q-switched fiber laser utilizing new hafnium–bismuth–erbium co-doped fiber as saturable absorber. *Indian Journal of Physics*, 1-5.

Rajini, J. H., & Selvi, S. T. (2015). Performance Analysis of Hybrid Optical Amplifiers for 64× 10 Gbps DWDM system. *Asian Journal of Applied Sciences, 8*(1), 46-54.

Rivera-López, F., Babu, P., Jyothi, L., Rodríguez-Mendoza, U., Martín, I., Jayasankar, C., & Lavín, V. (2012). Er3+–Yb3+ codoped phosphate glasses used for an efficient 1.5 μm broadband gain medium. *Optical Materials, 34*(8), 1235-1240.

Saifi, M. A. (2001). Optical Amplifiers. In K. H. J. Buschow, R. W. Cahn, M. C. Flemings, B. Ilschner, E. J. Kramer, S. Mahajan, & P. Veyssière (Eds.), *Encyclopedia of Materials: Science and Technology* (pp. 6416-6423). Oxford: Elsevier.

Senior, J. M., & Jamro, M. Y. (2009). *Optical fiber communications: principles and practice*: Pearson Education.

Shah, A., & Mankodi, P. (2017). *Analysis and simulation on gain flattening filter of an erbium doped fiber amplifier for multi-channel WDM system.* Paper presented at the 2017 International Conference on Wireless Communications, Signal Processing and Networking (WiSPNET).

Shukla, P., & Kaur, K. P. (2013). Performance analysis of EDFA for different pumping configurations at high data rate. *International Journal of Engineering and Advanced Technology (IJEAT), 2*(5), 487-490.

Singh, M. (2018). A review on hybrid optical amplifiers. *Journal of Optical Communications, 39*(3), 267-272.

Singh, S., & Kaler, R. S. (2015). Review on recent developments in hybrid optical amplifier for dense wavelength division multiplexed system. *Optical Engineering, 54*(10), 100901.

Suzuki, N., Yoshima, S., Miura, H., & Motoshima, K. (2016). Demonstration of 100-Gb/s/λ-based coherent WDM-PON system using new AGC EDFA based upstream preamplifier and optically superimposed AMCC function. *Journal of Lightwave Technology, 35*(8), 1415-1421.

Teyo, T., Leong, M., & Ahmad, H. (2003). Power conversion efficiency of erbium-doped fiber amplifiers with optical feedback.

Varshney, R., Singh, A., Pande, K., & Pal, B. (2007). Side-polished fiber based gain-flattening filter for erbium doped fiber amplifiers. *Optics Communications, 271*(2), 441-444.

Volet, N., Spott, A., Stanton, E. J., Davenport, M. L., Chang, L., Peters, J. D., . . . Bowers, J. E. (2017). Semiconductor optical amplifiers at 2.0-μm wavelength on silicon. *Laser & Photonics Reviews, 11*(2), 1600165.

Wang, J., Xu, P., Gu, X., Ma, L., & Hu, Z. (2018). *High-efficiency Stimulated Brillouin Effect in Short-length Fibers Assisted by Twisted-mode Linear-cavity Erbium Doped Fiber Lasers.* Paper presented at the Optical Fiber Sensors.

Xiao, Z., Yi, L., Xue, L., & Hu, W. (2018). Single-Fiber Bi-Directional Burst-Mode EDFA for TWDM-PON. *IEEE Photonics Journal, 10*(6), 1-6.

Yang, J., Dai, S., Dai, N., Xu, S., Wen, L., Hu, L., & Jiang, Z. (2003). Effect of Bi 2 O 3 on the spectroscopic properties of erbium-doped bismuth silicate glasses. *JOSA B, 20*(5), 810-815.

Yang, J., Meng, X., & Liu, C. (2016). Accurately control and flatten gain spectrum of L-band erbium doped fiber amplifier based on suitable gain-clamping. *Optics & Laser Technology, 78*, 74-78.

Yin, A., Li, L., & Zhang, X. (2010). Analysis of modulation format in the 40 Gbit/s optical communication system. *Optik-International Journal for Light and Electron Optics, 121*(17), 1550-1557.

Yucel, M., & Aslan, Z. (2013). The noise figure and gain improvement of double-pass C-band EDFA. *Microwave and Optical Technology Letters, 55*(11), 2525-2528.

Yucel, M., & Yenilmez, G. (2015). The comparison of the gain flattening techniques EDFA configurations in the C/L band. *Journal of Optoelectronics and Advanced Materials, 17*(9–10), 1450-1457.

Yusoff, N. M., Abas, A., Hitam, S., & Mahdi, M. (2012). Dual-stage L-band erbium-doped fiber amplifier with distributed pumping from single pump laser. *Optics Communications, 285*(6), 1383-1386.

Yusoff, N. M., Bakar, M. A., Sheih, S., Adikan, F. M., & Mahdi, M. (2010). Gain-flattened erbium-doped fiber amplifier with flexible selective band for optical networks. *Laser physics, 20*(8), 1747-1751.

LIST OF PUBLICATIONS

Journals indexed by Clarivate Analytics, Web of Science (WoS).

Al-Azzawi, A. A., Almukhtar, A. A., Reddy, P., Dutta, D., Das, S., Dhar, A., . . . Harun, S. (2018). Compact and flat-gain fiber optical amplifier with Hafnia-Bismuth-Erbium co-doped fiber. Optik, 170, 56-60.

Al-Azzawi, A. A., Almukhtar, A. A., Reddy, P., Dutta, D., Das, S., Dhar, A., . . . Harun, S. (2018). A flat-gain double-pass amplifier with new hafnia-bismuth-erbium codoped fiber. Chinese Physics Letters, 35(5), 054206.

Al-Azzawi, A. A., Almukhtar, A. A., Reddy, P., Das, S., Dhar, A., Paul, M. C., . . . Harun, S. W. (2019). An efficient wideband hafnia-bismuth erbium co-doped fiber amplifier with flat-gain over 80 nm wavelength span. Optical Fiber Technology, 48, 186-193.

Al-Azzawi, A. A., Almukhtar, A. A., Hamida, B., Das, S., Dhar, A., Paul, M., . . . Harun, S. (2019). Wideband and flat gain series erbium doped fiber amplifier using hybrid active fiber with backward pumping distribution technique. Results in Physics, 13, 102186.

Al-Azzawi, A. A., Almukhtar, A. A., Reddy, P. H., Dutta, D., Das, S., Dhar, A., ... & Harun, S. W. (2019). Wide-band flat-gain optical amplifier using Hafnia and zirconia erbium co-doped fibres in double-pass parallel configuration. Journal of Modern Optics, 66(16), 1711-1716.

Al-Azzawi, A. A., Almukhtar, A. A., Dhar, A., Paul, M. C., Ahmad, H., … Harun, S. W. (2020) Gain-flattened hybrid EDFA operating in C + L band with parallel pumping distribution technique, **(Submitted to IET Optoelectronics)**